Master Thesis

OPERATION, CONTROL AND OPTIMIZATION OF A MESHED-HVDC SYSTEM

A Thesis submitted by Alejandro Bayo Salas for the degree of MSc in Electrical Engineering in the Universitat Politècnica de Catalunya

June 2013

Supervised by:
Agustí Egea Álvarez
Andreas Sumper

Màster d'Enginyeria en Energia especialitat Elèctrica
Universitat Politècnica de Catalunya

'I remember Tom [Edison] telling them that direct current was like a river flowing peacefully to the sea, while alternating current was like a torrent rushing violently over a precipice. Imagine that! Why they even had a professor named Harold Brown who went around talking to audiences... and electrocuting dogs and old horses right on stage, to show how dangerous alternating current was.'

George Westinghouse

Resum

Aquest projecte estudia el control de l'operació de les xarxes multi-terminals d'HVDC. Les dos estratègies més generalitzades, la centralitzada i droop, són estudiades així com el seu efecte en la operació del sistema. Per tal de fer aquest estudi, es presenta també la modelització i el disseny i control dels convertidors VSC. Posteriorment s'han dut a terme diferents simulacions mitjançant l'eina d'estudi PSCAD. Per tal d'analitzar aquest sistema, es presenta un mètode per calcular el flux de càrregues amb control droop.

Posteriorment, es proposa un control terciari amb l'objectiu de donar una solució al problema de la operació òptima en xarxes MTDC controlades distribuïdament. Finalment, per tal de validar, estudiar el seu comportament i extreure conclusions, s'han simulat diferents casos.

Abstract

The M-HVDC system is seen as the most feasible solution for the massive integration of renewables energies, the interconnection among power systems located in remote areas and the interconnection of asynchronous ac grids. However, there are several outstanding issues and it is necessary to further research before its development. One of the research areas which generates greater attention is the operation and control of such grids. A system of these characteristics must be capable of maintaining the power balance, distributing the load flows between converters after a change in load or generation conditions and accomplishing the N-1 security requirements.

In the thesis, the two most generalized strategies for its control, centralized and droop, are explained, and their effect on the network operation is studied. The droop control is generally promoted thanks to the autonomous control, the collaborative scheme in the system stabilization and the N-1 provision. Nevertheless, its inherent proportional characteristic leads to deviations with reference to the nominal values and, thus, it is not possible to control the injected power in each of the stations. This can be solved with secondary controller which allows following references values only determined by the line resistances. Thus, not any desired load flow scenario is possible and it is not capable of optimizing the overall system according to a desired operation.

It is proposed a tertiary control based on an OPF which allows the system optimization according to the minimization of losses and the frequency support of the connected ac power systems. This controller is based on the droop characteristic and, therefore, the system does not require critical communications for its stability. Moreover, it satisfies a hierarchical coherence respect to the lower controllers and defines its possible functions on such network.

In order to validate and study the behaviour on the operation, simulations of the control are perfomed by means of the power systems study tool PSCAD.

Resum

Els sistemes M-HVDC són considerats com la solució més viable per a la integració massiva d'energies renovables, la interconnexió entre sistemes de potència localitzats en àrees remotes i la connexió entre sistemes asíncrons. No obstant encara resten per resoldre diferents qüestions i reptes prèviament al seu desenvolupament. Una de les àrees que genera major interès és l'operació i control d'aquesta xarxa. Un sistema d'aquestes característiques ha de ser capaç de mantenir el balanç de la xarxa i de distribuir els fluxos de càrrega entre els convertidors desprès de qualsevol canvi a més de complir els requeriments de seguretat N-1.

En el projecte s'han estudiat les dos estratègies més generalitzades en el seu control, el centralitzat i droop, així com el seu efecte en la operació del sistema. Generalment, el control droop ha estat afavorit degut a la no necessitat de comunicacions per a la seva regulació, l'estratègia col·laborativa entre els convertidors a l'hora d'estabilitzar el sistema i la provisió de seguretat N-1. No obstant, la pròpia característica proporcional implica desviacions respecte els valors de referència i, per tant, les potències injectades als terminals no poden ser absolutament controlades. Això pot ser solucionat gràcies a un control secundari que permeti l'eliminació d'aquests errors de potència en règim permanent respecte les referències. No obstant, les referències calculades per aquest no permeten per si mateixes l'operació òptima del sistema per unes determinades condicions.

En el present projecte es proposa un control terciari basat en un OPF mitjançant el qual s'optimitzi el sistema en relació a la minimització de pèrdues i a la redistribució de reserves dels sistemes connectats per tal de reduir les desviacions de freqüència. El control està basat en la característica droop i, per tant, no són requerides comunicacions crítiques per a la estabilitat del sistema. A més, se satisfà una coherència jeràrquica amb la resta dels nivells de control i es defineixen les seves possibles funcions dintre un sistema d'aquestes característiques.

Amb l'objectiu de validar els resultats i estudiar el seu comportament en l'operació s'han dut a terme diferents simulacions mitjançant l'eina d'estudi de sistemes de potències PSCAD.

Resumen

Los sistemas M-HVDC son considerados como la solución más viable para la integración masiva de energías renovables, la interconexión entre sistemas de potencia localizados en áreas remotas y la conexión entre sistemas asíncronos. Sin embargo todavía quedan por resolver diferentes cuestiones y retos previamente a su desarrollo. Una de las áreas de investigación que suscita mayor interés es la operación y control de esta red. Un sistema de estas características debe ser capaz de mantener el balance de la red y de distribuir los flujos de carga entre los convertidores después de un cambio en las condiciones además de cumplir los requisitos de seguridad N-1.

En el proyecto se han estudiado las dos estrategias más generalizadas en su control, el centralizado y droop, así como también su efecto en la operación del sistema. Generalmente, se ha favorecido el control droop debido a la no necesidad de comunicaciones para la regulación, la estrategia colaborativa entre los convertidores en estabilizar el sistema y la provisión de seguridad N-1. Sin embargo, la propia característica proporcional implica desviaciones respecto a los valores de referencia y, por lo tanto, las potencias inyectadas en los terminales no pueden ser controladas. Esto puede ser solucionado gracias a un control secundario que permita la eliminación de estos errores de potencia en régimen permanente respecto a las referencias. Sin embargo, estas referencias calculadas por este no permiten por si mismas la operación óptima del sistema para unas condiciones determinadas.

En el presente proyecto se propone un control terciario basado en un OPF mediante el cual se optimice el sistema en relación a la minimización de pérdidas y a la redistribución de reservas de los sistemas conectados a la red para reducir las desviaciones de frecuencia. El control está basado en la característica droop y, por tanto, no son requeridas comunicaciones críticas para la estabilidad del sistema. Además, se satisface una coherencia jerárquica con el resto de niveles de control y se definen sus posibles funciones dentro de un sistema de estas características.

Con el fin de validar los resultados y estudiar su comportamiento en la operación, se han llevado a cabo simulaciones mediante la herramienta de estudio de sistemas de potencia PSCAD.

Acknowledgements

Foremost, I would express my deepest gratitude to Agustí Egea for investing a lot of time and effort on me and satisfying my regular consultations for which I were able to gain enough insight in the Thesis subject. Moreover, I would like to thank him to the contributions in the research subject proposal.

I would also extend my gratitude to Mònica Aragüès for dealing with some questions related to control and optimization areas and enabling me the further handling of power system simulation programmes.

My gratitude also goes particularly to my supervisor Dr. Andreas Sumper for the guidance during the course of the project and for giving me the opportunity to explore this interesting topic.

Last but not least, I would like to thank my parents for allowing me the study at the university and encouraging me during these years.

Nomenclature

FRT	Fault Ride Through
GSVSC	Grid Side Voltage Source Converter
HVDC	High Voltage Direct Current
ICC	Inner Current Controller
IGBT	Insulated Gate Bipolar Transient
LCC	Line Commutated Converter
M-HVDC	Meshed High Voltage Direct Current
MMC	Multi Modular Converter
MTDC	Multi-Terminal Direct Current
OPF	Optimal Power Flow
PCC	Point of Common Coupling
PI	Proportional-Integral Control
PLL	Phase-Locked Loop
PSO	Particle Swarm Optimization
SPWM	Sinusoidal Pulse Width Modulation
SVPWM	Space Vector Pulse Width Modulation
TSO	Transmission System Operator
VSC	Voltage Source Converter
WF	Wind Farm
WPP	Wind Power Plant

Contents

List of Figures

List of Tables

Chapter 1

Introduction

1.1 Background

The continuous increasing in electrical energy demand coupled with the need of produce it without depending of fossil resources has favoured the development of renewable energies for generating electrical energy the last decades. Wind energy has emerged as one of the most interesting sources. As stated in a document from the European Commission, wind energy could provide one fifth of the EU's electricity demand in 2020 and one third by 2030 [13]. In order to meet this goal, according to the European Wind Energy Association (EWEA), offshore wind power capacity should increase from 3 GW (2010) to 40 GW - 55 GW in 2020 [14]. Technological advances have allowed the location at the sea or offshore which has the advantages of a more favourable wind source and the placement in unexploited locations. These installations have promoted the submarine HVDC transmission because of technical reasons.

HVDC systems allow a reduction of losses in long distance transmission, the possibility of interconnecting asynchronous power systems and the undersea power transmission. However, the massive installation of offshore wind farms provides an opportunity of deprecating the classical point-to-point connections in favour of the concept of a meshed dc grid which would interconnect more than two terminals. M-HVDC is seen as the solution to the massive integration of renewable energies and large interconnection of power systems while increasing the reliability of the system by providing redundancy in paths and allowing a greater power exchange capability. However, the technology is still under development and knowledge superficial. One of the research areas to investigate further is the operation and control of such systems. This is the focus of the research work described in the thesis.

1.2 Contributions of the Research Work

The contributions of the research work reported in the Msc Thesis is divided into different aspects of M-HVDC systems described below:

- *Contribution in the M-HVDC control area.*
  A control method for power trading definition within terminals has been

proposed. This control is defined as the tertiary controller of such network and, hence, an entire hierarchical control structure is presented.

- *Contribution in the M-HVDC operation area.*
  An easy and intuitive methodology in dc droop design for achieving a scheduled power flow operation is presented. Moreover, it is defined a power trading for the tertiary control level in order to support frequencies in the ac power systems connected to the grid.

- *Contribution in the M-HVDC optimization area.*
  The main contribution in this area is present an Optimal Power Flow for a network with bidirectional and droop-controlled terminals and its integration in the operation control of such system. Another contribution is the utilization of Particle Swarm Optimization to solve the problem.

- *Contribution in the M-HVDC steady-state analysis area.*
  A Newton-Raphson-based methodology to solve the load flow analysis of a droop-controlled dc network is presented.

1.3   Outline of the Thesis

- Chapter 2 provides a general introduction of HVDC systems. Some converter topologies of HVDC transmission are described. As the multi-terminal system is the scope of the thesis, its possibilities, challenges and state-of-the-art are presented.

- Chapter 3 describes the modelling of a voltage source converter. Control strategies in a point-to-point connection are also explained. Finally, some simulation are performed in PSCAD for the purpose of validating and studying the dynamical behaviour.

- Chapter 4 explores different control strategies for the primary control in meshed dc systems. An easy and intuitive methodology based on the scheduled power flow for the droop design is explained. The dc load flow analysis of a network of such characteristics is developed. Moreover, the secondary control for a distributed control is also presented. Finally, three cases are simulated in order to study the influence of the voltage control strategy in the MTDC operation.

- Chapter 5 is focused on the tertiary control of a M-HVDC system. A tertiary control for a distributed control is proposed in order to optimize the operation and define a hierarchical coherence between control levels. The optimization is performed by an optimal power flow in dc grids solved with particle swarm optimization.

- Finally, in chapter 6 some simulations are performed in PSCAD in order to examine the behaviour and capability of the tertiary controller and verify its operation.

Chapter 2

Meshed HVDC Grids

This chapter provides a general overview of HVDC systems with the aim of explaining their history and evolution. First of all, the concept of the multi-terminal HVDC system and its need is presented, together with its advantages with respect to the common ac grids. Secondarily, the main HVDC converter technologies are described and the main advantages and drawbacks of each of them are briefly discussed. Finally, a general state-of-the-art is explained and an introduction to dc networks topologies is done.

2.1 Introduction

A multi-terminal HVDC grid, hereinafter M-HVDC, is the interconnection of more than two converter stations within one or several ac power systems located at remote areas through a dc grid. It is the evolution of the traditional HVDC transmission systems that are based on a point-to-point system in which the dc line connects two ac buses, generally within the ac network and the generation plant. The M-HVDC system provides the possibility of connecting more than one energy source located in less viable areas for the direct connection with the ac power system. This grid is seen as the solution to allow the massive integration of renewable sources into the power system and as a transmission system that safely spreads electric power across national borders and beyond [15].

Because of the development and growth of renewable energies installed power, the old concept of power systems in which energy is generated by the generation plant and transferred through ac lines to the demand points, has been deprecated. Despite economical and environmental advantages, renewable energies have brought along different drawbacks such as its variable energetic production or its grid integration. Every time an increase in the installed power has occurred, the Transmission System Operator or other organizations have been forced to execute actions aimed to ensure the power supply quality such as FACTS installation, interconnection conditions at the PCC or fault ride through requirements. Notwithstanding, the continuous increase and the current installation of offshore wind farms of higher ratings oblige to assume the solution of a stronger interconnection within power systems and borders. In countries like Denmark, with high percentages of renewable generation installed, the in-

terconnection capacity represents about a 40 % of power capacity and 75 % of the maximum power demand [16]. However, in other countries like Spain where its production has reached until the 64.25 % of the overall power demand with 17.056 MW on February 6th, 2013 [17], the cross-border interconnection represents only a 4% of the power capacity and 7% of its maximum power demand [16]. This capacity is going to be increased by 2014 with the installation of the MAT transmission line between France and Spain with first European onshore HVDC connection of two links of $\pm$320 kV and 1000 MW for each of them [18]. On their behalf, UK has proposed a long-term plan for offshore wind energy consisting on the installation of 30 GW of such generation by 2020 which increase ten time the current power capacity whereas Nordic countries are planning the increase of wind generation until the 18 GW the year 2020. In addition, the Nordic hydro-power has been proposed to serve as a battery for Europe by which the wind energy surplus is absorbed by pumping stored water and then exporting it in off-peak hours [19]. Nevertheless, these areas have an insufficient interconnection available for geographical reasons and they have made important efforts to research, develop and install this new concept of energy transmission. An international meshed connection is conceived as a solution that will strengthen the energy security by coordination of power systems across regions. Up to date, HVDC emerges as the most reliable and feasible solution for the massive integration of renewable energy resources.

2.2 HVDC Transmission

The decision of choosing between an ac or dc transmission dates from the beginning of electrical power generation in the late 1880s. The so called "War of the Currents" opposed Thomas Edison, who promoted the dc current for electric power distribution, and Westinghouse and Nikola Tesla, who advocated for the alternating current. Finally, the choice of ac prevailed due to the easier transformation in high voltages thanks to ac transformers. Meanwhile, dc transmission was not capable of achieving high voltages and therefore produced higher transmission losses.

The manipulation of dc voltages became possible with the development of devices such as mercury arc valves in 1910s and semiconductor devices such as thyristors and recent IGBTs later. The continuous development in semiconductor devices and their increase of power ratings have made possible higher voltages reaches. Currently, power and voltage limits are set out by power and voltage ratings of such devices. In HVDC systems, the three-phase ac power is transformed by means of a terminal into dc power, which is then distributed in a dc network.

A dc connection within ac systems is for the below mentioned reasons the most feasible solution.

- The long distance transmission of energy through the already heavily loaded lines put an extra pressure on them. Moreover, because of the variability of the renewable energy sources, more transmission lines are needed for the same amount of energy delivered [20].

4

- New transmission lines have been limited in densely populated areas because of environmental, health or politic reasons. In this aspect, dc transmission occupies less volume and area for a determined power than ac lines.

Figure 2.1: Example of installations for 6000MW transmission lines [1].

- Transmission of large power underground or undersea are impossible in ac and must be done with dc transmission because of its lack of capacitive charging current.

- Charging current in ac cables intensifies as length increases. Due to the reactive power increase, less active power can be transferred as cable length grows. This phenomenon sets a limit to cable length. Charging current lack in dc cables turns this option into the only feasible for long-distance cables.

- Cable resistive losses for an ac cable are larger than those of an equivalent dc cable. However, power losses at the converter stations in ac systems are lower than those in the equivalent dc system.

- It makes possible the interconnection between two asynchronous power systems.

- HVDC does not increase the short-circuit level on the connected ac system.

- Magnetic fields from HVDC lines are negligible unlike the corresponding magnetic fields of HVAC lines.

- Dc systems are more economically feasible for long-distance cables. Dc transmission systems have larger terminal losses and investment costs but lower cable losses and cable costs. Figure 2.2 shows the generalized approach of the cost calculation as a function of cable length.
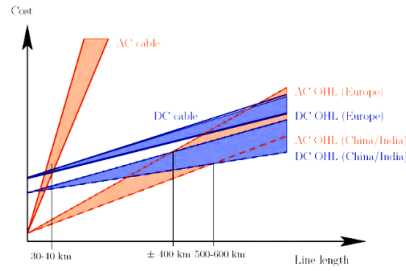
Figure 2.2: Costs comparison between ac and dc connections [2].

2.3 Converter technologies

The converter is the most important part of the HVDC transmission system being as it is the responsible to convert the ac into dc voltage and vice-versa and achieve a correct and efficient power transmission. Inside the converter, the control will take care of getting the correct system dynamic response.

The fast increasing process of thyristor and fully controlled semiconductor technologies has driven the HVDC transmission rapidly to its actual position. In a way, it has been the semiconductor technologies development which has enabled the progress of this kind of transmission.

2.3.1 Line-commutated current-sourced converters

The LCC converter depends on the ac voltage for its satisfactory operation. These converters are operated by delaying the current phase ideally between 0 and π rad respect to a determined voltage. Therefore, the current is always lagging behind the voltage and always absorbing reactive power [21].

The commutation process also generates a substantial harmonic current, principally at harmonics of 12n± 1 order on the ac side. Hence, a large ac filter is needed to reduce the harmonic distortion. The filter is capacitive at the fundamental frequency to provide the reactive power compensation and to filter the low frequency harmonics. This high capacitance can derive as well in large over-voltages during some dynamic conditions, i.e. fault recovery.

Typically, a LCC transmission needs to be connected to a PCC on the ac network with a short-circuit power at least 2.5 times the rating of the HVDC in order to assure stable operation [22].

In figure 2.3 is shown the six-pulse valve LCC transmission system where the basic configuration of the converter is a six-pulse bridge converter, also known as Graetz Bridge, composed by thyristors.

6
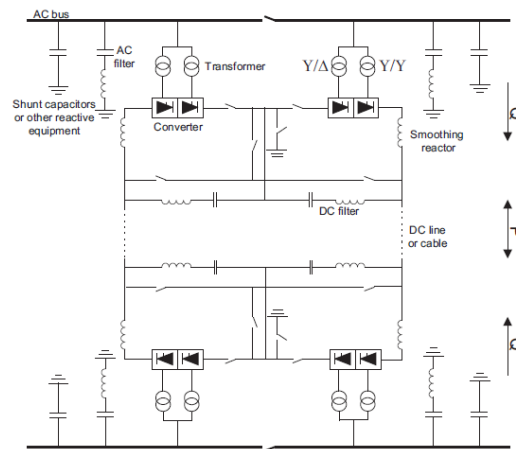
Figure 2.3: LCC transmission system [3]

The bridges are connected separately to the ac grid through transformers, one with Y-Y winding and other with an Y-Δ configuration to reduce the harmonic distortion, being the 5th a 7th harmonic current through the two transformers in opposite phase. A dc filter is also present to reduce the ripple produced on the dc voltage.

In meshed HVDC systems, LCC technology is not feasible as the voltage must also be reversed if the direction of power is reversed and a complete system recovery can only be achieved through the connection to a strong ac system at each terminal.

2.3.2 Voltage source converter

The development of the fully controlled semiconductor technologies has made possible the promotion of this technology after reaching important voltage levels. In fact, its maximum feasible rating is principally limited by present-day ratings of devices. The voltage source converter, VSC, is composed by IGBTs which are a fully controlled device. They are switched by a gate signal, generally generated by a PWM. The IGBTs withstand voltage and conduct current in one single direction; for this reason, a diode is connected in anti parallel in order to enable current conduction in both directions. The converter is typically operated at a switching frequency of about 1 kHz and is switched in order to eliminate low order harmonics. Thereby, a filter is required only to high order harmonics unlike the LCC smoothing filter. The figure 2.4 shows a diagram of a VSC transmission system.

7
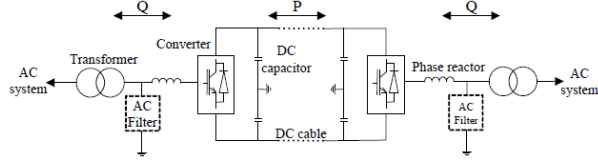
Figure 2.4: VSC transmission system [3].

From the ac network point of view, the VSC is seen as an equivalent voltage source with an amplitude and phase angle determined by the control system. There are three factors that limit the capability curve of the VSC transmission system. The first one is the maximum current allowed across the IGBTs, which gives a maximum PQ circle for a given maximum current. The second limit is the maximum dc voltage level, which due to reactive power mainly depends on the voltage difference between the ac voltage that the converter can generate from the dc bus and the grid ac voltage. With a low ac voltage, the reactive power capability is higher, which takes sense from a stability point of view. Finally, the third limit is given by the dc cable thermal rating which principally dependent on the maximum dc current passing through it and will limit the active power capability. In figure 2.5, the capability curve is shown.
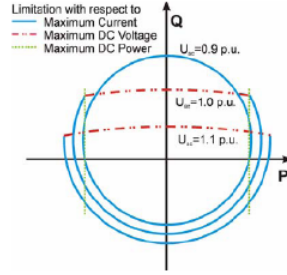
Figure 2.5: The capability curve of a VSC [4].

The active power exchange with the ac network is mainly controlled by the phase angle of the generated voltage. On the other hand, the reactive power is controlled by the magnitude of the generated voltage. Because of this, the reactive power exchange can be independently controlled at the different converters. The active and reactive powers are defined by equations 2.1 and 2.2.

$$p = \frac{u_c u_s \sin \delta}{X_r} \tag{2.1}$$

$$q = \frac{u_s \left(u_s - u_c \cos \delta \right)}{X_r} \tag{2.2}$$

Where δ is the phase angle and X_r is the series reactor reactance.

To sum up, the voltage source converter can be considered as a controllable voltage source. From the ac system point of view, the VSC acts as a synchronous

machine without mass that can control the active and reactive power instantaneously. It is also capable of controlling the active and reactive power flow independently since the generated output voltage can be virtually synthesized at any angle and amplitude with respect to the bus voltage.

Afterwards, the need of improving the voltage waveform and reducing power switching losses has led to the development of multi-level converters. When more switching levels are included in a leg, the voltage waveform should be more identical to a sinusoidal one; theoretically, the higher number of levels is included, the better waveform is obtained. Different multi-level topologies exist, including the flying capacitor and diode clamped converter. In [23] and [24] the two converters are explained in detail. A comparative between these topologies can be found in [25].

The main advantages and disadvantages of VSC with respect to the classical HVDC transmission are:

- In VSC active and reactive power can be controlled independently. LCC needs reactive power from the ac grid.

- The risk on commutation failure in VCS is reduced thanks to the use of self-commutated devices, whereas the classical converters need the presence of an ac voltage to commutate.

- Communication is not needed in VSC transmission since the converter controllers operate independently.

- VSC can operate at weak grids while LCC requires a stronger system with SCR greater than 2.

- VSC has a more compact site area, typically 50 - 60% of LCC site area.

- VSC has higher losses than LCC converters, 1% versus 0.75%.

- VSC has an insignificant harmonic distortion and does not require filters in most cases.

- VSC has a limited overload capability provided by the available IGBT devices whereas LCC has a better capability provided by robust power thyristor devices.

2.3.3 Multi modular converter

The Modular Multilevel Converter (MMC) is the most promising power converter for high power applications in the near future, particularly in HVDC links [26]. With the objective of reducing the voltage step size and the gradient voltage, more levels can be introduced. While in previously proposed multi-level strategies such as NPC or FCC a limited number of levels - usually three or five - can be practically realized [27], a MMC could use hundreds of levels. In fact, there is a commercial model of 401 levels nowadays which has been installed, among others, in the Spain-France interconnection. A high number of voltage levels produce a higher quality in output voltage waveform with low zero-sequence voltage in a 3-ph ac system [28]. Thus, the higher the number of

steps, the smaller harmonic distortion will be and only a small or even no fil-
ter are required. Another advantage is the adoption of low switching frequency
schemes which traduces in a reduction of semiconductor switching losses [28,29].

The operating principle of the MMC topology is the insertion and bypassing of
each sub-module composed by a capacitor and two switches as shown in figure
2.6 in order to obtain a multilevel waveform. The MMC is build using a series
connection of half-bridge sub-modules (SM).
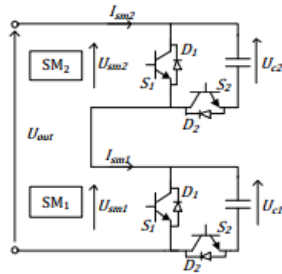
Figure 2.6: Series connection of two sub-modules [5].

By the correct switching of SMs, their respective capacitances are either con-
nected in series or bypassed in order to obtain the desired waveform of the
output voltage. Series connection of the two SMs in figure 2.6 can produce
three levels in the output voltage. For example, both SMs are inserted if S_1 is
conducting in both SMs and the two S_2 are blocked giving an output voltage
equal to $U_{SM1} + U_{SM2}$. If the two S_1 are conducting and both S_2 are block-
ing, both sub-modules are bypassed and the output voltage is equal to zero.
Depending on the direction of the current flow, the inserted capacitor either
charges or discharges.

Figure 2.7 sketches a MMC with series connections of the sub-modules. Phase
legs are connected in parallel on the dc side. Hence the dc current is split equally
between the three legs of each phase.
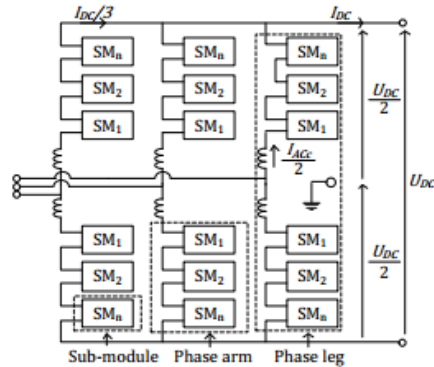
Figure 2.7: Simplified scheme of the three phase multi-level converter [5].

2.3.4 Hybrid LCC and VSC Converter

Finally, the hybrid converter configuration concept is presented. Hybrid converter is a converter that can appear with either series or parallel arrangement of LCC and VSC converters. The composite idea of a hybrid converter combines the main points of strength of both LCC and VSC converter while minimizing their disadvantages.

An ideal converter should permit operation at full power range at any desired power factor and importation/exportation of reactive power as well as eliminate commutation failure, cause an insignificant harmonic distortion and have low losses. A well-designed hybrid converter could overcome some weaknesses of LCC such as the need of an external reactive source, a large filter, control in active and reactive part or control at terminal voltage; and, the opposite way, some weaknesses of VSC could be improved, such as lower power ratings and less switching losses thanks to the fact that an amount of power is shared with the LCC.

The two main configurations of hybrid converters are in series or parallel.

A series hybrid converter consists on a series connection of one LCC and one VSC as shown in figure 2.8. In this configuration the VSC generates the reactive power demand of the LCC and also supports the ac terminal voltage while participates in active power transfer.
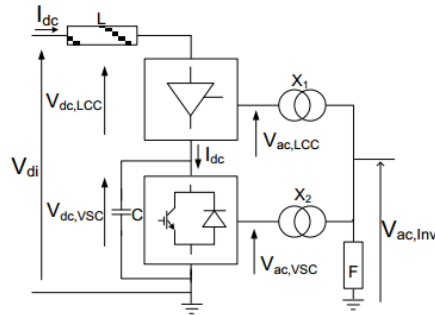
Figure 2.8: Simplified series hybrid converter transmission system [6].

On the other hand, a parallel hybrid converter consists on a parallel connection of one LCC and one VSC as shown in figure 2.9. This configuration is considered in situations such as the connection to a weak system and upgrading it.
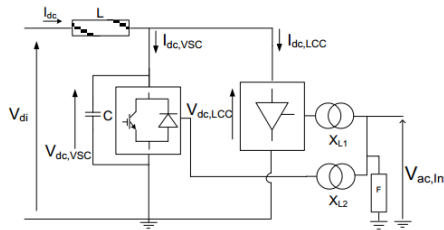
Figure 2.9: Simplified parallel hybrid converter transmission system [6].

Hybrid converters have as a drawback the complexity in power reversal which needs two sets of operations. The first is the change in oltage polarity in the LCC and the second is to switch in order to interchange inputs and outputs for reversing the voltage polarity across the VSC.

2.4 State-of-the-art of M-HVDC grids

The evolution of classical point-to-point interconnections to multi-terminal schemes has required a great number of research and development activities in many areas. All this progress has been performed by the time the technological advances in semiconductor devices have allowed higher ratings and new operation capabilities. Multi-terminal based HVDC transmission is not a new topic. LCC-based interconnections have been studied since decades. In fact, several installations based on this technology were installed and are still operating.

Up to date, only three MTDC networks have been commissioned. The first to use LCC technology was the Sardinia-Corsica-Italy Transmission in which the third terminal was added in 1991 to the initial point-to-point system build

in 1967. The power ratings are 200 MW in two terminals and 300 MW for the third, and voltage level is ±200 kV [30]. The first large scale multi-terminal transmission was the Quebec-New England Transmission commissioned between 1986 and 1992, where an initial classical HVDC two terminal interconnection was extended further to a third terminal with power ratings in all converters of 2000 MW and a dc voltage level of ±450 kV [31].

Nevertheless, the appearance of the VSC has been the advance which has caused the most important improvements and expanded initial concepts. The first multi-terminal network using VSC technology was the Shin-Shanano substation in 1999. This transmission consists of three back-to-back connections used for power exchanges between ac grids at different frequency levels [32]. Due to the lack of a dc transmission, this system does not represent a typical multi-terminal-based network.

One of the most important challenges is the operation of a MTDC network. Since the evolution of point-to-point interconnection, the new system has to respond to the need of characterizing the new power sharing or power responses within converter at changes in power flows. As a result, an important research working area has focused on control of VSC for reliable M-HVDC operation and different strategies are suggested in the literature. These strategies have been divided into two groups, a centralized and a distributed control. In a master-slave control, one converter is responsible of controlling the voltage at a given reference and it needs communications. On the other hand, coordinated control mode can regulate the transmitted power instantaneously at the cost of voltage deviation without the need of communications. Two examples of this strategy are the voltage margin method [33] and the droop control [34–38]. The droop control has achieved a relevant importance with respect to other strategies due to its capability of controlling voltage in several stations and its greater skill to provide N-1 security condition. Another outstanding issue of this area is the control of wind farms connected to ac systems by a MTDC. Since large offshore plants are completely disconnected from the ac onshore areas, WFs must continue being capable of supporting all ac grids to which they are connected in different conditions. Some authors focused in this area have proposed different methods such as reducing the generated power of WFs by a dc chopper [39], emulating an inertia for supporting primary frequency control [40–42], defining the current-voltage characteristics for a MTDC controlled with droop [37] or presenting possible topologies to transport power in such networks [43].

Another research area has focused on the power flow analysis in a dc system including some of them a power flow analysis of the overall ac/dc system. These solution methods are divided in a unified [44–46] and sequential approach [47–49]. The solution by an optimal power flow formulation has been also studied [50].

There are also research works related to the small-signal stability of a M-HVDC system [51–53].

However, the weakest point in M-HVDC transmission might be the protection. In a dc network, the fault current limit is the resistance of the dc line unlike ac systems where the line impedance reduces the effect of the fault further back in

the system. For this reason, a fault at one location can bring down the entire transmission system. The feasibility of a M-HVDC depends on the capability of withstanding dc faults on a fast and selective way. Due to the fact that it is not acceptable to disconnect the entire system each time a fault occurs, the meshed system have to isolate only the faulted part of the grid while keeping the remaining system in operation. The new system must be robust towards fault clearance: after fault clearing, there shall be a distribution of power flows and it need to be acceptable in N-1 security criteria [54]. The most important challenge in this area is the difficulty to achieve an available circuit breaker for dc systems due to the technological challenge of interrupting short-circuit currents in these networks. There are significant differences between ac and dc breakers mainly due to the absence of a natural current zero crossing in dc systems. Numerous ideas for HVDC breaker schemes [55] have been published and patented, but up to date only one has been invented, an Hybrid HVDC Breaker [56] solving a '100-year-old barrier to the development of DC transmission' [57] though it is not commercially available yet. Moreover, the detection of faults in the HVDC lines is also important in order to ensure a fast fault clearance. New fault detection methods has been developed such as wavelet [58],travelling wave detection [59] or fourier transformation [60] but they have not been yet implemented due to their complicated practical application and immature RD state.

2.5   DC Grids

The evolution of classical point-to-point schemes to multi-terminal schemes leads to a new interconnection scheme. The classical interconnection through a dc line becomes a meshed topology with more nodes. Some dc network topologies can achieve the objective of a multi-terminal system.

A possible configuration is a network with independent dc lines where all nodes are connected to an ac system as sketched in figure 2.10. In this topology, each circuit is composed by a dc line and two converters and all the converters are independently controlled as in classical point-to-point connections. For this reason, each circuit can operate at a different voltage level and it is feasible to adapt current HVDC installations into a M-HVDC system. As a drawback, this topology needs two converters for each dc line and therefore the overall network control might be rather complex.
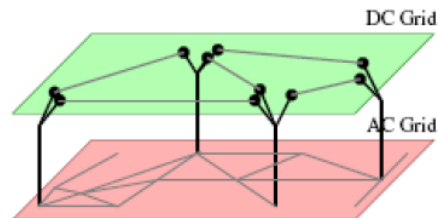
Figure 2.10:   M-HVDC system of independent dc lines [2].

Another topology is a meshed dc network. This network is the equivalent to

ac systems where the network nodes are connected between them without the need of converters, as is shown in figure 2.11. A meshed system makes possible a power flow with multiple possible paths between nodes and provides redundancy in converters which has a direct influence on the system reliability. However, protection requirements and its operation and control become more difficult.
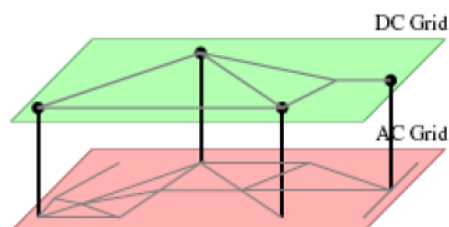
Figure 2.11:   Meshed dc grid. [2].

The operation and control of a meshed dc grid has to fulfil several functions:

- Maintaining the power balance between converter stations. A deviation in balance leads to a variation in dc voltage due to the charging of converter dc capacitor and may leading to a dc system black-out.

- Being able to redistribute power between converters after a power change.

- Accomplishing N-1 security requirements and relocating the power between converters after the fault.

Control strategies are explained in detail in chapter 4.

According to the two main topologies for a dc grid, some considerations must be done in order to ensure a reliable performance of this network.

On the one hand, the dc grid with point-to-point connection has the advantages related to the protection, operation and availability of the technology required. The switching technology is only required for the ac side in case a fault occurs. So the necessary protection components are indeed available in market. The capability of combining different voltage levels in dc transmission and circuit transmission, as monopolar or bipolar, is also an advantage. In this topology, power flow control of the overall network is not needed since each circuit is controlled by itself. Furthermore, line overloads cannot occur according the previous reason. However, the existence of a higher number of converter becomes a straightforward increase of electrical losses. This system is expandable with the corresponding installation of a converter.

On the other hand, the dc meshed network is also expandable and easier to construct with VSC technology. The main advantages are the integration of wind farms to the existing transmission cables and the higher line redundancy which becomes a higher transmission capability through lines thanks to the lower load on these. Because of this redundancy in transmission paths, load flow can be fully transmitted and used even during outages and abnormal conditions.

Nevertheless, in this topology it is not possible to operate at different voltage levels without the installation of special equipment such as dc/dc converters. Moreover, dc breaker technology is not yet available and dc circuit protection research is still immature. The capabilities of primary and secondary control of such network play as well an important role in this topology. In that case, a power flow control is required in order to avoid line overloads and accomplish ac network requirements.

To sum up, a point-to-point interconnection turns out to be currently the only technically favourable solution to construct an overlay grid with a low mesh although its cost is higher. But at the extent that the network increases in complexity and meshing due to more interconnected wind farms and ac nodes, the dc meshed grid becomes the most feasible and less expensive solution to the dc system development, even if it requires the advance in technology.

A meshed dc network has conceived the further challenging idea of building a Supergrid. This concept has become the main spearhead of the 2050 challenge destined to achieve the goal of reducing greenhouse gases by 80-95 % by 2050 [61]. This idea is based on the creation of a 'pan-European transmission network facilitating the integration of large-scale renewable energy and the balancing and transportation of electricity, with the aim of improving the European market' [62]. There are several projects and initiatives focused on that such as the European Supergid or Desertec.

As a future step, a grid code for the Supergrid needs to be defined, such as standard voltage levels or concepts to interconnect local and inter areas. Organisations such as CIGRÈ, CENELEC and IEC are studying various aspects of dc systems in order to prepare guidelines and technical reports and standards on common operational procedures to facilitate an open market for future system expansions. Some of the current working groups are listed below.

CIGRÉ

- B4-52 HVDC Grids Feasibility Study (2009-2012)

- B4-56 Guidelines for Preparation of Connection Agreements or Grid Codes for HVDC Grids (2011-2013)

- B4-57 Guide for the Development of Models for HVDC Converters in a HVDC Grid (2011-2013)

- B4-58 Devices for Load flow Control and Methodologies for Direct Voltage Control in a Meshed HVDC Grid (2011-2013)

- B4/B5-59 Control and Protection of HVDC Grids (2011-2013)

- B4-60 Designing HVDC Grids for Optimal Reliability and Availability Performance (2011-2013)

CENELEC

- European Study Group on Technical Guidelines for DC Grids (2010-2012)

IEC

- TC-57 (WG13 CIM) Power systems management and associated information exchange

Chapter 3

VSC Modelling and Control

In this chapter, the model of a VSC is presented and all the parts which compose it are explained. Different control strategies for the converter station are suggested as a result of the different grid operation which is required. This chapter also includes a model of the dc circuit used to connect the different stations. Finally, some simulations are presented to validate the desired behaviour of the explained model.

3.1   VSC Modelling

As explained previously, a M-HVDC grid is composed by different stations which interconnect the dc grids to the wind farms or ac grids by means of a voltage source converter. The behaviour of the overall system at varying situations depends mainly on the device dynamic response. In order to simulate this response, a model of a M-HVDC is built.

Roughly, the VSC is composed by the converter, in the different structures which have been explained in the previous chapter, a phase reactor on the ac side, for controlling the active and the reactive power flow by regulating currents through them, the capacitors on the dc side and the dc cable.

3.1.1   Averaged VSC Model

Firstly, a reduced averaged converter model, a non-harmonic model, is used. According to the required steady state and large time simulations, performing the simulation is preferably in a study of these characteristics so that IGBT switching has no interest. Thus, considering the switching functions of the transistor, instantaneous values of the current and voltage variables can be calculated whereby it is obtained the dynamics of the average values of variables rather than the dynamics of the instantaneous values. In the time-averaged model, different modulation techniques and modulation levels are no concern. Nonetheless, all phenomena related to the current components and fundamental frequency can be studied.

The model is based on the power balance between dc and ac side. This model

is represented by a current source on the dc side with a value equal to the current needed to obtain the active power injected for a determined voltage and three controllable voltages sources with the instantaneous magnitude from the modulator. The model also includes the ac series reactor and the dc capacitor. The presented model is lossless but in case of considering converter losses it can be achieved by adding a current source in parallel. Figure 3.1 shows the averaged VSC model.
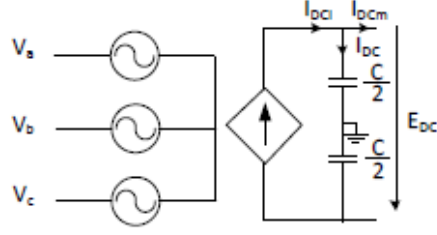
Figure 3.1: Averaged converter model circuit [7].

If converter and commutation losses are neglected, the powers on ac and dc side are equal. The power on dc side is expressed in the equation 3.1 and instantaneous active power on ac side in the equation 3.2.

$$P_{dc} = E_{dc}I_{dc} \tag{3.1}$$

$$p = u_a i_a + u_b i_b + u_c i_c \tag{3.2}$$

Applying the Park transformation [63] in order to obtain instantaneous stationary values, active and reactive power are calculated according to Akagi's dq Instantaneous Power Theory [64] in a simpler and faster form for the purpose of optimizing control. The calculation is expressed in equations 3.3 and 3.4.

$$p = \frac{3}{2}(v_d i_d + v_q i_q) \tag{3.3}$$

$$q = \frac{3}{2}(v_q i_d - v_d i_q) \tag{3.4}$$

An ideal phase locked loop, PLL, can provide a fast and accurate voltage angle and angular speed information allowing the synchronization between the grid-interfaced converter and the electrical network. Thereby, a stationary voltage component can be equal to zero. In this case v_q is oriented with the voltage, so v_d is equal to zero being the equations as follows:

$$p = \frac{3}{2}v_q i_q \tag{3.5}$$

$$q = \frac{3}{2}v_q i_d \tag{3.6}$$

3.1.2 Switched VSC Model

Figure 3.2 shows the two level basic structure of a Voltage Source Converter. As shown in the figure, it is composed by six pulse bridge employing self commutating switches, in high voltage applications commonly Insulated Gate Bipolar Transistor with diodes connected in anti-parallel. Depending on the active power flow within the converter, it will work as a rectifier or inverter.
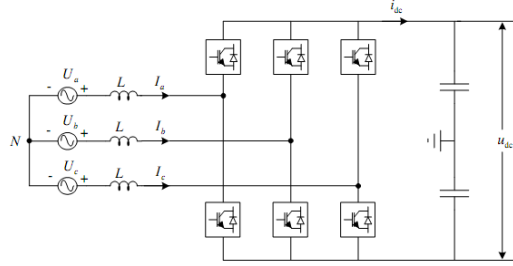
Figure 3.2: Two level switched converter model circuit [8].

This model is required for the study of modulation techniques, different topologies of the converter and high frequency components for a detailed study of losses.

In order to generate the sinusoidal wave shape and the phase angle and magnitude changes on it, instantaneously modulation techniques are used. In the thesis the Sinusoidal Pulse Width Modulation and the Space Vector Pulse Width Modulation are used. Their theories and implementations are explained in appendix B.

3.1.3 The DC Capacitor

The dc capacitor is the element in charge of reducing voltage ripples on the dc side as well as maintaining the voltage for the operation of the VSC. It also acts as an energy storage buffer for providing the dynamic response between ac and dc side.

The capacitor is sized based on dc voltage link and power handling capacities of the converter. Its size is commonly given in terms of a time constant τ which responds to the time required to charge it at the nominal voltage at the rated current and gives information about its dynamic response to voltage changes. Application of large capacitors results in dc voltage small changes in response to changes in power exchange on the dc side. On the other hand, if capacitor is small, there is an improvement on system dynamics, resulting in faster response to changes in the instantaneous power exchanged at the expense of a worse dc voltage support. The capacitance can be approximated by equation 3.7 obtained from the quotient between the energy stored in the capacitor and the electrical

energy [3].

$$C = \frac{2\tau S_b}{e_{dc^2}} \tag{3.7}$$

Where C is the total capacitance of capacitors in $[\mu F]$, τ is the time constant of capacitor [ms], S_b is the rated capacity of the converter in [VA] and e_{dc} is the nominal direct voltage. The time constant must be selected between 5 and 10 ms in order to obtain a small ripple and a fast response of voltage upon fluctuations in the power exchange.

3.1.4   Phase Reactor

Phase reactors are used to control active and reactive power flow by regulating the current through them. They are also required as the interface between the modulated voltage obtained in the converter and the ac grid voltage. Phase reactors are low-pass filters which reduce the high harmonic content of ac current caused by the switching operation. They provide as well the required attenuation of current ripples. The reactor inductance is calculated by the desired maximum peak-to-peak ripple current as,

$$i_{ripple} = \frac{E_{DC}}{2L} \frac{1}{2f_s} \tag{3.8}$$

A large phase reactor would mean a higher impedance to the ripple current, and hence, lower current ripples. However, too high value would slowdown the dynamics of the converter. A phase reactor of size 0.12 pu is commonly used.

Another method for the phase reactor dimensioning is to take the usual values of the transformer parameters, concretely the short-circuit impedance, ε_{cc}, and the joule winding losses, w_{cc}. A common value for ε_{cc} is contained within the range of $8\% \div 0.12\%$ and w_{cc} can be chosen as 0.4%. The equivalent resistance and inductance of the phase reactor is then calculated according to the following equations,

$$R = w_{cc} \frac{U_N^2}{S_N} \tag{3.9}$$

$$Z = \varepsilon_{cc} \frac{U_N^2}{S_N} \tag{3.10}$$

$$L = \frac{\sqrt{Z^2 - R^2}}{\omega_e} \tag{3.11}$$

3.1.5   DC Cable

The connection of VSC is done by means of a dc cable. The dc circuit of a VSC system consists on a bipolar connection. Since the dynamic modelling takes into account transients, the model consists on an inductance and a resistance in series with two capacitors in parallel as sketched in figure 3.3.
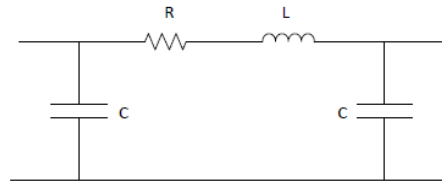
Figure 3.3: π model of a dc transmission line.

3.2 VSC Control

The VSC permits to control two electrical variables in the *qd0* frame allowing the independent control of reactive and active power. Reactive and active power references come from a higher level control of the system or are determined on a previous calculated value. According to the nature of the connected source, the VSC control strategy may differ.

In the present thesis, the HVDC system control structure has to accomplish that all the power produced by the generation power plant is transferred first to the dc grid through a rectifier and then being injected to the ac grid by means of inverters.

The main control scheme of a voltage source converter is based on a two-level cascaded control system where the lower level, or inner controller, allows to regulate the ac current while the higher level, or outer loop, deals with the regulation of the references.

The control system stability is based on the response speed of typical cascaded control systems where the inner control loop is set to be faster than the several outer loops. The ac currents controlled by the faster loop must follow the references provided by the slower loops.

There are different strategies to control the VSC according to the desired converter output which are divided into two different outer loops: the active and the reactive loop. The active loop is in charge of calculating the reference related to the voltage angle while the reactive provides the reference related to the modulation voltage. The active power flow can be controlled by means of the dc voltage on the dc side, by variation of frequency on the ac side or imposing to follow an active power reference while the reactive power flow is controlled through the voltage drop within the series reactor on the ac line, the voltage on the ac side or following a reactive power set-point. Obviously only one control in each loop can be used at the same time and its choice is made depending on the application.

3.2.1 GSVSC Control

The main objective of the grid side voltage source converter is to inject in the ac grid the active power on the dc side and to control the ac voltage on the ac side.

It is desirable that converters inject all the generated active power to the ac grid. Depending on the dc system and the number of onshore stations which compose it, many strategies to achieve the power balance can be realised. Moreover in this case, voltage regulation within the dc network must be performed. The control of two variables in a HVDC system will be discussed from this point forward.

3.2.1.1 Inner Current Control

The grid side converter control must allow to inject reference currents from the imposition of a drop voltage between converter nodes and ac grid nodes and the generated currents must follow the references with a behaviour determined by the first order plant of the phase reactor. For the purpose of controlling the system, the electrical circuit is studied first. The system plant is composed by the series reactor resistance and inductance as it is shown in figure 3.4 and expressed in equation 3.12.

$$v_{zabc} - v_{labc} = r \cdot i_{abc} + l\frac{d}{dt}i_{abc} \tag{3.12}$$
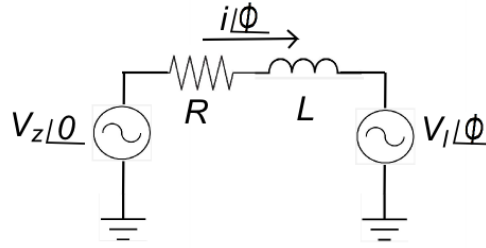
Figure 3.4: Series reactor between the grid (0rad) and the converter (θrad).

The ICC is implemented in the *qd0* frame. Applying the Park Transformation, explained in Appendix A, the equation system results:

$$\begin{bmatrix} v_{za} \\ v_{zb} \\ v_{zc} \end{bmatrix} - \begin{bmatrix} v_{la} \\ v_{lb} \\ v_{lc} \end{bmatrix} = \begin{bmatrix} r_l & 0 & 0 \\ 0 & r_l & 0 \\ 0 & 0 & r_l \end{bmatrix} \begin{bmatrix} i_a \\ i_b \\ i_c \end{bmatrix} + \begin{bmatrix} l_l & 0 & 0 \\ 0 & l_l & 0 \\ 0 & 0 & l_l \end{bmatrix} \frac{d}{dt} \begin{bmatrix} i_a \\ i_b \\ i_c \end{bmatrix} \tag{3.13}$$

$$\begin{bmatrix} v_{zq} \\ v_{zd} \end{bmatrix} - \begin{bmatrix} v_{lq} \\ v_{ld} \end{bmatrix} = \begin{bmatrix} r_l & -l_l w_e \\ l_l w_e & r_l \end{bmatrix} \begin{bmatrix} i_q \\ i_d \end{bmatrix} + \begin{bmatrix} l_l & 0 \\ 0 & l_l \end{bmatrix} \frac{d}{dt} \begin{bmatrix} i_q \\ i_d \end{bmatrix} \tag{3.14}$$

And decoupling equations are written in equation 3.15

$$\begin{bmatrix} v_{lq} \\ v_{ld} \end{bmatrix} = \begin{bmatrix} -\widehat{v}_{lq} + v_{zq} - l_l w_e i_{ld} \\ -\widehat{v}_{lq} + l_l w_e i_{ld} \end{bmatrix} \tag{3.15}$$

Where $\widehat{v}_{ld}$ and $\widehat{v}_{lq}$ are the outputs of the current controllers and v_{ld} and v_{lq} are the voltages to be applied by the converter.
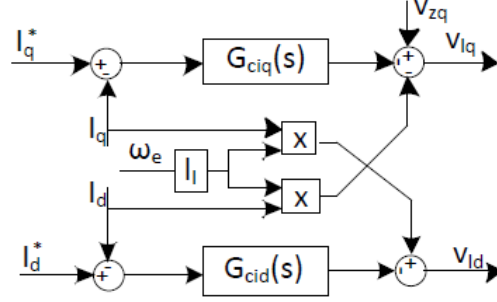
Figure 3.5: Inner Current Controller scheme [7].

Substituting 3.14 with 3.15 and applying the Laplace transformation, the system plant transfer function results as

$$\frac{i_{dq}(s)}{\widehat{v}_{ldq}(s)} = \frac{1}{l_l s + r_l} \tag{3.16}$$

In order to obtain v_{dl} and v_{ql}, a PI controller is used. It is designed in base of Internal Model Control Theory [7]. The PI controller transfer function is

$$G_{cd}(s) = G_{cq}(s) = K_p \left(1 + \frac{1}{T_i s}\right) \tag{3.17}$$

Then, the proportional and the integral constant are:

$$K_p = \frac{l}{\tau} \quad K_i = \frac{r}{\tau} \tag{3.18}$$

Where τ is the closed time constant of the electrical system.
The overall current loop is sketched in figure 3.5.

3.2.1.2 Outer Controllers

Main designs objectives of outer loops are the optimal regulation and control stability. They are responsible of calculating the reference currents, i_d^* and i_q^*, which are the inputs at the inner loop for assuring the main control objectives.

In the thesis, the two chosen strategies for the GSVSC are to control the dc voltage for the active loop and the ac voltage for the reactive and the reason of their choice is explained in the respective paragraphs.

3.2.1.3 DC Voltage Controller

The dc voltage controller is required for controlling the power exchange between converters. The control objective is to maintain the dc voltage at a given reference value by regulating the power exchange by means of i_q^*. Controlling the dc voltage, the converter ensures that the active power available in the dc grid is transferred to the ac grid. So the converter acts as an energy buffer between
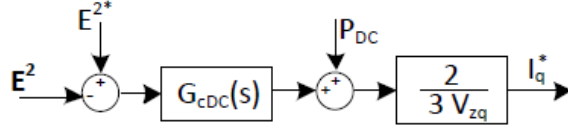
Figure 3.6: DC Voltage Controller [7].

dc and ac side.

Any unbalance between ac and dc powers leads to a voltage fluctuation over the capacitor. So the active power reference is calculated by means of operating this dc voltage error. A common practice to design this control is to operate on the error proportional to the square of the dc voltage [7] as E^2 is proportional to the energy stored in the capacitor $W \propto E^2$ as it is expressed in equation 3.19 and this power is the output after the proportional integral control. So the power reference is easily calculated as the sum of the power at the capacitor and the active power measured at the dc line before the capacitor as it is sketched in figure 3.1.

$$P_c\left(s\right) = \frac{1}{2}sCW\left(s\right) \tag{3.19}$$

Assuming the converter lossless, power balance equation between two grids remains according to equations 3.5 and 3.1:

$$P = \frac{3}{2}v_q i_q \tag{3.20}$$

The dc Voltage Controller scheme is shown in figure 3.6. The PI controller constants are calculated according to Internal Model Control technique as it is explained in the above reference,

$$K_p = C\xi\omega \tag{3.21}$$

$$K_i = \frac{C\omega^2}{2} \tag{3.22}$$

where ξ is the desired damping ratio of dc voltage loop, and ω is the desired angular velocity of the voltage loop.

Other dc voltage controller is a proportional-controlled strategy. In this control, the dc voltage difference is multiplied by a droop constant obtaining an active power reference. Its usefulness is focused on the control possibilities in a multi-terminal grid. The dc droop control is explained in detail in chapter 4.

3.2.1.4   AC Voltage Control

The main goal of the ac Voltage Controller is to regulate the voltage at the ac bus to a given reference. That implies that the converter will generate an amount of reactive power so that the voltage is maintained at the reference value by modifying the reference current i_d. For a voltage drop in the phase reactor with and inductive impedance higher to the phase resistance, $X_L \gg R$,
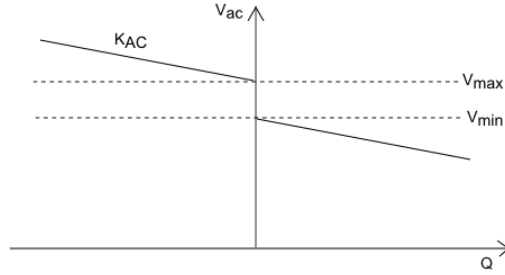
Figure 3.7: V_{ac}-Q characteristic of the reactive droop.
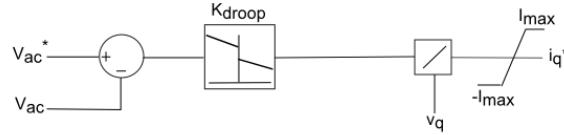
Figure 3.8: AC voltage droop control scheme

the voltage drop will only depend on the reactive power flow [3]. The ac outer loop is mathematically expressed in equation 3.23.

$$i_q^* = (v_{ac}^* - v_{ac}) (G(s)) \tag{3.23}$$

Reactive Power compensation and Fault Ride Through in a wind farm point of common coupling, PCC, is required. Since the dc grid decouples the generation plant, the converter must support the TSO requirements of ac voltage control.

In order to accomplish Grid Code requisites in which it is indicated that within a determined voltage range, generally $\pm 5\%$, can not be injected neither absorbed reactive power from the grid, a dead-band is implemented. Thus, a combined droop and dead-band control has been implemented for controlling the reactive loop as it is illustrated in figure 3.7. A more detailed explanation and theory of the ac voltage droop control can be found in [65]. The ac droop constant is then calculated as,

$$U - U^* = K_{ac} (Q - Q_0) \tag{3.24}$$

Where U is the measured voltage, U^* is a reference voltage, K_{ac} is the droop constant and Q is the reactive power. Parameters can be expressed in international system units or in pu.

The control scheme implemented in the thesis is shown in figure 3.8.

3.2.1.5 Current Saturation

In practice, the current absorbed or delivered by the converter flows through semiconductor switches. These have a limited current carrying capability which

27
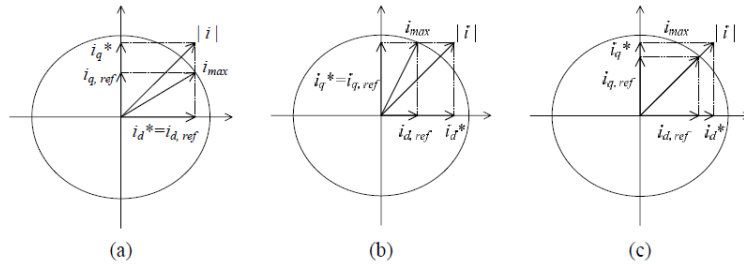
Figure 3.9: Current saturation strategies.

in the case of being exceeded could lead to the fail and damage of the converter.

In order to avoid an excessive current, a current saturation scheme is implemented. The current limiter compares the current reference values calculated by outer controllers with the maximum permitted. If the magnitude of the reference value exceeds the maximum current, then the magnitude is limited to the saturation value.

The magnitude of the current reference value is,

$$|i| = \sqrt{i_q^{*2} + i_d^{*2}} \tag{3.25}$$

where $|i|$ is the magnitude and i_q^*, i_d^* are the q-axis and d-axis current reference values.

There are three different strategies to saturate the exceeded current through switches. Firstly, it can be given the priority to i_d^* as is shown in figure 3.9.a. In second place, the priority may be given to i_q^* as is sketched in figure 3.9.b and the last strategy is scaling equally i_d^* and i_q^* as in figure 3.9.c.

In the thesis, the limiting strategy used is the one which gives priority to the reactive current.

3.3 Model validation

In order to validate, the model implemented in EMTDC/PSCAD as given in figure 3.1 has been tested for the controller performance under different cases.

PSCAD is an electromagnetic transient simulation tool specialised in transient analysis of power system involving non-linearities such as power electronic systems (HVDC,FACTS,distributed generation...), transformers with saturation, flicker, asymmetrical faults, frequency models of cables, etc and provides a fast and accurate simulation.

The system has been simulated for the voltage and power values presented in table 3.3. The VSC model components have been sized by means of the equations

28
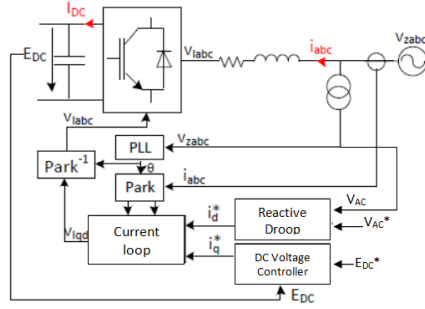
Figure 3.10: Voltage Source Converter control strategy [7].

detailed in this chapter and the resultant parameters used during the simulation are shown in table 3.3.

TABLE 3.1: HVDC transmission parameters.

VSC Model Parameters	
V_{ac}	320 kV
V_{dc}	380 kV
S_{base}	1000 MW
Series Reactor	
L	13.5 mH
R	0.2116 Ω
Inner Current Controller	
K_p	13.5
K_i	4.73ms
DC Voltage Controller	
C	300 μF
K_p	0.0287
K_i	8.5050s
AC Droop Controller	
K_{Droop}	-0.06 [pu/pu]

The simulated system is composed by a wind farm modelled as a current source at constant power and the voltage source converter controlled by the PI-dc voltage controller and the ac droop controller as it is shown in figure 3.10. Voltages are initially set up to the reference values and the initial generated active power is equal to zero. The system is subjected to the following transients:

- An active power step of 1000 MW at 1.5 s.

- A 3ph fault in the ac grid at 2 s, and the consequent clear fault after 50 ms.

- A change in the dc voltage reference which varies from 1 pu to 1.02 pu.
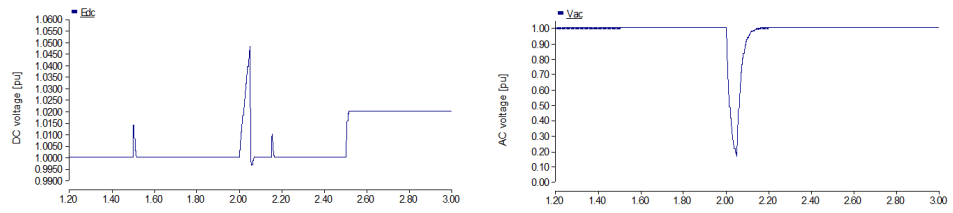
Figure 3.11: Measured dc voltage and ac voltage.
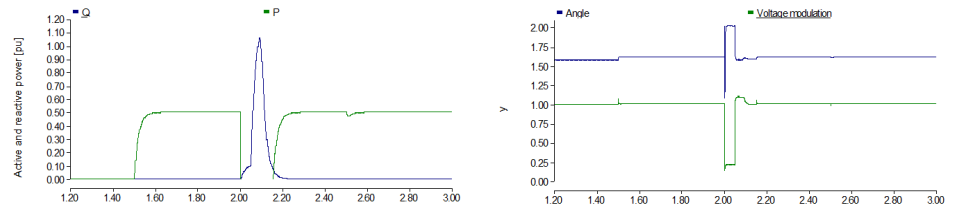
Figure 3.12: Active and reactive power measured in PCC and angle and modulation obtained from control.

For the purpose of verifying the correct operation of the model and all controllers, the previous transients are simulated. Focusing on transients in dc voltage, an active power step and a change of the dc voltage reference are applied. As the converter is controlled by means of a dc voltage controller, the converter should behave as a constant voltage source at the reference voltage. Also, a fault in the ac system is applied to observe the correct operation of the ac voltage controller and the converter fault ride through capability. In this case, the ac voltage should maintain constant at the reference value after cleared the fault.

The waveforms of dc voltage, active and reactive power at terminal, ac voltage and d and q components of current as well as the load current through the converter are plotted in figures 3.11, 3.12 and 3.13. Active power measurements are made on the ac side.

In first place, transients due to changes in the dc voltage controller are discussed.
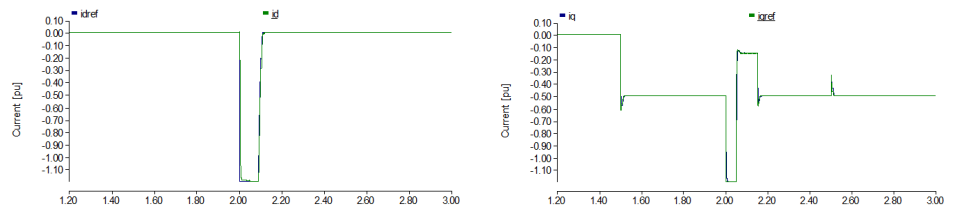
Figure 3.13: Measured and reference d and q components of current.
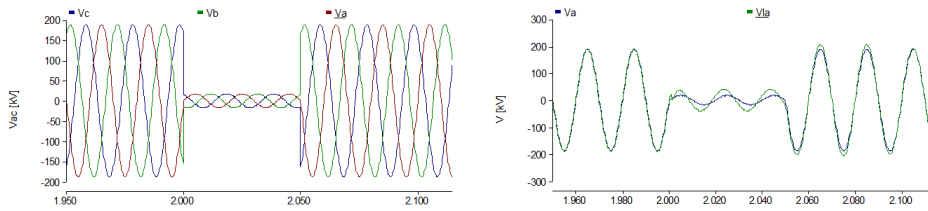
Figure 3.14: Measured ac voltage in PCC and measured ac voltage in VSC of a-phase when the ac fault is produced.

It is observed in figures that the applied power step at the dc current source from 0 pu to 1 pu while dc voltage reference is held at 1 pu is reflected in the power measurement at the ac system after a first order response. The active power change is reflected as well in the q-component of current. The power step cause a transient dc over-voltage. According to the dc voltage reference change, it is observed that the reference value is correctly followed by the measured dc voltage and it requires a change in current reflected in the q-component of current to maintain the generated active power balance. So the PI dc voltage controller performs correctly in tracking the reference. It is also observed that the effect of these transients is not present in the reference d-component of current. Hence the decoupled control of active and reactive power is also ensured.

Reference to the fault at ac side, the VSC produce an amount on reactive power in order to maintain the ac voltage at the PCC. Once cleared the fault, the ac voltage at the PCC is instantly recovered towards its nominal value and it accomplish the grid requirements of FRT, so the VSC control demonstrates its black start capability. According to the dc voltage measured, it is observed that the ac fault produces an important transient on it. The first over-voltage is due to the wind farm power injection which transforms on a current unbalance leading to the charge of the capacitor which directly causes an increase on the dc voltage. In this case, a power reduction control must be implemented on a wind farm in order to reduce the extracted power and avoid that the voltage exceeds the voltage limits. This power reduction can be physically implemented by a dc chopper [39] in charge of dissipating the surplus energy. Once cleared the ac fault, the dc voltage recovers its previous value.

In figure 3.14, it is shown the ac voltage behaviour of the 3-ph system and a comparative between the ac voltage at PCC and the voltage at VSC of phase a. In the second figure it is observed the different voltage modulation which causes the reactive power flow. And in figure 3.15 it is shown the behaviour of the dq frame voltages obtained by the control according to the angle and modulation voltage and the measured 3-ph currents where it can be observed the power step at 1.5s and the ac fault at 2s. It is observed that the ac fault produces an over-current which is reduced by means of the wind farm power reduction.

From the simulation results, it is concluded that the system response is fast; control accuracy can be achieved and the active power and the reactive power can be controlled independently and bidirectionally.

31
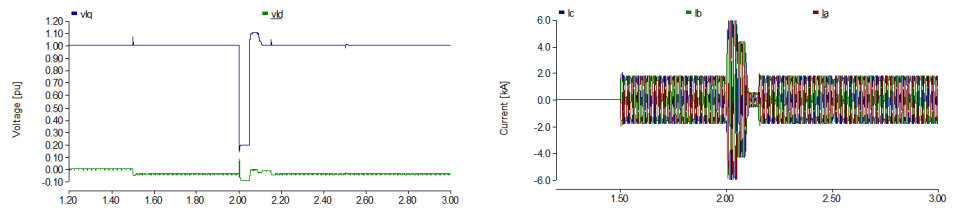
Figure 3.15: *dq* voltages of the control and measured 3-ph currents.

To sum up, by means of simulations it has been shown that the model and control strategies are able to provide the requested and desired behaviour and power distribution.

Chapter 4

Operation and Control of Meshed-HVDC Systems

The objective of this chapter is to provide enough insight in the topic of operation and control and analyse the load flow in a M-HVDC grid according to different control schemes. Firstly, the two most common strategies, i.e. centralized and distributed control, are explained. It has focused on the study of the droop control. An easy and intuitive droop design in order to obtain a scheduled power flow has been proposed. Furthermore, a load flow analysis for both control strategies is detailed. Secondly, the concept of the secondary control in such networks is presented. Finally, a case is defined in order to study the effect in power sharing of the both strategies and simulations has been performed for this purpose.

4.1   Introduction

Since more than two converters of a point-to-point scheme are connected to the dc system, different control functions in the converter are needed for a reliable operation of the M-HVDC system.

On the side of the ac system, the terminals directly connected to the grid should be capable of making up for all the functions of an ac generator. Whilst on the dc side, the system must be able to maintain the power balance among all the converters. The sum of all injected powers must be equal to the sum of all the powers; if not, the current unbalance causes a variation in dc capacitor charge which results as well in a dc voltage fluctuation may leading in the worst of the cases to a system black-out. The system must be capable of redistributing the active power variations between converter stations without larger time lags preferably while maintaining the same balance after a terminal disconnection by means of redistributing the surplus power to the remaining converters and maintaining the dc voltage within a acceptable range. In a system of such characteristics, the power injections are controlled by the converters which are in charge of changing dynamically the power flow into, or out of, the network without a reconfiguration of the overall system.

As explained previously in chapter 3, some challenges emerges on the operation and control of a meshed dc grid such as maintaining the power balance, redistributing the power flows after changes and accomplishing the N-1 security requirements and these functions must be fulfilled by the converters.

4.2 Operation and Control strategies

Commonly, the strategies to control the M-HVDC grid has been divided into two groups, a centralized point of view and a distributed control.

4.2.1 Centralized Control

The first strategy is based on the extension of control principle of a point-to-point scheme where a converter is in charge of maintaining the dc voltage within the system on a constant value and the power set-points are provided to the rest of converters. As explained in chapter 3, the dc voltage controller regulates the power exchanged at the converter in order to maintain the dc voltage at a reference value by modifying i_q^*. This strategy is also known as master-slave or centralized bus slack, as the ac approach where the slack converter maintains the voltage at the expense of compensating the power variation from the nominal references. In such control, the master terminal is in charge of accommodating all power unbalances that might occur in the system.

The main drawback of this strategy is the impossibility of controlling when the master or slack terminal fails. The slack converter disconnection leads to the dc system outage immediately due to the lack of converter controlling the voltage. The voltage control function of this converter can be duplicated to another converters as back-up slacks to take over the voltage control in case the master converter fails; though it does not disregard the main drawbacks of a centralized dc slack converter [66]. Another problem comes from the need of over-sizing the slack converter since it must be capable of compensating not only the power variation but also the transients caused by converters or lines outages. Other disadvantages derived from this are the requirement of being connected to a strong ac grid capable of supporting the severe transients and all the problems in the dc grid and the controversial associated to its geographical location and the system operator which would accept to develop this function.

Moreover, a M-HVDC grid implies a greater difficulty in regulating the voltage level in the grid unlike the common point-to-point connections. Due to the larger number of nodes in the grid is not possible to guarantee that the equilibrium in one terminal implies the stability within the dc network, may leading to unwanted voltages and power oscillations or unbalances.

In figure 4.1 it is shown a system composed by one WF terminal and two GS terminal in parallel with no resistive losses and voltage and power dynamic behaviour to an active power step of 1000 MW at 1.5 s. The two GSVSC are controlled with the dc voltage controller with PI control in order to maintain the dc voltage at a given reference. The figure shows the impossibility of con-

trolling the dc voltage at a given reference by more than one converter. While the two GS should share the total generated power, the injected active power in the two grid side converters is unbalanced and the dc voltage is correctly maintained during the simulation on its value.

A smart approach in a system of such typology is to combine the mas-
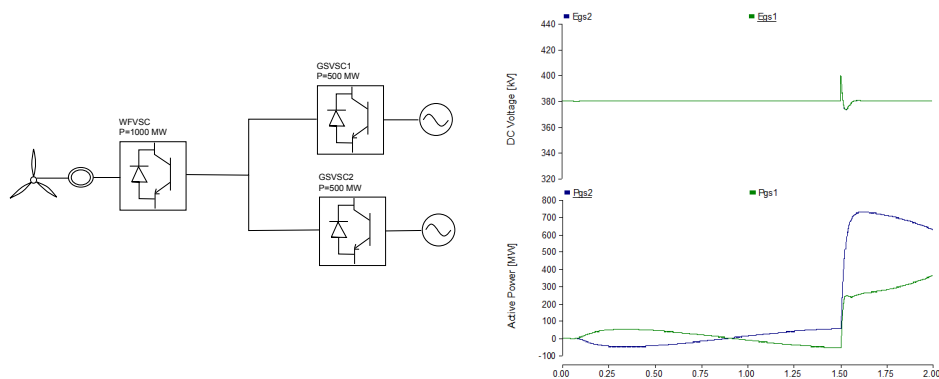
Figure 4.1: a. Circuit composed by one WF and two GSVSC. b. DC voltage and Active Power in the onshore terminals.

ter controller with droop-controlled converters. By this, voltage controlling is performed by more terminals which in case of a slack outage can ensure the stability of the system. Thus, this strategy can ensure the provision of N-1 security. Moreover, it can achieve an approximated scheduled power flow in droop-controlled stations. However the problems related to over-sizing the slack converter and being connected to a strong ac system still remains because of the fact that the master controller continues accommodating the most of the contingencies.

4.2.2 Distributed Control

On the other hand, the second strategy is based on the idea that the dc voltage control is distributed between several converters by means of adopting their input powers when the dc voltage changes at the expense of not keeping powers and voltages at the reference values. As an example, two methods that operate at this principle are the dc voltage droop control [34–38] or the voltage margin method [33]. These methods enable to share load among dc voltage regulating converters which operate in parallel.

The dc droop control is a similar strategy to the power-frequency droop control implemented in ac grids for primary control, in which the frequency droop is used for the control system to adjust the power of all generators in the network. The droop controller performs the function of primary control (synchronization and power balance) in meshed dc grids. However, its implementation is different since , in the one hand, the synchronization parameter is the frequency which is constant in the entire power system while, in the other hand, taking the dc voltage as the reference value has a less straightforward and more complicated implementation due to the variation of the voltage among nodes.

This control strategy regulates the power flow from the dc voltage at the terminal. Multiple terminals can support the dc voltage by adjusting their power or current according to their droop characteristic. At each power flow change, the system operates in a new equilibrium point determined by the voltage droop characteristic.

The method employs a proportional controller which emulates a resistance in the dc circuit behaviour and describes the relation between the dc voltage and the current at the terminal as it is represented in figure 4.2 in which the slope is the inverse of k_{droop}. According to this, a change in dc voltage implies a change in power sharing and vice-versa. This constant indicates the degree of compensation of power unbalance at the cost of a variation or a steady state error in the dc voltage.
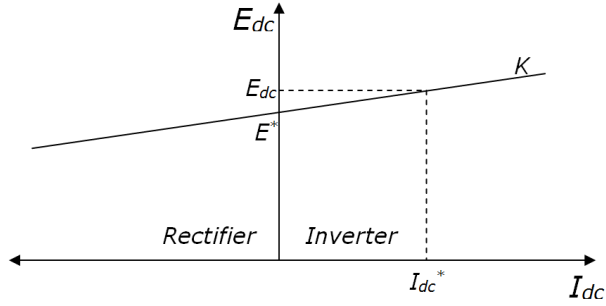
Figure 4.2: DC Voltage droop characteristic.

The control is based on calculating the injected current to the terminal as it is shown in equation 4.1.

$$i_{DC}^* = k_{Droop} \left(E_{dc} - E_{dc}^* \right) \tag{4.1}$$

Where i_{DC}^* is the reference current, E_{dc} is the measured voltage and E_{dc}^* is the dc voltage value for a null power injection at the converter, i.e. the minimum voltage desired at the inverter dc bus and depends on the system control design. Taking into account equation 3.5, the reference current at the inner loop, i_d^* can be calculated in per unit as:

$$i_d^* = \frac{2 \cdot E_{dc} I_{dc}}{3 \cdot v_d} \tag{4.2}$$

Some authors use a power-voltage droop characteristic [66, 67]. This approach has the advantage of having an easier integration and a conceptual simplicity in outer loops of vector control and making easier the calculation of power flows because of the linearity between voltage and power. At the operating point or around it, both controls behave identically but at the time the point is deviated, differences become larger due to the quadratic relation between current and droop. It may even the case of having high reference currents at low voltages in P-V droop. For this reason, the current-voltage approach is a more

realistic control since it relates proportionally two variables linearly dependent.

Droop control presents another characteristics useful for M-HVDC grids explained below:

- Communications are not needed among converters since the control is directly performed from the measured voltage at nodes.

- The control distribute the power injected by the generation to the different inverters controllably according to its design.

- It is a control very simple and easy to implement because of being defined by a proportional characteristic.

- It provides N-1 security criteria.

During the different power flow changes in the grid, the converters work on different operating points according to their respective droop characteristics. This operating points can be analytically calculated with the voltage-current characteristic of the M-HVDC grid. This consists on representing on voltage and current axis the v-i characteristic for each converter and find the operating points of each converter in which the stability is reached for the different power flow situations. These points are called equilibrium points. A more accurate and extensive description of v-i characteristic of a M-HVDC grid and the operating modes of converters can be read in [12,37] and some examples are performed in appendix C.

The calculation of the constants k_{droop} and E_{dc}^* are chosen in the control system design. The lower the voltage droop is, the more the converter adapts its output power at voltage deviations; while the higher k_{Droop} is, the more the converter generates a steady state error at dc voltage by maintaining the output power. In fact, a droop constant equal to zero can be considered as a dc voltage slack controller while P-control is obtained with a value tending to ∞. The droop design and the reference voltage set-point can be calculated based on the steady state system conditions. It must be taken into account that a voltage regulation of approximately 3 % between minimum and maximum dc voltage is commonly used to ensure stability in the system. Examples of its calculation and operation are explained in appendix C and a procedure to achieve a scheduled power flow according to the system references is explained in section 4.3.

As detailed in appendix C, dc droop control is also capable of performing a determined power sharing between terminals according to a certain ratio only varying the droop slope and defining a power sharing between converters during lack of generation. Moreover, the dc voltage offset as well as in charge of limiting the voltage regulation, it can prioritize the power injection to a determined converter in a situation of lack of generation.

Furthermore, some authors have proposed droop design methodology based on performance criteria in dynamic models [12] of meshed grids such as a design based on the frequency-response analysis [52] or solved by a convex optimization problem with linear matrix inequalities [68].

4.3 Droop design for a scheduled power flow

In this section it is explained a simple procedure to achieve a scheduled power flow in a dc meshed network. In a real network, the system have some electrical losses due to, among others, resistive losses in lines. These losses by effect Joule lead to large deviations respect to the operating point previously calculated by the droop characteristic in a lossless system. These deviations mainly depend on the equivalent resistance of the line and are determined by the network topology, cable characteristics, converter situation and the droop slope.

The dc line voltage drop between two nodes after a current flow is sketched in figure 4.3. When no current flows, $E_{dc,i}$ and $E_{dc,k}$ are equal while, on the contrary, a voltage difference between nodes generates a current flow. The new current caused by the drop is calculated in equation 4.3 in which small signal terms are included.
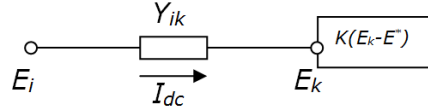
Figure 4.3: Voltage drop between two nodes.

$$I_{dc} = Y_{ik}(E_k - E_i) = K(E_k - E^*) = Y_{ik}\Delta E = K\Delta E \qquad (4.3)$$

The impact of dc line voltage drop in the injected power in a converter is shown in figure 4.4. If the system is designed for a reference voltage, i.e. the bus voltage for a lossless system, the flow of a current between nodes causes a variation on the converter voltage which straightforward leads to a deviation on the controlled current proportional to the droop constant.
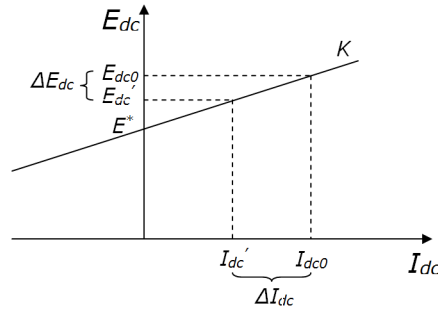
Figure 4.4: Impact of a voltage drop in the droop characteristic.

This deviation is calculated as,

$$P - P_0 = Y_{ik}(\Delta E)E_i - K(\Delta E)E_i \qquad (4.4)$$

$$\frac{\Delta P}{\Delta E} = Y_{ik}E_i - KE_i \qquad (4.5)$$

A scheduled power flow in a master-controlled grid or a slack with droop-control system is not a problem since the power injection at each node is given by the reference value, except the master terminal which is in charge of maintaining the power balance by accommodating all the deviations in the grid and compensating the system losses by adapting automatically the injected power.

Haileselassie et al. [69] propose a precise power flow of a MTDC grid with power and droop-controlled converters. On the work, reference powers and voltages for a lossless system are defined. Then, the precise power flow is achieved by defining a converter as slack, i.e. imposing on it a voltage equal to the reference, calculating the load flow and defining the injected power of the 'slack' converter as the necessary to compensate transmission losses.

In order to achieve a precise scheduled load flow in a distributed meshed network without defining a 'slack' and compensating transmission losses by all droop converters, a procedure to calculate droop constants is detailed in the following steps,

- Perform a power flow with all generation/load nodes as P-controlled as explained in section 4.5 with $P = [P_{ref1}, Pref_{ref2}, ..P_{refk}, 0..0]$ in a grid with k-controlled nodes. Obtain the voltages at the converter nodes.

- Generate the dc voltage offset vector using the obtained voltage values in the previous step and imposing the voltage regulation according to a certain criteria such as voltage control or power injection priority, $Edc^* = [Udc_1 - x\%, ..Udc_k - x\%]$ with k-onshore stations. Taking as a starting point the common value of a voltage regulation of a 3%, the higher x is, the more power-controlled is whereas the lower it is, the more voltage-controlled the converter is. Moreover, its sizing can be performed by a desired load flow in lack of generation situation in order to obtain two v-i points to calculate the droop coefficient.

- Calculate the droop constants as

$$k_{Droop,i} = \frac{\frac{P_{ref,i}}{E_{dc,i}}}{\left(E_{dc,i} - E_{dc,i}^*\right)} \qquad (4.6)$$

- Perform a load flow analysis for the distributed system as explained in section 4.5.2 in order to verify the results.

However, in a system of such characteristics, the system experiences steady-state power deviations respect to the lossless system references due to the existence of transmission losses which must be accommodated by the converters in the new equilibrium point of the system at the cost of this deviation.

In order to decrease the steady state error of power in all converter, it is performed a correction of the offset according to figure 4.5.
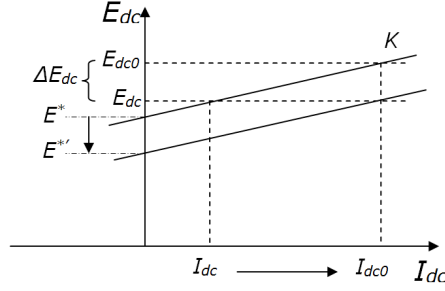
Figure 4.5: Correction of the droop offset.

The steady state error can be partially removed by means of decreasing the difference between the measured and reference current, i.e. doing $I - I^* = 0$, which can be achieved by adapting the droop characteristic in the new operating point. Due to the impossibility of removing all steady state error respect the measured powers and the reference powers for a lossless system, the modification of the offset is inversely proportional to the droop constant as indicated in equation 4.7. If the correction is only made in one terminal, this achieves to follow the scheduled power reference at the cost of the rest of terminals compensate losses while increasing deviations. In this way, the compensation of losses is performed by all droop converters while minimizing the overall deviation.

$$E_i^{*'} = E_i^* - \frac{\Delta E_i}{K_i} \tag{4.7}$$

Where ΔE_i is the voltage difference between the initial lossless voltage in a node and the current calculated voltage.

4.4 Secondary Control

As seen, droop control has an intrinsic relation between voltage regulation and current sharing between converters. This proportional characteristic which ensures the power balance between onshore stations without need of communications leads to a steady-state power deviation after a power flow change. In order to remove the steady-state deviation of primary control and achieve the power set-points, the secondary control is conceived. This concept has been in large power systems for decades in order to control the frequency of a larger ac electrical network.

The secondary control is divided in two parts. The first is located at the converter control and is in charge of performing the following of given references while the second is located remotely and carries out the function of calculating the references which are sent via communications to the converter control. This concept is known as a master controller, central reference calculation or reference power dispatch. In order to ensure a correct schedule operation, this controller must recalculate the power references ensuring that $\Sigma P = 0$ after any contingency or load flow condition. Otherwise, references can not be maintained

at the reference value.

The solution of a secondary controller for the purpose of achieving a more reliable and more optimized operation is suggested and developed by some authors [53, 70–72].

Egea et al [70] proposes a hierarchical control structure for M-HVDC systems composed by a primary control, consisting on the droop characteristic, and a secondary control. The control structure is based on a PI controller that follows the power references while removing the steady state error by means of modifying the droop offset. By combining in the same structure the secondary controller and the droop characteristic, the system does not require a critical communication thanks to the intrinsic safe operation of the droop method. The strategy is shown in figure 4.6.
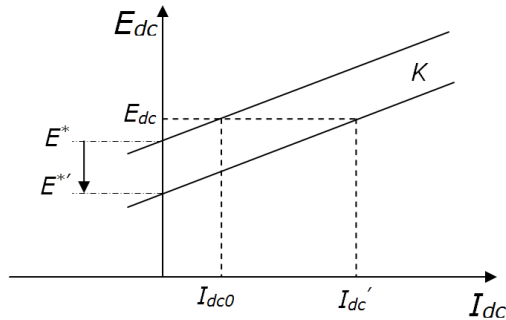
Figure 4.6: Droop characteristic modification by means of secondary control.

4.5 Power Flow in a M-HVDC system

One of the main research areas is the steady state behaviour of these integrated ac/dc grids to achieve the power flow solution of both networks. The solution methods of ac/dc grids are generally divided into sequential and unified methods. The unified method, suggested by *Arrillaga et al* [44], solves the ac/dc equations together [45] whereas in the sequential method equations are solved sequentially [47, 48].*Haileselassie et al* [46] propose a numerical iteration based on Newton-Raphson method for lossless converter using the unified approach. *Beerten et al* [49, 73] propose a sequential ac/dc power flow algorithm based on Newton-Raphson method and a detailed steady-state VSC model including converter losses and defining power set-points. In [66] the same author includes the concept of distributed dc voltage control with a droop characteristic. On his behalf,*Gonzalez-Longatt et al* [74] has developed a sequential power flow algorithm based on Gauss-Seidel method.

In the thesis only the dc network is considered, so ac/dc power flow solution is not included neither explained. So all calculations, analysis and operations are

focused on the dc system.

4.5.1   Load flow analysis in a centralized dc meshed grid

For a system composed by n nodes, the current injected at the ith node is calculated as,

$$I_{dc,i} = \sum_{j=1,j\neq i}^{n} Y_{dc,i,j} \left(U_{dc,i} - U_{dc,j} \right) \tag{4.8}$$

Where $Y_{dc,i,j}$ is the branch admittance equal to $1/R_{dc,i,j}$ and formed according to the following equations,

$$\begin{cases} Y_{i,j} = -\frac{1}{R_{i,j}} & \text{if } i \neq j \\ Y_{i,j} = \sum_{i=1,i\neq j}^{n} \frac{1}{R_{i,j}} & \text{Otherwise} \end{cases} \tag{4.9}$$

In case the dc voltage is considered as the phase-to-phase measure, admittance values must be taken as the total resistive value of the cable, i.e. the equivalent resistance of the two cables which compose the connection. In case not, the admittance is based on the line resistance and the power expressed in next equations is the calculation on a single line.

Combining all currents injected in a n buses dc network into a matrix form,

$$I_{dc} = Y_{dc}U_{dc} \tag{4.10}$$

Where $I_{dc} = [I_{dc1}, I_{dc2}, ...I_{dck}, 0...0]$ with $n - k$ zero elements due to dc buses without power injection and converter outages, $U_{dc} = [U_{dc1}, U_{dc2}, ...U_{dcn}]$ and Y_{dc} the network admittance matrix.

For a bipolar dc grid and assuming lossless converters, active power injected at i-th node can be written as,

$$P_{dc,i} = U_{dc,i}I_{dc,i} \tag{4.11}$$

And taking into account equation 4.8, active power at i-th node becomes

$$P_{dc,i} = E_{dc,i} \sum_{j=1j\neq i}^{n} \left(Y_{dci,j}(U_i - U_j) \right) \tag{4.12}$$

Since the non-linear nature in terms of the voltage at a node, the system must be solved by a numerical method which provides a solution within a given tolerance. The solution can be achieved by different methods as Newton-Raphson or Gauss-Seidel Method.

The following steps describe the used procedure performed with Gauss Seidel for a centralized control, i.e. with a slack bus:

- Formulate a nxn admittance matrix, Y_{dc}.

- Assign initial voltage to n unknown nodes voltage. In the case of slack bus, assign the reference value.

$$U_{dc,i}^{(k+1)} = 1.00pu \quad i = 1..n \tag{4.13}$$

- Find voltages at nodes for a reference power controlled converter.

$$E_{dc,i}^{(k+1)} = \frac{1}{Y_{dc,i,i}} \left[\frac{P_{dc,i}}{U_{dc,i}^k} - \sum_{j=1\,j\neq i}^{n} Y_{dc,i,j} E_{dc,j}^k \right] \quad i = 1..(n-1) \quad (4.14)$$

Where k is the iteration number and n is the slack bus.

- Check if the system converges. That is, the difference between successive voltages is less than a tolerance value.

- Calculate the power at the slack bus

$$P_{dc,slack} = E_{dc,slack} \sum_{j=1}^{n-1} Y_{dc,i,j} \left(E_{dc,slack} - E_{dc,j} \right) \quad (4.15)$$

4.5.2 Load flow analysis in a distributed dc meshed grid

The load flow in a system of such characteristics is solved by expanding equations of currents and not powers as it is commonly done [66]. Since powers at nodes are variable according to a droop characteristic and therefore unknown, terminals can not be considered as power sources. On the other hand, currents at converters are proportional to the droop constant and therefore are easily calculated.

The load flow analysis of a network can be simply performed by an iterative method such that the mismatch between the actual current calculated and a specified previous calculated current is within a required tolerance. Convergence of load flow is tested by equation 4.16.

$$max|\Delta I_i| \leq \varepsilon \quad (4.16)$$

Since the load flow study is a non-linear problem, the Newton-Raphson method is used to solve it and achieve a faster convergence respect to other iterative methods.

According to the Ohm's Law, the current between two nodes is equal to,

$$I_i = \sum_{i=1,i\neq j}^{n} Y_{i,j}(E_i - E_j) \quad (4.17)$$

The currents injected vector for m droop-controlled nodes, k-m power-controlled nodes and n-k outage or non-injection nodes (according to Kirchhoff's Law) is,

$$I_n = \left(K_1(E_1 - E_1^*), K_2(E_2 - E_2^*), ..., K_m(E_m - E_m^*), \frac{P_{m+1}}{E_{m+1}}, ..., \frac{P_k}{E_k}, 0, ..., 0 \right) \quad (4.18)$$

The current mismatch at nodes is calculated as,

$$\Delta I_i = \sum_{i=1,i\neq j}^{n} Y_{i,j}(E_i - E_j) - I_i^{k-1} \quad (4.19)$$

NR method consists on the linearisation of the system by expanding it in Taylor Series as,

$$I(E) = I(E^*) + \frac{dI(E^*)}{dE}(E - E^*) \tag{4.20}$$

By iterations, the system is solved by finding a solution E^* such that $I(E) = 0$ by means of equation 4.21.

$$E^{k+1} = E^k - \left[\frac{dI(E^*)}{dE}\right]^{-1} I\left(E^k\right) \tag{4.21}$$

Where $\frac{dI(E^*)}{dE}$ is defined as the jacobian which is obtained by,

$$J_{dc} = \begin{pmatrix} \frac{\partial I_1}{\partial E_1} & \frac{\partial I_1}{\partial E_2} & \cdot & \cdot & \cdot & \frac{\partial I_1}{\partial E_n} \\ \frac{\partial I_2}{\partial E_1} & \frac{\partial I_2}{\partial E_2} & \cdot & \cdot & \cdot & \frac{\partial I_2}{\partial E_n} \\ \cdot & \cdot & \cdot & & & \cdot \\ \cdot & \cdot & & \cdot & & \cdot \\ \cdot & \cdot & & & \cdot & \cdot \\ \frac{\partial I_n}{\partial E_1} & \frac{\partial I_n}{\partial E_2} & \cdot & \cdot & \cdot & \frac{\partial I_n}{\partial E_n} \end{pmatrix} \tag{4.22}$$

The terms of the jacobian are given by,

$$\frac{\partial I_i}{\partial E_j} = \begin{cases} \frac{\partial I_i}{\partial E_j} = \frac{\partial}{\partial E_j}\left(\sum\limits_{i=1,i\neq j}^{n} Y_{i,j}(E_i - E_j)\right) & \text{if } i \neq j \\[3mm] \frac{\partial I_i}{\partial E_i} = \frac{\partial}{\partial E_i}\left(\sum\limits_{i=1,i\neq j}^{n} Y_{i,j}(E_i - E_j)\right) + \frac{\partial}{\partial E_i}\left(\frac{P_{dc,i}}{E_i}\right) & \text{if } i = j \text{ and P-node} \\[3mm] \frac{\partial I_i}{\partial E_i} = \frac{\partial}{\partial E_i}\left(\sum\limits_{i=1,i\neq j}^{n} Y_{i,j}(E_i - E_j)\right) + K_{droop} & \text{if } i = j \text{ and droop-node} \end{cases} \tag{4.23}$$

And powers at nodes are obtained as,

$$P_{dci} = E_{dci}I_{dci} \tag{4.24}$$

4.6 Effect of dc voltage control on the dynamic and steady state response

In this section it is studied the effect of the strategies in the control of a M-HVDC. By means of simulations, steady-state and dynamic behaviour of converter voltages are studied specially focusing on the operation of such grid after a change in generated power or a disturbance. Firstly, the test system in which simulations are performed is presented. Secondly, the control implemented in the network and the simulated transients are explained. The simulations and results obtained by a power systems simulation tool are presented next and finally the results obtained by each control strategy are discussed.

When the voltage at a node varies suddenly for the previous reasons, it leads to an immediate unbalance in the network which need to be promptly removed by the control strategy. That unbalance is removed by means of accommodating

the power deviation among the converters which perform the control of a M-HVDC. According to the different strategies, that adaptation of power injection in converters leads to some implication concerning the power sharing, feasibility and security of the M-HVDC grid and, thus, of the overall power system operation.

In this section the two most common strategies to be implemented in these networks are simulated: the centralized dc voltage and the distributed droop method.

All simulations have been carried out with PSCAD.

4.6.1 Multi-terminal test system

A network composed by four onshore converters and one wind farm is created to perform the study and the simulations. The grid is shown in figure 4.7 and the main parameters are written in table 4.1.
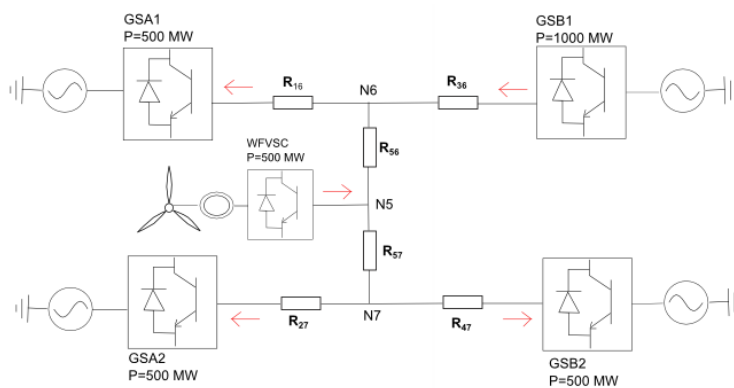
Figure 4.7: Multi-terminal test system.

TABLE 4.1: Test network parameters

Base values and Power ratings [MW]					
S_{base}	2400 MW	$E_{dc,base}$	800 kV		
P_{GSA1}	500	P_{GSB1}	-1000	P_{WF1}	-500
P_{GSA2}	500	P_{GSB2}	500		
Line parameters[Ω^{-1}]					
Y_{16}	2	Y_{27}	1.67	Y_{36}	1
Y_{47}	1	Y_{56}	5	Y_{57}	1.25
L	1e-3mH	C	1e-6μ F		
VSC parameters					
C	232.69 μF	R	0.241 Ω	L	15.3 mH

4.6.2 Case Study

In order to perform the simulations and analyse the results, the design of both control strategies is explained. In both strategies, the steady state is calculated for the purpose of comparing with the results obtained by the simulation tool. The simulated disturbances for the study of particular cases are also presented.

Master-Slack method   The test system is controlled by a centralized strategy by means of controlling the dc voltage in the station A2 at the reference voltage of 800kV with a PI-dc voltage controller (explained in Chapter 3) while the others stations are power-controlled at the references presented in table 4.1. The figure 4.8 sketches the adopted strategy and table 4.2 presents the results of voltages obtained by the steady state analysis explained in 4.5.
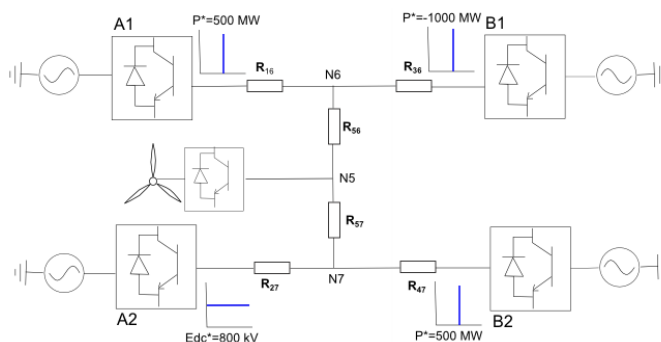
Figure 4.8:   Slack-controlled system.

TABLE 4.2: Steady state analysis of the studied system with master-slack method

Onshore stations	Voltage [kV]	Power [MW]
GSA1	802.342	500.000
GSA2	800.000	492.685
GSB1	805.449	-1000.000
GSB2	799.485	500.000
WF	802.719	-500.000

Droop method   In order to design the control parameters of the distributed strategy, it has been performed a droop design as explained previously in section 4.3. The parameters obtained are written in table 4.3.

In table 4.4 it is shown the deviation correction performed by the offset correction explained in section 4.3. The table shows the results of power and deviations respect to the nominal values for the design without and with correction. It is observed that the power deviation is decreased with the correction. In this case power deviations can not converge to zero because the nominal powers are defined for a lossless system and the droop terminals compensate the transmission

TABLE 4.3: Droop parameters

Onshore stations	K_{Droop}	E_{dc}^*
GSA1	26.0529	0.9915
GSA2	26.1307	0.9886
GSB1	51.9035	1.0115
GSB2	26.1472	0.9879

losses.

The voltages at converters and power injections obtained by the steady state

TABLE 4.4: Droop parameters

Stations	Without correction		With correction	
	P [MW]	ΔP [%]	P [MW]	ΔP [%]
GSA1	498.3	0.35	498.7	0.27
GSA2	498.4	0.32	498.6	0.27
GSB1	-1002.7	0.27	-1003.5	0.35
GSB2	498.5	0.3	498.7	0.27

analysis developed in section 4.5.2 are detailed in table 4.5. It is observed that the obtained power injections are rather approximated to the reference values and the deviation is due to system losses which are adapted by all droop-controlled converters as explained in section 4.3.

TABLE 4.5: Steady state analysis of the studied system with droop method

Onshore stations	Voltage [kV]	Power [MW]
GSA1	799.6168	498.65
GSA2	797.2371	498.64
GSB1	802.7405	-1003.46
GSB2	796.7359	498.66
WF	799.9898	500.000

4.6.2.1 Transient cases in study

It is analysed the response of the system controlled by both strategies in the three cases detailed in table 4.6 and sketched in figure 4.9.

TABLE 4.6: Cases of the simulated transients

Cases	Description
Case 1	Input of a slope in the WF injected power from the initial 500 MW at 3s to 620 MW at 3.8 s. The wind power plant is disconnected at 4s.
Case 2	Outage of converter B2 at 3s.
Case 3	Outage of the line between the WF node and node 7 at 3s.
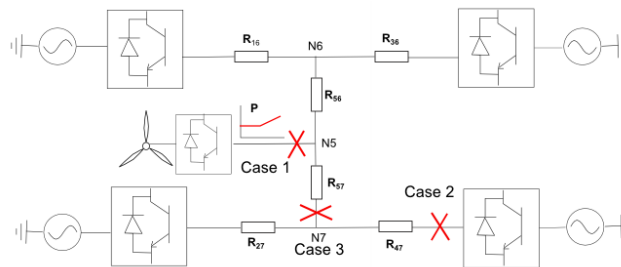
Figure 4.9: Cases of the simulated transients.

4.6.3 Simulations and results

Simulations based on the particular cases previously explained are presented. Results are divided for each case in which the two strategies are compared.

4.6.3.1 Case 1

In case 1 transients are caused by the wind farm. Initially the system remain at the normal operation. At second 3, a wind power slope is produced which leads to an increase in the generated power. And, finally, the power plant is disconnected at second 4.

The results obtained in the system controlled with the master-slack strategy are presented in table 4.7 and the simulations of power and voltage at converters are shown in 4.10.

TABLE 4.7: Voltages and powers in Case 1 with centralized control.

Voltage [kV]	2s	4s	5s
GSA1	802.240	802.785	800.621
GSA2	800.000	799.9980	800.000
GSB1	805.348	805.889	803.735
GSB2	799.366	799.574	798.744
WF	802.616	803.162	800.996
Power [MW]	2s	4s	5s
GSA1	499.969	500.624	499.486
GSA2	492.908	662.079	-3.132
GSB1	-1000.138	-999.395	-1000.733
GSB2	499.990	500.239	500.032
WF	-500.000	-672.031	0.000
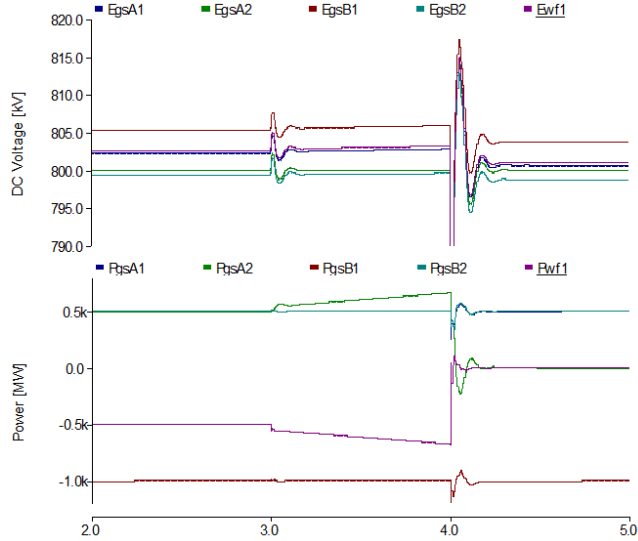
Figure 4.10: Voltages and powers at converters in Slack-controlled system in Case 1.

As seen in results and simulations, the dc voltage at the slack converter is well controlled at the reference value at steady-state operation. The injected power at power-controlled converters is also well followed at the respective reference values including after the disturbances. According to the dynamic behaviour, it is produced a transient in all dc voltages at the disturbance due to the power imbalance generated. At the power slope, dc voltage is lightly increasing until the slope is finished at 3.8 s. At the disconnection of the wind farm, an important transient in dc voltage is produced with an over-voltage peak of 817 kV and an under-voltage of 786 kV. The higher the power imbalance is, the higher the produced transient in voltage is. In reference to the power sharing among converters, it is clearly seen that power-controlled converters follow the references after transients and the higher power transient is produced at the plant

disconnection. According to the slack, it is seen that all the increasing power produced by the plant is allocated through it and at the disconnection all the power step is also immediately accommodated by it.

On the other hand, the results obtained in the system controlled by the droop strategy are presented in table 4.8 and the simulations of power and voltage at converters are shown in 4.11.

TABLE 4.8: Voltages and powers in Case 1 with droop control.

Voltage [kV]	2s	4s	5
GSA1	799.5471	800.1316	797.1624
GSA2	797.2852	797.7834	795.2559
GSB1	802.6687	803.1788	800.5907
GSB2	796.6669	797.1422	794.7315
WF	799.9183	800.5659	797.2735
Power [MW]	2s	4s	5s
GSA1	497.4706	521.467	396.983
GSA2	501.442	531.955	373.757
GSB1	-1003.104	-962.506	-1173.022
GSB2	496.836	521.147	395.854
WF	-499.999	-619.569	0.000
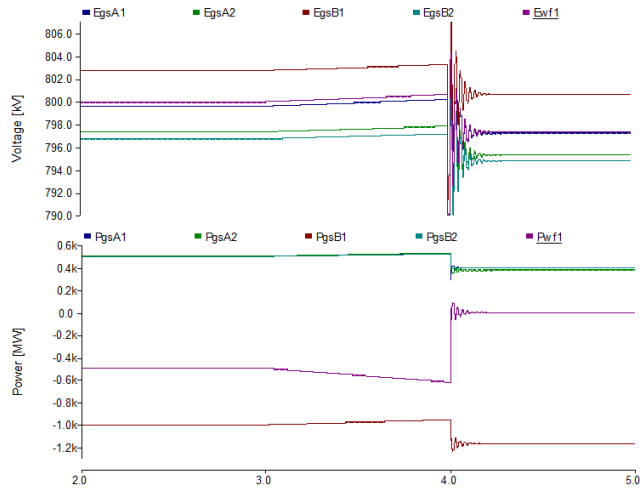
Figure 4.11: Voltages and powers at converters in the droop-controlled system in Case 1.

The simulations obtained in the system controlled by the droop method shows the collaborative scheme of all droop-controlled converters in the function of balancing power in order to obtain a new steady state operation. It is seen at the wind generation increase how all the converters share among them the power surplus from the offshore station. After the wind farm disconnection, the system recovers immediately a new steady state operation. In this case, the current

injection at each converter is logically adapted to a new value different to the nominal because of the current power flows and, consequently, it is generated a steady state error between current voltages and the values at normal operation.

4.6.3.2 Case 2

In case 2 the transients are caused by the outage of converter B2 at second 3. The results obtained in the system controlled with the master-slack strategy are presented in table 4.9 and the simulations of power and voltage at converters are shown in figure 4.12.

TABLE 4.9: Voltages and powers in Case 2 with centralized control.

Voltage [kV]	2s	4s
GSA1	802.241	802.869
GSA2	800.000	800.001
GSB1	805.348	805.980
GSB2	799.366	801.244
WF	802.616	803.244
Power [MW]	2s	4s
GSA1	499.976	500.197
GSA2	492.859	992.836
GSB1	-1000.101	-1000.686
GSB2	499.996	0.000
WF	-500.000	-500.000
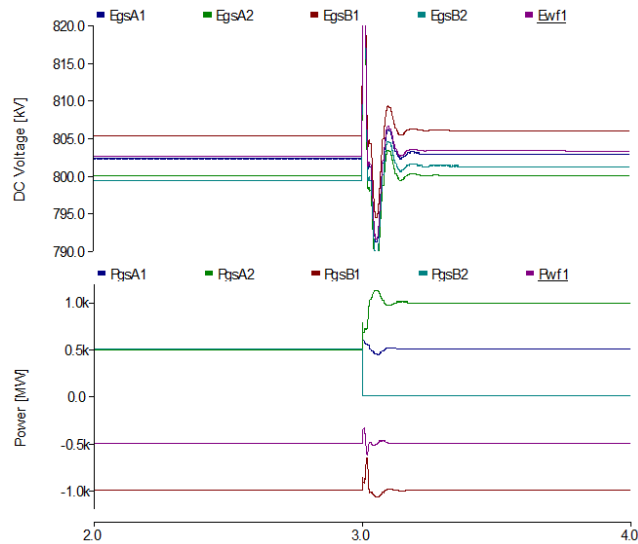
Figure 4.12: Voltages and powers at converters in Slack-controlled system in Case 2.

Simulations and results of this case show a correct following of voltage at the ref-

erence by the slack converter and a correct following of powers at the references by power-controlled converters at the steady state operation. Regarding the dc voltage, the transient caused by the converter outage produces an over-voltage of 826 kV and an under-voltage of 787 kV. As in the previous case, this transient is produced by the power unbalance after the contingency which consists on the loss of a P-controlled converter.

According to the powers at dynamic state, it is observed a transient after the disturbance which is removed rapidly on the P-controlled converters allowing the following of references by them. On its behalf, the slack converter has also a transient and after the outage accommodates all the loss of generation by injecting it on the network while removes the power unbalance leading to the fast recover of the system. In this case, the system controlled by the centralized method achieves the stabilization and performance after the loss of such converter.

On the other hand, the results obtained in the system controlled with the droop control strategy are presented in table 4.10 and the simulations of powers and voltages at converters are shown in figure 4.13.

TABLE 4.10: Voltages and powers in Case 2 with droop control.

Voltage [kV]	2	4
GSA1	799.5471	802.1399
GSA2	797.2852	800.5033
GSB1	802.6687	804.9280
GSB2	796.6669	801.3844
WF	799.9183	802.7939
Power [MW]	2	4
GSA1	497.471	607.399
GSA2	501.442	705.251
GSB1	-1003.104	-817.341
GSB2	496.836	0.000
WF	-499.999	-499.999
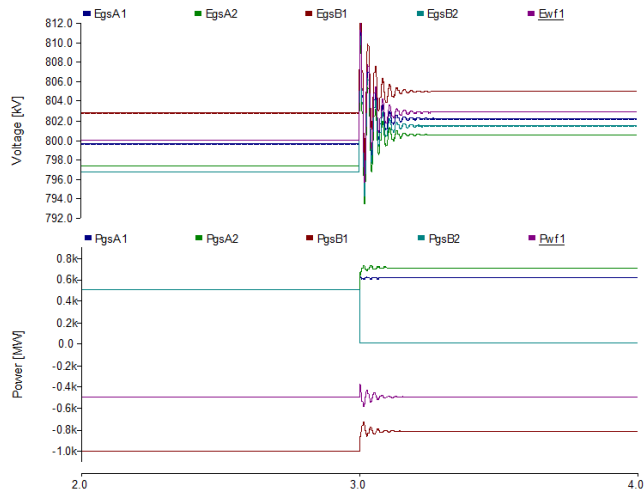
Figure 4.13: Voltages and powers at converters in the droop-controlled system in Case 2.

The simulations performed in the distributive system show the accomplishment of the N-1 security criteria with the loss of a converter. After the outage of B2, a converter involved in the dc voltage regulation, the system immediately reaches a new equilibrium point defined by the droop characteristics of the converters at operation. All droop-controlled converter performs the function of balancing the system in order to achieve a stable operation by means of adapting the current injected while deviating the voltages with reference to the respective nominal values. According to the transient caused by the contingency, it is produced an over-voltage of 812kV and 792kV which are less severe than the transients caused in the slack-controlled system.

4.6.3.3   Case 3

Finally, the Case 3 studies the outage of the line which connect the wind farm with the node 7 at second 3.

The results obtained in the system controlled with the master-slack strategy are presented in table 4.11 and the simulations of power and voltage at converters are shown in figure 4.14.

TABLE 4.11: Voltages and powers in Case 3 with centralized control.

Voltage [kV]	2s	4s
GSA1	802.240	—-
GSA2	800.000	799.9993
GSB1	805.348	—-
GSB2	799.366	798.1112
WF	802.616	—-
Power [MW]	2s	4s
GSA1	499.969	—-
GSA2	492.908	-502.884
GSB1	-1000.138	—-
GSB2	499.990	502.576
WF	-500.000	—-
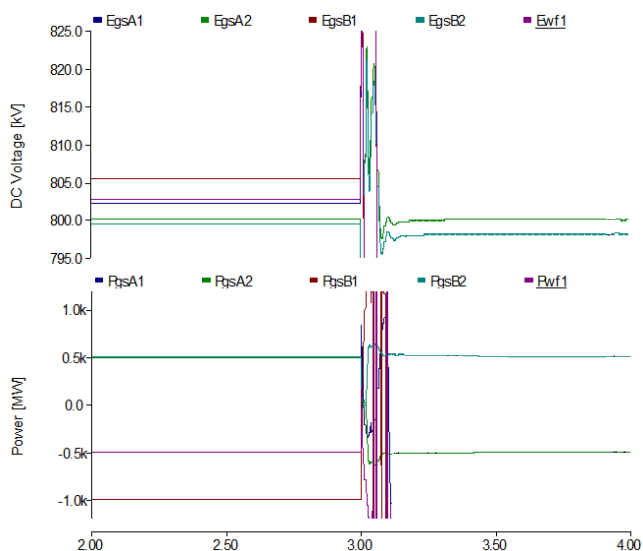
Figure 4.14: Voltages and powers at converters in Slack-controlled system in Case 3.

From the simulations it is clearly observed the instability produced after the outage of a line in the part of the network without voltage-controllers. Converters A1, B1 and the WF are completely unstable and in a real case it should lead to a disconnection. The overall system controlled by the centralized method can not operate after the outage of an element. Transients of these converters are not shown because of usefulness in the study. According to converters A2 and B2, it is seen the well performing of both controller in which the slack follows the voltage reference and B2 follows approximately the power reference. All the power injected to the power-controlled converter is supplied by the slack converter.

The results obtained in the system controlled with the droop method are pre-

sented in table 4.12 and the simulations of powers and voltages at converters are shown in 4.15.

TABLE 4.12: Voltages and powers in Case 3 with droop control.

| Voltage [kV]	2s	4s
GSA1	799.5471	808.2883
GSA2	797.2852	788.3785
GSB1	802.6687	810.2855
GSB2	796.6669	788.1723
WF	799.9183	809.618
Power [MW]	2s	4s
GSA1	497.471	870.868
GSA2	501.442	-54.187
GSB1	-1003.104	-372.616
GSB2	496.836	54.181
WF	-499.999	-499.999
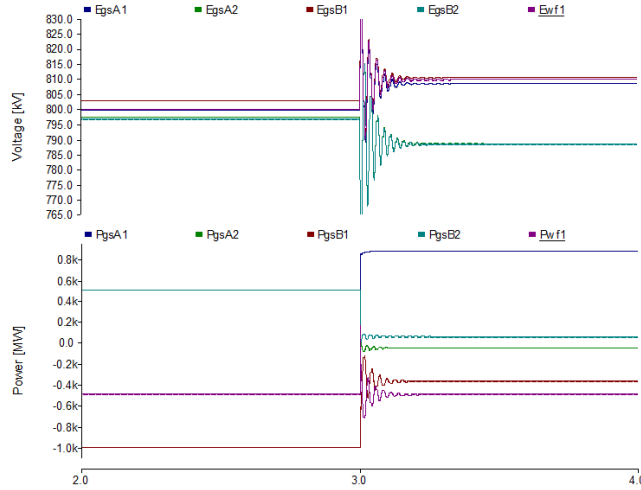
Figure 4.15: Voltages and powers at converters in the droop-controlled system in Case 3.

Simulations in the droop-controlled case show the feasible operation and the inherent secure characteristic of the droop scheme. Difference to the case controlled with slack, the system is capable of maintaining a stable operation in the different subsystems divided after the outage of a line. After the contingency, the two sub-areas reach a new operating point determined in each of them by the droop characteristics of the converters connected to them. This is clearly observed in the difference of voltage levels measured after the fault which each of them correspond to one of the subsystems. According to the area without generation, the two converters share the total amount of power being the converter A2 the station which injects the power to dc grid while the converter B2

55

is in charge of transferring it to the ac system. This load flow is defined by the droop offsets which determine the power flow direction. However, there is a considerable steady state error with reference to the nominal operation unlike the subsystem with slack control.

4.6.4 Discussion

From the simulations results some conclusions are drawn related to the effect of different dc voltage control strategy on the dynamic and steady state behaviour of voltages at converters and, consequently, about the responses of power flows within the network.

One the one hand, it has been analytically observed the previously and theoretically exposed. The voltage transient is straightforward related to the power unbalance. In fact, the higher it is, the higher transients are. According to the master-slack strategy, it is seen the correct following of voltage and power references in steady state operation by the grid side stations. After a perturbation, the slack converter is in charge of adapting all the power unbalance while power-controlled converters remain at the reference power. The central controller is the main responsible of the system stability. In accordance with this, all power steps generated by sudden disturbances are accommodated instantaneously by the slack which may cause instabilities in the ac system and requires to be connected to a strong ac power system. In case the network or a part of it losses the slack, i.e. the voltage regulation, the system is directly collapsed. For this reason, the system composed by one slack can not assure the N-1 security criteria.

On the other hand, when converters operate with a dc droop characteristic, it is observed a collaborative scheme for the dc voltage control among them by sharing the task of accommodating the power unbalance. The new steady state operation is defined by the v-i characteristics of converters which compose it and is achieved by means of generating a steady state deviation in reference to the nominal values. This method has a better performance on voltage regulation and it demonstrates the capability of N-1 security. Moreover, the collaborative scheme has a straightforward implication on the power systems connected to the meshed dc network. All transients produced in this grid are balanced by all droop-controlled converter which leads to less severe transients than the caused by the slack converter. However, the proportional characteristic has an inherent behaviour of considering equally the normal and the disturbed operation. The larger bus voltage differences lead to larger share of the power flow errors. For this reason, it is not possible to achieve a system optimization.

To sum up, it has been confirmed by means of simulations that a meshed dc system needs at least one converter controlling the dc voltage for a reliable operation. In the case of centralized control, the stability of the overall system is responsibility of the slack which is in charge of balancing all the contingencies. This may lead to high transients and a non-desirable in-operability in the ac node in which it is connected. For this reason distributed control is seen as a more feasible solution for the control of MTDC systems because of it is capable of assuring the provision of N-1 security and its collaborative strategy among

converters in balancing the grid. Notwithstanding, optimization is not possible because of its proportional and equally dealing with normal and disturbed operation leading to important deviations respect to the scheduled flow. This can be solved by a secondary controller which allows the following of a references values only determined by the line resistances. Thus, any desired load flow scenario is not possible and it is not capable of optimizing the overall system according to power references calculated by itself.

Chapter 5

Tertiary Control of a Meshed-HVDC Grid

In this chapter, the tertiary control of a M-HVDC grid is proposed. First of all, the traditional concept of the tertiary control is introduced. The research work performed up to date dealing with the optimization topic of such network is detailed. Secondarily, the algorithm and methodology used in order to solve the optimization problem of the proposed control is explained. Finally, the performance, procedure and capabilities of such control are detailed.

5.1   Introduction

The tertiary control of a M-HVDC is the upper level of the hierarchical control of a meshed dc network. Compared with the classical ac grids control, this level performs the function of the tertiary control which operates at the largest time margin and seeks an optimized power share in the area of a larger power system. In a dc network, the tertiary control should be capable of calculating control variables such as power or voltage references for a power system optimal operation according to market, losses or security criterion.

Traditionally, the tertiary control has to:

- Cope with a major or systematic imbalance in the control area.

- Remove the steady-state error of frequency when secondary control is unable to perform it.

- Manage congestions in the transmission network.

- Trade of power flows with balancing purposes.

Up to date, the research has focused on the secondary and specifically on the primary control strategies of a MTDC system. The optimal operation of a grid of such characteristics has not arise interest yet. There are deficiencies on the knowledge yet and it is necessary to further research on the combined operation of the dc and ac systems and the frequency balance by means of such network.

However, some authors have researched the optimization of such grid.

Aragüès et al. [75] propose an optimum voltage algorithm for minimizing losses. The OPF algorithm solved by Interior Point Method obtains the optimum voltages of grid side converters in a system composed by generation plants and inverter stations. The system is controlled by a distributed slack strategy in which converters are controlled by the optimum values sent via communications. In case of a communication loss, the converter control is reconfigured and the voltage droop control loop is then activated.

Teixeira-Pinto et al. [76,77] propose an OPF solved with Genetic Algorithms for minimizing losses in a meshed system controlled by a primary control strategy based on distributed slack nodes, which requires communications in order to calculate the voltage references of each converter while maintaining N-1 security. By this, the strategy controls the direct voltage at each converter to the value defined by the OPF allowing any possible load flow scenario. However, the operation behaviour after the loss of communication and contingencies is not defined due to the voltage-based control of each converter.

The latter references have defined systems composed by generation plants and inverter onshore stations which allows to define the total injected power among converters. However, it is not considered the possibility of bidirectional terminals and, hence, neither it is defined the power trading of such network nor any load flow is possible. Furthermore, the optimization into the upper hierarchical control structure has not been studied nor defined.

5.2 Optimal Power Flow

The Optimal Power Flow (OPF) is an intelligent load flow which automatically adjust the power control while simultaneously solving the power flow and optimizing the operating conditions within specific constraints. Basically, the main objective of an OPF is to determine the optimal way to operate a power system in which optimal is referred to the solution which achieves the desired condition to be minimized.

Generally, the OPF problem can be mathematically formulated as a non-linearly constrained optimization problem as discussed,

$$min f = F(u, x) \tag{5.1}$$

Subject to

$$h(u, x) = 0 \ g(u, x) \geq 0 \tag{5.2}$$

Where u is the set of controllable quantities in the system and x is the set of dependent variables. Equality constraints , $h(u, x)$, are the balanced power flow equations and inequality constraints, $g(u, x)$, represent the operating limits of the system.

The particular content of the function to be minimized determines the objective of OPF. Several minimization problems are commonly implemented such as the

minimum generation cost, which determine the most economically efficient dispatch while keeping security criterion, or minimum losses, in which controls are modified in order to decrease losses in transmission system.

The studies about OPF methods can be traced back to the 1960s when Carpentier and Siroux [78] discussed the problem firstly, and then H.W. Domme and W.F. Tinnety presented a simplified derivative algorithm which is the first practicable algorithm [79].

Since then, a wide variety of classical optimization approaches have been applied such as Non-Linear Programming, Quadratic Programming, Linear Programming, Newton-based techniques, Interior Point Methods or Parametric Models. All these aforementioned methods, are based on first and second derivative information so they are possible to fall into a local optima. Many of these conventional methods are suitable to have an insecure convergence due to the non-linear nature of the OPF problem where exists more than one local optima. Although important improvements have been performed in classical methods, they maintain some disadvantages such as they are computationally difficult in larger systems, have a poor convergence, are weak in handling some qualitative constraints and in most cases it is necessary to simplify the mathematical formulation to get the solutions. Therefore, different non-classical optimization methods emerged to overcome these drawbacks and handle possible difficulties. The main modern optimization techniques are genetic algorithm (GA), evolutionary programming (EP), artificial neural network (ANN), simulated annealing (SA), ant colony optimization (ACO), and particle swarm optimization. In this context, heuristic methods appear as a possible solution to solve complex and multi-objective optimization problems without a computational effort but at expense of a lack of mathematical meaning in solving the problem.

5.3   Particle Swarm Optimization

The Particle Swarm Optimization (PSO) is one of the modern heuristic methods for solving the optimization problem. The increasing development in computers and software has played a key role in prosperity and use of this optimization method. Widely used in many applications and electrical engineering research, the PSO can be in some cases a good choice for solving the Optimal Power Flow.

The original PSO suggested by Kennedy and Eberhart is based on the analogy of social behaviour of swarm of bird and school of fish [80]. PSO shares many similarities with evolutionary computation techniques such as Genetic Algorithms (GA). However, while GA generates random populations and searches for optima by upgrading next generations, PSO use the same population which moves around the problem search space according to social and cognitive behaviours. The PSO optimizes a problem by iteratively trying to improve a candidate solution with regard to a given measure of quality.

5.3.1 PSO algorithm

PSO provides a swarm-based search procedure in which particles change their positions with iterations. In a PSO algorithm, particles fly around in a multi-dimensional search space until a satisfactory solution is discovered or computational limitations are exceeded. During flight, each particle updates its position according to its own experience and the experience of neighbour particles, making use of the best position encountered by itself and its neighbours. In a social context, this means that each particle has a cognitive-based and a social-based component.

The following is the conventional terminology of variables in PSO: x and v denote a particle position and its corresponding velocity in a search space, respectively. Therefore, the ith particle is represented as $x_i = [x_{i1}, x_{i2}, ...x_{id}]$ where d is the particle dimension or coordinates number.
The best position of the ith particle is represented as, $pbest_i = [pbest_{i1}, pbest_{i2}, ..., pbest_{id}]$.

The best particle position among all the particles in the group is represented by $gbest_d$.

The velocity for the ith particle is $v_i = [v_{i1}, v_{i2}, ...v_{id}]$ and the modified velocity and position of each particle after each iteration can be calculated as,

$$v_{id}^{k+1} = wv_{id}^k + c1 random(pbest_{id}^k - x_{id}^k) + c2 random(gbest_d^k - x_{id}^k) \qquad (5.3)$$

$$x_{id}^{k+1} = x_{id}^k + v_{id}^{k+1} \quad \text{for i=1,2,...,n and d=1,2,...,m} \qquad (5.4)$$

Where:
n	number of particles
m	dimension of a particle
k	pointer of iterations
w	inertia weight factor
c1,c2	acceleration factors

The search mechanism of the PSO is performed by modifying velocity and position of each particle according to equations 5.4 and 5.3 as it is illustrated in figure 5.1.
 The constants $c1$ and $c2$ represent the weighting of the acceleration terms which quantifies the influence of each particle towards *pbest* and *gbest* positions and they influence directly on the search space movement according to the cognitive-based and social-based behaviour. On the one hand, $c1$, also known as 'self-confidence', has a contribution towards the self-exploration (or experience) of a particle. On the other hand, $c2$ or 'swarm confidence' has a contribution towards motion of the particles in a global direction. These coefficients are in the interval [0,4] and their values are selected depending on a criterion such as imposing one social behaviour or prioritizing the local search or the acceleration.

The inertia weight factor is used to control the impact of the previous velocity on the current velocity. Hence, it influences the trade-off between global and
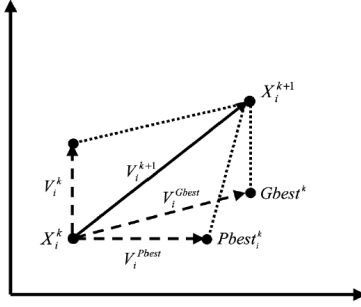
Figure 5.1: PSO search mechanism.

local exploration abilities. For initial stages of the search, large inertia weight to enhance the global exploration is recommended while it is reduced at the last stages for a better local exploration. The inertia weight factor is calculated as,

$$w = \frac{(W_{max} - W_{min})(iter_{max} - iter)}{iter} + W_{min} \qquad (5.5)$$

Where W_{max} and W_{min} are set to 0.9 and 0.4 respectively.

For the purpose of handling the problem of a premature convergence in PSO, the concept of craziness is used. The main idea is to randomize the velocity of some of the particles referred as 'crazy particles'. According to this, a number of particles determined by a certain probability moves around the space without any influence of social behaviour. The probability of craziness, ρ_{cr}, is defined as a function of inertia weight,

$$\rho_{cr} = W_{min} - e^{-\frac{w_k}{W_{max}}} \qquad (5.6)$$

Then, velocities of particles are randomized according to the following conditions,

$$v_{id}^{k+1} = \begin{cases} rand(0, V_{max}) & \text{if} \rho_{cr} > random(0,1) \\ v_{id}^{k+1} & \text{Otherwise} \end{cases} \qquad (5.7)$$

5.3.2 Implementation of PSO for OPF Problem

Most of power system optimization problems including optimal power flow have complex and non-linear characteristics with restrictive constraints and the addition of more objective functions. By the complexity and the need of simplification of these OPF problems, many modern methods have been developed between which PSO is placed. Abido introduced PSO to solve the OPF problem [81] and the method has been widely applied in this application since then.

The formulation of OPF PSO-based is done by separating the problem variables to state variables,x, and control variables, u, as it was described in equations 5.1 and 5.2.

The equality constraints are the non-linear power flow equations while inequality constraints are the functional operating constraints such as transmission line limits, bus voltages, power capabilities, etc.

Each particle in PSO is a vector containing the control variables, u, which suggests a possible solution for the OPF problem. Then the position of the ith particle represents the total number of control variables which means that particles are moving in a $n-$control variables dimensional space. Therefore, each particle attempts to minimize the following OPF objective function,

$$f = F(x_d) + \lambda \left[\sum_{i=1}^{restr.} \mu_i(x_d, u) \right] \tag{5.8}$$

$$\mu_i = \begin{cases} 1 & h_i(x, u) > 0 \\ 0 & h_i(x, u) \leq 0 \end{cases} \tag{5.9}$$

Here the objective function becomes an unconstrained objective function by using the classical penalty functions principle. All inequality constraints are replaced by their respective penalty terms while equality constraints, the load flow balance, is solved for each particle by an iterative power flow algorithm.

5.3.2.1 PSO-based OPF algorithm

The steps involved in the implementation of PSO for the OPF problem are:

Step 1 Definition of parameters of system such as particle dimension and boundaries for each variable.

Step 2 Generation of a random initial population. The initial particles have to be feasible solutions, therefore, apply restrictions to particle coordinates.

Step 3 To each particle of the population, application of the a power flow algorithm and evaluation of the objective function.

Step 4 Set the initial evaluation value for each particle and set the particle to *pbest*. Find the best value among the population and set the particle to *gbest*.

Step 5 Initialization of iterations from 1 maximum number of iterations.

Step 6 Generation of two random numbers and update the inertia weight given in 5.5.

Step 7 Modification of the velocity according to eq.5.3 and set its value to the proper limits $\pm V_{max}$.

Step 8 Modification of the particle position according the equation 5.4 and set its value within restriction limits.

Step 9 Evaluation of each updated particle by means of OPF problem and obtain the objective function value. If the evaluation is best than the previous, set *pbest* to the new particle. In opposite case, maintain the previous particle as *pbest*.

Step 10 Update *gbest* as the best evaluation particle, *pbest*, among the population in the current iteration.

Step 11 If a stopping criterion is satisfied as completed such as a number of iterations or obtained $|gbest_{k+1} - gbest_k| < \varepsilon$ go to Step 12. Otherwise, go to Step 6.

Step 12 The latest *gbest* is the optimal solution.

5.4 Tertiary Control of a M-HVDC system

The proposed control corresponds to the upper level of the meshed dc voltage control. It operates on the largest time margin and it execute an optimized power share while guaranteeing restrictions related to the operability and reliability of the system.

The operation and control of a meshed dc network must accomplish the following functions:

- Maintaining the power balance between converters.

- Redistributing the power flow between terminals.

- Providing N-1 security.

The tertiary control has to fulfil the functions also performed by the lower control levels while optimizing the power share and operation in a larger area and following a coordinated scheme respect to the local controllers.

For this reason, the proposed control scheme is set out to the following purposes:

- Being connected to the lower levels of control in order to follow a coordinated scheme.

- Setting the power references to the central controller and then to the secondary controllers.

- Defining the power exchange between areas.

- Optimizing the operation according to a criterion.

5.4.1 Problem definition

The optimized operation of such system is performed by an Optimal Power Flow in which load flow, operating conditions and restrictions are defined. In a problem of such characteristics, a given data sent by communications informs about the network state. Then, the OPF is solved according to the control and state variables while minimizing an objective function. After that, the solution contained in the state variables vector is sent via communications to the converters in which the signal is introduced on its control system finally obtaining the desired operation.
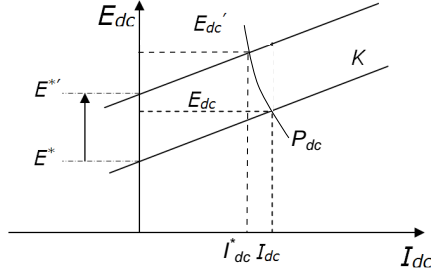
Figure 5.2: Tertiary control strategy in the droop characteristic.

An OPF for the operation of a M-HVDC grid is presented. The objective function of the problem is the loss minimization of the dc network. The algorithm gives the voltage offsets of droop control of the optimal operation as solution. The strategy of loss minimization by means of the offsets is sketched in figure 5.2. Transmission losses are determined by currents or voltage drops in lines. Therefore, the minimization is achieved by modifying them. In a control of such characteristics, it is necessary that control follows a hierarchical connectedness respect to the lower levels; i.e., the power references followed by the tertiary control must also be followed by the secondary control at the same time that the operation is optimized. Since injected powers are not desirable to be modified, losses minimization is achieved by modifying voltages at nodes. The optimal power flow problem for a meshed dc network can be defined as,

$$[MIN]z = \sum_{i=1}^{n} \sum_{j=1}^{n} Y_{dci,j}(E_{dci} - E_{dc,j})^2 \tag{5.10}$$

Subject to the electrical grid restrictions:

$$I = Y_{dc}E \tag{5.11}$$

$$P_i = E_i I_i \tag{5.12}$$

The problem is also subject to the voltages and current limit restrictions

$$E_{min} \leq E_i \leq E_{max} \tag{5.13}$$

$$I_{min-node} \leq I_i \leq I_{max-node} \tag{5.14}$$

$$I_{min-branch} \leq Y_{ij}(E_i - E_j) \leq I_{max-branch} \tag{5.15}$$

The equality constraints are solved by the equation 5.16 which is solved by an iterative power flow method as explained in section 4.5.2.

$$P_{dc,i} = U_{dc,i} \sum_{j=1j \neq i}^{n} (Y_{dci,j}(U_i - U_j)) \tag{5.16}$$

And the solutions obtained are the node voltages needed to calculate the transmission losses in equation 5.10.

Moreover, inequality constraints are fulfilled using penalty factors as in 5.8. A penalty factor is an algorithm for solving constrained problems. A penalty method transforms the original constrained problem into a series of unconstrained problems whose solutions converge to the solution of the constrained problem. This unconstrained formulation is performed by adding a term to the objective function consisted on the parameter and a measure of the violation respect to the constraints. The measure of violation is the quantification of the difference between the measured variable and the constraint and solutions remain interior the boundary of the feasible region as the difference converges to zero. This achieves to favour the solutions which converge to the reference or find interior the bounds while penalizing the solutions which violates the constraints.

Furthermore, it is essential that an input power equal or similar to a reference value is being injected to the onshore stations as sketched in figure 5.2 in order to make reliable the operation and controllability of the system and impose a hierarchical coherence respect to the lower operation levels. In a meshed network controlled with the droop method, power injections can not be controlled because of these are directly determined by the equilibrium point between the onshore rectifiers and inverters which compose the system. Due to the OPF with droop controls can not guarantee the following of the power references, another lagrange multipliers are added in order to penalize deviations from power references.

Depending on the value of λ, the algorithm can achieve a correct following of power references or a loss reduction to the detriment of an error between powers and references. For this reason, a correct dimensioning of the different penalty factors is fundamental in order to obtain an optimum and desirable system operation.

Finally, the objective function is formulated as,

$$[MIN]z = \sum_{i=1}^{n}\sum_{j=1}^{n} Y_{dci,j}(E_{dci} - E_{dc,j})^2 + \lambda_E \sum \lim ts_{i=1} n(E_{dci} \pm E_{bound})^2$$

$$+\lambda_I \sum_{i=1}^{n+1}(I_{dci} \pm I_{bound})^2 + \lambda_P \sum_{i=1}^{GS}(P_{dci} - P_{refi})^2 \quad (5.17)$$

The challenge in solving the OPF for a droop-controlled meshed dc grid comes from the non-convexity caused by the quadratic and non-linear equality constraints in equation 5.16. The objective function , i.e. transmission losses, is a non-linear function of the line flows or voltage drops ($P_{loss} \propto I_{line}^2 \propto \Delta V^2$). Moreover, the solutions to be optimized, i.e. voltage offsets E^*, do not find into the objective function while the variables involved in resistive losses are determined by a load flow analysis of the system which, at the same time, is a non-linear function. Furthermore, the calculated powers included in penalty terms are also determined by the load flow. Therefore, any marginal error in equations or solutions leads to greater deviations due to the droop characteristic. For this reason, the optimal power flow problem is solved by means of an heuristic method as explained in section 5.3.2 with a correct solution and estimation but at the expense of a random solution and the possibility of falling

into a local minimum.

5.4.1.1 Power Distribution Scheme

As explained previously in section 5.4.1, the algorithm requires the power references in order to define a power sharing between converters. In normal operation, the references can be set to those defined in the normal steady state. The proposed method does not need to maintain the calculated powers at these references because of it minimizes the power deviation of all the terminals, i.e. the algorithm defines the power sharing after a disturbance as the situation in which the power differences respect to the determined references are minimum.

In the case of prioritizing the loss minimization, it can be achieved by decreasing the penalty factor of powers at the same time that the loss reduction in the objective function gets greater importance. As an example of this case, after the disconnection of a converter the terminal in charge of compensating the power balance is the nearest to the disconnected one. This example in a simulated situation can be seen in table 6.5.

In order to define the power distribution among converters in abnormal conditions, a minimization of overall frequency deviations in control areas is performed. The frequency is linked to the power system balance and the system frequency and the flows through lines are the variables to control while the powers through converters are the variables employed on controlling them. Therefore, in the event of a control area connected to the dc grid experiences a frequency deviation, the power distribution among terminals shall be such that the unbalanced ac system restores approximately the frequency to a narrower range with reference to the nominal value at the expense of the rest of converters adapt their respective injected powers.

The minimization of frequency deviations is achieved by adding the term in equation 5.18 in the objective function in equation 5.17.

$$\text{pf} \quad \Delta f = \lambda \sum_{i=1}^{areas} (f_i - f_N) \tag{5.18}$$

The complexity of a frequency system model depends on the objectives which have been defined and the application. In the thesis, the objective is to develop a simple model capable of quantitatively predicting the steady-state frequency deviation after an unbalance without paying attention on the frequency response. The frequency variation in a power system after a disturbance of the balance between the injected power to the system and the consumed power is defined by,

$$\Delta f = K_{net} \Delta P \tag{5.19}$$

Where K_{net} is a estimated gain of the system inertia.

5.4.1.2 OPF Algorithm

The PSO algorithm for solving the OPF problem with an objective function of minimization of transmission losses is shown in figure 5.3.
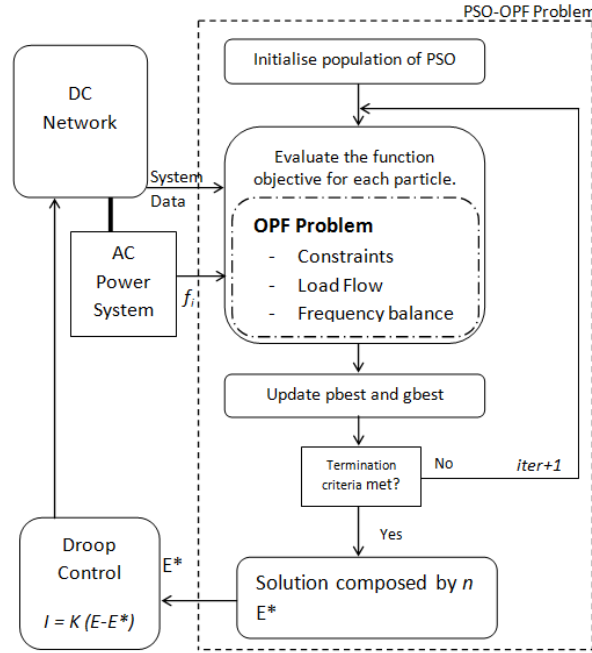
Figure 5.3:   Tertiary control algorithm flowchart.

5.5   Tertiary Control of a Distributed M-HVDC system

A tertiary control for a distributed M-HVDC system is proposed. It is defined by an Optimal Power Flow based on Particle Swarm Optimization. The algorithm requires a data detailed in section 5.5.1 and calculates the optimum droop offsets for the converters which compose the system. The obtained solutions respond to the optimal way to operate the system according to the frequency support of the ac power systems and the minimization of the dc network transmission losses.

From the point of view of the control scheme, i.e. primary, secondary and tertiary control of a meshed dc system, the fact that solutions are the offsets imposes a coordinated scheme respect to the lower levels given that the overall system is controlled in a distributed form. After the calculation of the optimal offsets, in the event of an oscillation or a transient in power flows, the system returns to the equilibrium or produce a new power sharing according to the primary control from the last optimum operation point determined by the optimum offsets. Then, the system returns to be controlled by the primary and secondary control until after a determined period when tertiary control optimizes again the system operation in the new situation.

Furthermore, the fact of imposing the solutions into the primary or droop control allows that the system does not require critical communications for the safe
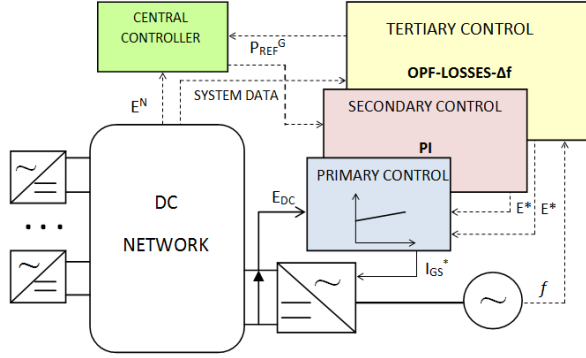
Figure 5.4: Hierarchical control strategy of a M-HVDC.

operation. In case of lack of communications, the droop strategy controls the system around the last point of operation determined by the tertiary which can not optimize again the operation in the new situation. Therefore, the proposed method ensures by itself the provision of N-2 security, i.e. loss of a terminal and communication.

The overall hierarchical control strategy is shown in figure 5.4. The time constant of actuation for primary control loop is in the order of a few ms while for secondary control it is set to some seconds [70]. Traditional tertiary controllers in ac systems react in a time period between 20 minutes and 1 hour which is due to the response times of the reserve services of ac power systems. In the case of the meshed dc grid, there is no specific recommendation although there must be a coordinated time actuation between control levels.

Therefore, the proposed tertiary control accomplish the requirements of a M-HVDC system for the following reasons:

- It defines a coordinated scheme and operation with primary and secondary controllers by means of optimum droop offsets for a determined situation.

- It defines a power exchange between terminals and control areas according to a criterion based on the frequency support of the connected power systems and it sends the power references to the central and secondary controller respectively.

- It optimizes the operation according to the minimization of dc network transmission losses.

- It provides N-2 security, i.e. loss of a station and communications, without reconfiguring the local control scheme.

5.5.1 Communications Flow

The centralized controller receives status information from the network and terminals in order to calculate the new operating point and define the power

exchange between areas. Its outputs are the power references and the droop offsets which are sent to the respective elements.

Table 5.1 explains the required and sent data in the algorithm.

TABLE 5.1: Data required by the centralized control.

	Data required
Dc network	The algorithm needs the current status of the dc network such as the unavailability of a line.
Wind farms	The centralized controller requires to fully aware of the power injected and the disconnection of it.
GS converter	It is required to know the state of outage and unavailability of a terminal.
	Output data
Central controller	The power references are sent to the central controller in order to the secondary controller match those given by the criterion adopted.
Autonomous controller	The solutions are the voltage offsets required in the droop control.

Chapter 6

Simulations results

In this chapter the simulations performed using the software PSCAD are presented and discussed in order to evaluate and validate the proposed control. Some cases are performed for the purpose of studying the behaviour through disturbed situations. Finally, the results are discussed and conclusions are drawn.

6.1 Introduction

In order to examine the behaviour and capability of the tertiary controller and check the reliable and safe network operation, it is defined a system and different cases of study are selected. The main objective is to study the performance of the proposed method in operating some of the common situations which can occur in a power system.

The network defined in section 4.6.1 is simulated in order to study analytically the behaviour of the operation. The system is composed by four onshore stations, one of which is a rectifier, and an offshore wind farm. Figure 6.1 shows the studied network implemented in PSCAD.

The control system is composed by the droop controllers in each of the converter
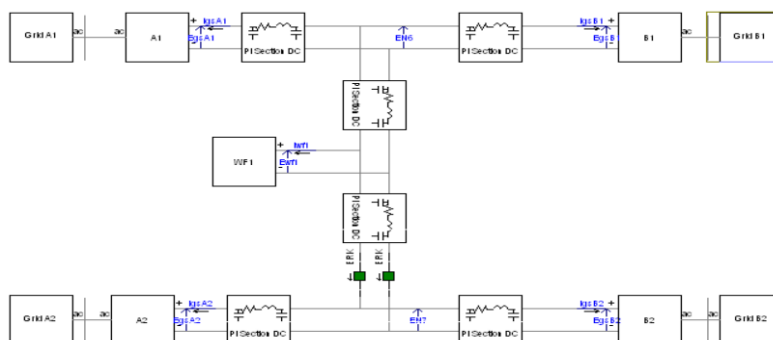
Figure 6.1: M-HVDC network implemented in PSCAD.
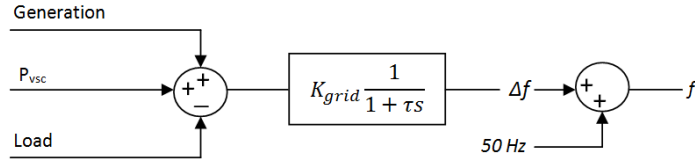
Figure 6.2: Inertial response of a ac power system.

stations and a centralized controller based on the proposed tertiary control in section 5.4 in charge of optimizing the system operation according to the frequency support and minimization of losses. The algorithm requires the network data, i.e. generated powers and outages, and sends the optimum droop offsets to the droop control loop of each converter. The optimization algorithm is built in Matlab and a component is elaborated in order to establish the communication between the latter and PSCAD.

Reference to the ac grid, it is modelled as a controllable voltage source with an external input for the frequency. The latter is calculated according to section 5.4.1.1 as a gain which relates a frequency deviation with a power deviation as it is shown in figure 6.2. Each grid is modelled with a different gain written in table 6.1 in order to observe a clear tendency in the power flow trading according to the frequency support to ac systems of different inertial response. According to the gains, the system connected to the terminal A1 is the one which has the greatest impact on frequency at a power unbalance while the system connected to A2 is the one which has the lowest.

TABLE 6.1: Inertial response gains of the ac systems.

Ac system	$K_{Grid}[MW/Hz]$
A1	$3.125 \cdot 10^{-3}$
A2	$1.042 \cdot 10^{-4}$
B1	$2.083 \cdot 10^{-4}$
B2	$3.125 \cdot 10^{-4}$

Some cases have been considered in order to analyse the control response to different contingencies. Table 6.1 contains a detailed description of all examined cases and transients.

6.2 Previous considerations

In chapter 4, it has been studied the primary droop and secondary control and some conclusions have been inferred. Briefly, when a contingency is caused, the system can not maintain the nominal powers and a steady-state error is generated in order to balance the system. Moreover, normal and disturbed operation are not distinguished. For this reason, a new power sharing must be defined

.

TABLE 6.2: Simulated cases and transients.

Scenario	Description
Case 1	The case is based on the tertiary control start-up at 5s.
Case 2	A comparison between different algorithm sizing according to the frequency support behaviour is performed. An outage at the converter B2 is caused at 5s and the tertiary control is executed at 0 and 10s.
Case 3	It is simulated a wind ramp between 1 and 20s from 200 to 700 MW. The tertiary control is performed at 0, 10 and 20s.
Case 4	It is simulated the outage of the line which connects the wind farm with the node 7 at 5s. The tertiary control is executed at 0 and 10s.
Case 5	The WF is disconnected at 5s and the loss of communications is caused at 15s. The WF is connected at 20s and communications are not recovered. The tertiary control is performed at 0 and 10s.
Case 6	It is caused a contingency in the ac power system connected to the onshore station A1 which consists on the loss of 500 MW of generation at 5s. The optimization is performed at 0 and 10s.

and, in this case, it is determined by the proposed tertiary control of the dc network in order to support the frequencies on the ac systems.

In classic ac systems, after a disturbance, there is a primary, secondary and tertiary regulation in charge of maintaining the equilibrium between generation and load. These controls have the objective of removing the steady-state error of the frequency by means of the control reserves.

In order to make easy the understanding of the tertiary control operation of a dc network, the ac system power-frequency control is not taken into account neither simulated. Moreover, the amount in which the wind farms connected to the dc network could contribute in the frequency support by means of a virtual inertia [82] is nor studied.

Hence, the frequency support to the onshore ac grids is obtained by merely redistributing the power amongst the onshore power systems.

6.3   Case 0: Minimization of losses without operation control

Firstly, the algorithm is executed in order to demonstrate the capability of the OPF solved by PSO in minimizing the objective function. Thus, the objective function is only composed by the transmission losses and the penalization of

powers and frequencies are not considered. The obtained voltages and power are written in table 6.3.

TABLE 6.3: Steady-state voltages and powers in Case 0.

	GSA1	GSA2	GSB1	GSB2	WF
Voltage [pu]	1.0995	1.0995	1.0995	1.0995	1.1000
Power [MW]	229.13	97.50	114.56	58.50	500
Frequency [Hz]	49.16	49.96	50.23	49.86	
Losses	0.2368 MW				

As it is observed in results, the algorithm achieves the minimization of losses. The voltage at the WF is 1.10 pu which is the maximum value permitted and powers at terminals are shared in a form such that the higher powers are injected to the nearer stations. Therefore, it is demonstrated the capability of minimizing the objective function by the PSO method. However, this solution has not sense from the point of view of operation controllability. The nominal references are not followed and the converter defined as a rectifier acts as an inverter, in fact, the only injected power to the dc grid is the generated power from the wind farm. As explained in chapter 5, according to the sizing of penalization factor, the algorithm prioritizes the different functions for which it is defined.

6.4 Case 1: Tertiary Control start-up

The tertiary control start-up procedure is simulated in order to study the dynamic behaviour of the voltages and powers after the change of voltage offsets in the droop controller at 5s. Initially, the system is controlled by the droop characteristic as explained in section 4.3. The system is at the nominal values and no disturbance is caused. The calculated steady-state values of voltages and powers are shown in table 6.4.

TABLE 6.4: Steady-state voltages and powers according to the implemented control in Case 1.

	Droop Control		Tertiary Control	
Station	Power [MW]	Voltage [pu]	Power [MW]	Voltage [pu]
GSA1	498.30	0.9995	498.60	1.0930
GSA2	498.40	0.9966	497.70	1.0903
GSB1	-1002.70	1.0034	-1002.20	1.0966
GSB2	498.50	0.9959	499.40	1.0897
Losses	7.42		6.21	

Figure 6.3 shows the voltages and powers at converters and the transmission losses respectively. It is observed the behaviour in the voltage increases as a first order system with $\tau = 0.5s$ which is stabilized after 3.5s. According to the active powers, there is a inappreciable transient thanks to the smooth increase of voltages. Finally, the transmission loss minimization after the optimization

76
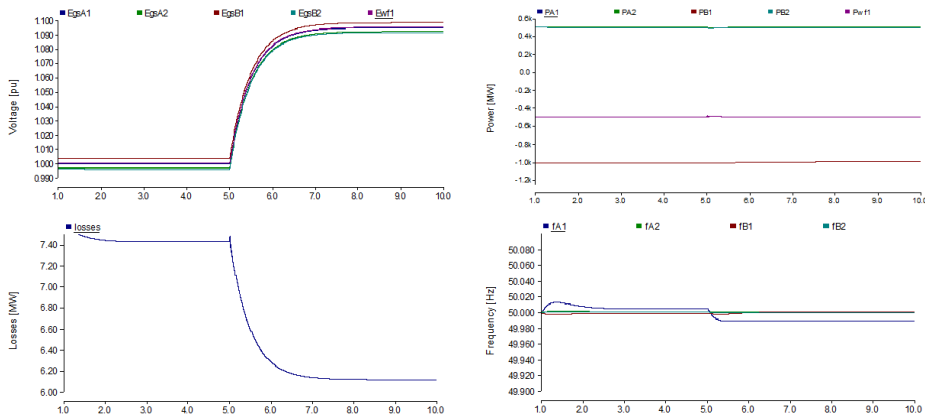
Figure 6.3: Voltages, powers, transmission losses and frequencies responses in the start-up case.

procedure start-up is confirmed.

6.5 Case 2: Comparison between minimization of losses and frequency support

As explained in section 5.4.1.1, the power trade among converters is such that the unbalanced ac systems restore approximately the frequencies into a range nearer the nominal value. In order to observe the performance of such control in the ac and dc grid, a comparison between a strategy supporting grid frequencies and optimizing transmission losses is performed. According to the value of the penalty factor λ, the system achieves to prioritize and optimize the different possible objective functions, in this case the minimizations of losses or the ac system frequency support.

The system is simulated for the outage of the converter B2 at 5s and is initially controlled by the optimization problem at the initial values. After that, the system is already optimized by the tertiary controller at 10s. In table 6.5 the calculated power an frequency values are shown according to the differents lagrange multiplier values.

It is clearly observed that, in the case with a lower penalty factor, transmission losses are lower but power deviations from the respective nominal values are more important while, in the case with higher λ, power deviations are negligible but transmission losses are higher, they are the double concretely. As expected, the penalty factor in powers and frequencies has a straightforward influence on the system optimization. A smaller penalization of powers and frequencies violations leads to prioritize the minimization of losses while in the opposite way a higher frequency support is achieved.

77
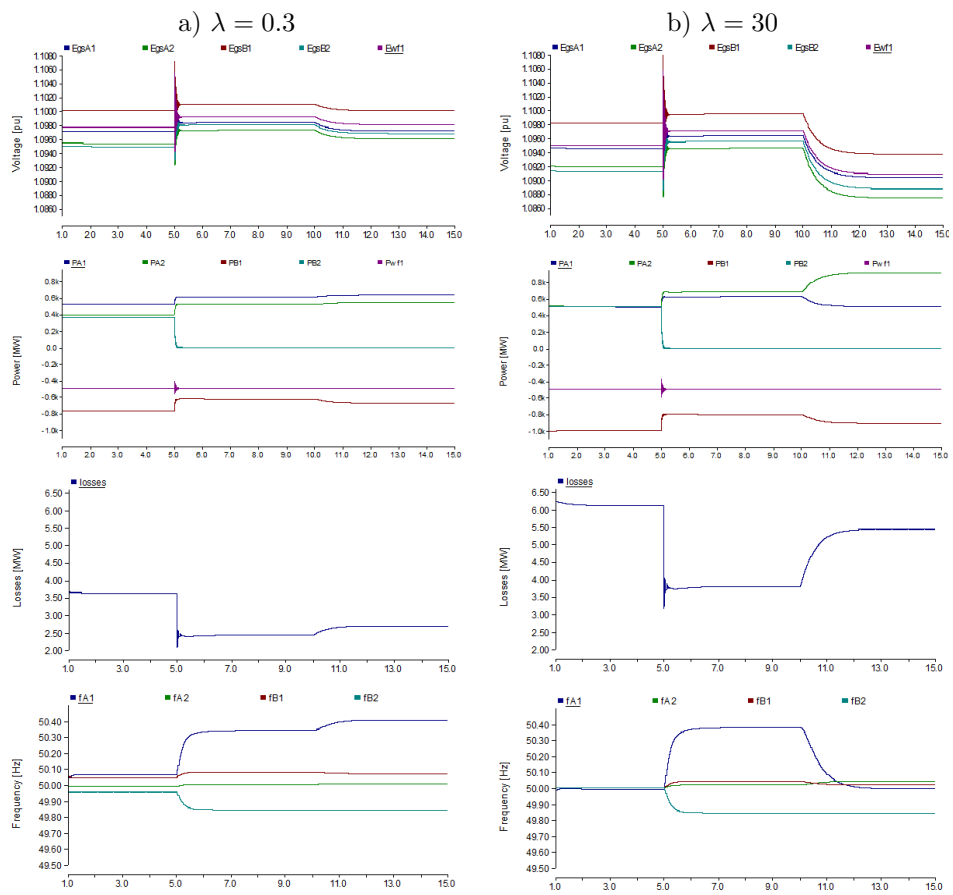
Figure 6.4: Measured voltages, powers, frequencies and losses according the different penalization factor in the algorithm.

TABLE 6.5: Steady state powers according to the penalization factor in Case 2.

	$\lambda = 0.3$		$\lambda = 30$	
	P_1[MW]	P_2[MW]	P_1[MW]	P_2[MW]
GSA1	517.63	628.97	498.50	498.92
GSA2	387.55	536.53	498.20	897.78
GSB1	-769.59	-668.29	-1001.10	-902.30
GSB2	360.6	0.00	498.23	0.00
Losses	3.65	2.72	6.19	5.52

In figure 6.4 are shown the voltages, powers, frequencies and losses of both cases respectively. According to the dc voltages, it is seen that voltages in $\lambda = 0.3$ case are higher than voltages in the $\lambda = 30$ case. In the second case, the higher penalization leads to a convergence to the operating points which satisfy smaller frequency deviations while not optimizing losses.

Reference to the power flows, initially, the injected power by the rectifier is smaller than the nominal reference and the greater amount of injected power through a converter is in terminal A1 which is the nearest to the rectifier and the WF. The latter has sense from the point of view of the minimization of transmission losses. In fact, the best solution with respect to such problem is the null power injection from the rectifier.

It is observed that in the first case the converter in charge of compensating the contingency in their majority are the more distant to the station disconnected, i.e. the converters A1 and B1, in order to minimize the flow to the most distant converter respect to the power injection stations, i.e. the terminal A2. In the second case, after the outage, the terminal connected to the weakest grid, i.e. the converter A1 remains approximately at the reference value while the converter in charge of compensating the powers is the A2 which is the station connected to the strongest ac system.

According to the frequencies, the second case controls the grid in a form such that the most deviated frequency, in this case the related to the weakest ac system connected to the converter A1, is recovered to a narrower range with reference to the nominal frequency. Frequencies in the $\lambda = 0.3$ case are more deviated with reference to 50 Hz at any given moment. Finally, the transmission losses are considerably lower in the $\lambda = 0.3$ case. Hence, it is confirmed the analytically expected that a minor penalization of powers and frequencies contributes to prioritize the minimization of losses at the expense of generating higher deviations from reference powers and frequencies.

6.6 Case 3: Wind ramp

The case is based on a increasing generation ramp on the WF from 200 MW at 1s to 700 MW at 20s while the optimization from the tertiary control is
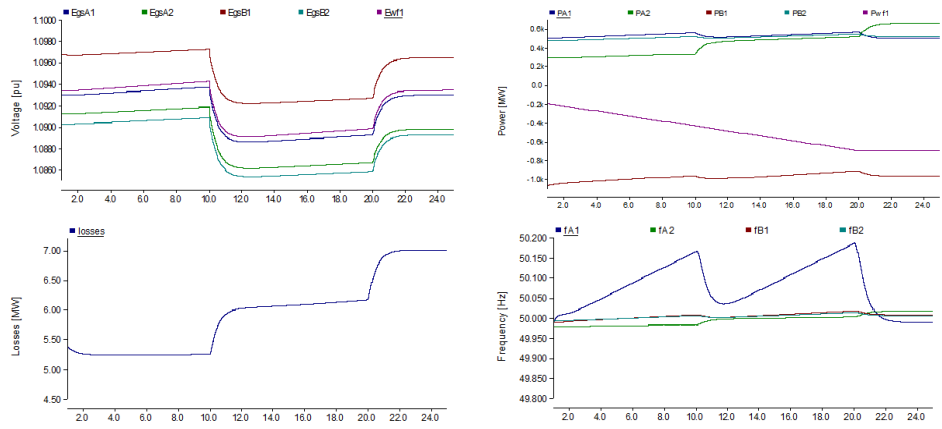
Figure 6.5: Voltages, powers, transmission losses and frequencies responses in the wind ramp case.

performed at 0, 10 and 20s. The calculated powers, frequencies and losses are shown in table 6.6.

As seen in the simulations in figure 6.5, the primary droop controller balances

TABLE 6.6: Steady-state voltages, powers and frequencies in Case 3.

	0s		< 10s		> 10s		< 20s		< 25s	
Station	P [MW]	f [Hz]	P [MW]	f [Hz]	P [MW]	f [Hz]	P [MW]	f [Hz]	P [MW]	f [Hz]
GSA1	498.2	50.00	553.5	50.17	498.4	50.00	559.5	50.19	498.6	50.00
GSA2	278.3	49.98	326.1	49.98	451.9	50.00	506.6	50.00	644.7	50.02
GSB1	-1055.6	49.99	-964.2	50.01	-1012.6	49.99	-914.1	50.02	-964.9	50.01
GSB2	473.7	49.99	516.2	50.01	493.1	50.00	541.9	50.01	514.5	50.01
WF	200		436.8		436.8		700.0		700.0	
Losses	5.29		5.27		6.05		6.15		7.07	

the system while the generated power is increasing in a collaborative scheme around the operating point initially calculated by the tertiary control. The latter determines the new voltages at 10 and 20s which are found interior the boundaries but in that case the new voltages are lower than the voltages in the first period, which is a demonstration of the problem ease to fall into local minimum.

According to the powers, it is also observed the coordinated scheme within converters in accommodating the generation power surplus. The injected power in converters A1 and B2 are approximated to the nominal value while the converter A2 is the terminal which generates the higher steady-state error respect the nominal reference in order to balance the system. Moreover, stations A1 and B2 are connected to the two weakest ac systems while A2 is connected to the strongest grid. Hence, the systems with best inertial response are in charge of supporting the frequencies of the systems with the worst inertial response by means of generating larger deviation with reference to the nominal powers.

In reference to the frequencies, the larger deviation is caused in the system A1, the weakest one, and after 10 and 20s the optimization problem removes par-
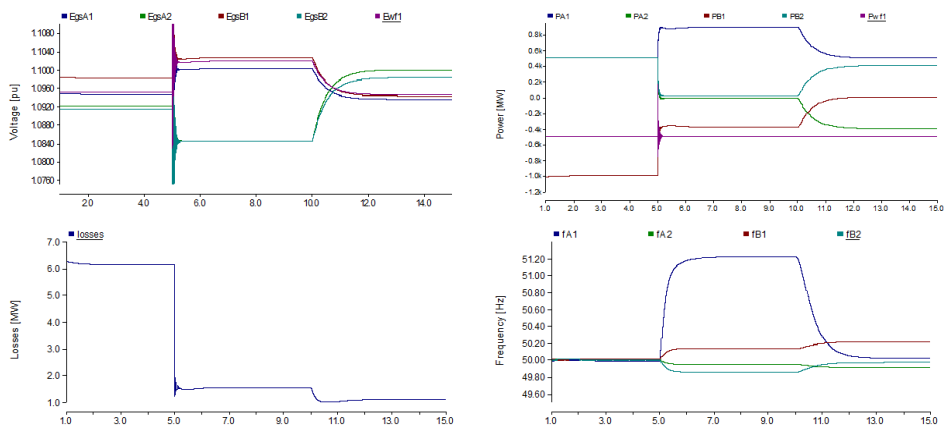
Figure 6.6: Voltages, powers, transmission losses and frequencies responses in the case related to the outage of a line.

tially the error though the continuous wind ramp leads to a continuous increase in the deviation. The frequencies of the rest of systems remains nearer the nominal value. Therefore, and taking into account the powers and frequencies results, the power trading within converters in order to the frequency support of all the systems is observed.

Finally, transmission losses increase each time the tertiary control is performed including after second 20 when voltages are higher than in the period comprised between 10 and 20s which is due to the new load flows situation.

6.7   Case 4: Outage of a line

In the case 4 it is studied the outage of the line which connect the wind farm with the node 7 at second 5. Calculated voltages, powers and frequencies at the different steady-state situations are shown in table 6.7.

TABLE 6.7: Steady-state voltages, powers and frequencies in Case 4.

Station	< 10s			< 15s		
	P [MW]	V [pu]	f [Hz]	P [MW]	V [pu]	f [Hz]
A1	887.6	1.1002	51.22	502.6	1.0941	50.01
A2	-17.6	1.0843	49.95	-401.84	1.1000	49.91
B1	-398.2	1.1026	50.13	-3.1	1.0981	50.21
B2	17.64	1.0843	49.85	400.77	1.0981	49.97
WF	500.0	1.1017		500.0	1.0942	

Figure 6.6 shows the response of dc voltages, powers and frequencies at terminals and transmission losses. Voltages after the outage of the line are divided

81

into two levels inasmuch as the two subsystems appeared after the contingency operate at the new equilibrium points determined by the droop characteristic as happened in section 4.6.3.3. Moreover, some voltages at nodes exceed the imposed voltage boundaries. Due to the deviation in the dc voltages, power injections are also deviated from the nominal values which leads to a deviation in frequencies as well.

After the optimum offsets are sent, the dc voltages are arrived at a point below the maximum limit. The injected powers are also changed according to the voltages and the frequency support criterion. By the latter, the frequencies are recovered from the deviation but the frequency on the power system connected to the converter B1 because the needed power by the power system connected to A1, with the worst inertial response, is injected by the wind farm. According to the transmission losses, they are decreased after the optimization despite having a different load flow.

6.8 Case 5: WF disconnection and loss of communication

In the case 5, it is caused the WF disconnection at 5s and the loss of communication at 15s. At 20s the WF is connected again but communications continue being inoperative. This scenario is simulated in order to study the performance of tertiary and droop control separately and the system operation after the loss of communication. Table 6.8 details the steady-state powers, voltages and frequencies before the transients.

TABLE 6.8: Steady-state voltages, powers and frequencies in Case 5.

	< 10s			< 20s			< 25s		
Station	P [MW]	V [pu]	f [Hz]	P [MW]	V [pu]	f [Hz]	P [MW]	V [pu]	f [Hz]
A1	377.4	1.0928	49.62	496.7	1.0923	49.99	616.1	1.0940	50.36
A2	398.8	1.0904	49.99	134.2	1.0911	49.96	234.4	1.0925	49.97
B1	-1183.7	1.0967	49.96	-1092.6	1.0961	49.98	-906.6	1.0975	50.02
B2	404.2	1.0899	49.97	456.9	1.0900	49.98	551.1	1.0913	50.02
WF	0	1.0929		0	1.0926		500	1.0947	
Losses	6.19			4.92			4.85		

Simulations are shown in figure 6.7. It is observed the both voltage responses at a contingency according to droop and tertiary control. As expected, power flows after the wind farm disconnection are deviated from the nominal values which also leads to a deviation in frequencies. The optimization control determines the new power trading which results in the decrease of steady-state error in frequencies. After the loss of communication at 15s, the system remains in the previous operating point and no transient is caused. When the wind farm is connected again at 20s, the system is only controlled by the droop characteristic which means that the new equilibrium point is determined by generating steady-state errors in voltages and powers but, in this case, around the latter operating point determined by the tertiary control. According to transmission
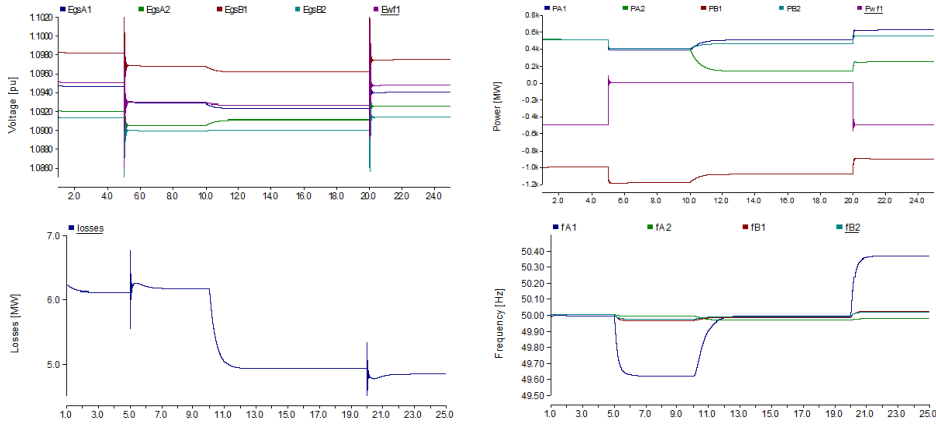
Figure 6.7:   Voltages, powers, transmission losses and frequencies responses in the outage of the wind farm and loss of communication case.

losses, they are decreased after the second optimization.

6.9   Case 6: Contingency in an ac power system

In the case 6, it is caused a contingency in the ac power system connected to the converter A1 of a loss of 500 MW of generation at 5s leading to a decrease on the frequency of such grid. The tertiary control is performed at 0s and 10s. In table 6.9 the steady-state powers, voltages and frequencies are detailed.

TABLE 6.9: Steady-state voltages, powers and frequencies in case 6.

| Station | < 5s | | | < 10s | | | < 15s |
	P [MW]	V [pu]	f [Hz]	f [Hz]	P [MW]	V [pu]	f [Hz]
A1	496.7	1.0946	50.00	48.43	997.3	1.0904	49.99
A2	496.5	1.0919	50.00	50.00	131.3	1.0902	49.96
B1	-997.8	1.0980	50.00	50.00	-1094.2	1.0950	49.98
B2	498.3	1.0913	50-00	50.00	459.8	1.0891	49.99
WF	500.0	1.0950			500.0	1.0918	

According to the simulations shown in figure 6.8, the frequency on the power system connected to A1 is deviated with reference to the nominal value because of the contingency while the load flow in the dc network remains unchanged. After the optimization is performed at 10s, some of the steady state error is removed at the cost of an important power deviation in the terminal A2, which is the station connected to the system with best inertial response. Reference to powers, it is observed that after the contingency in the ac grid load flow is not redistributed among converters due to the droop control is only in charge of balancing the dc network.
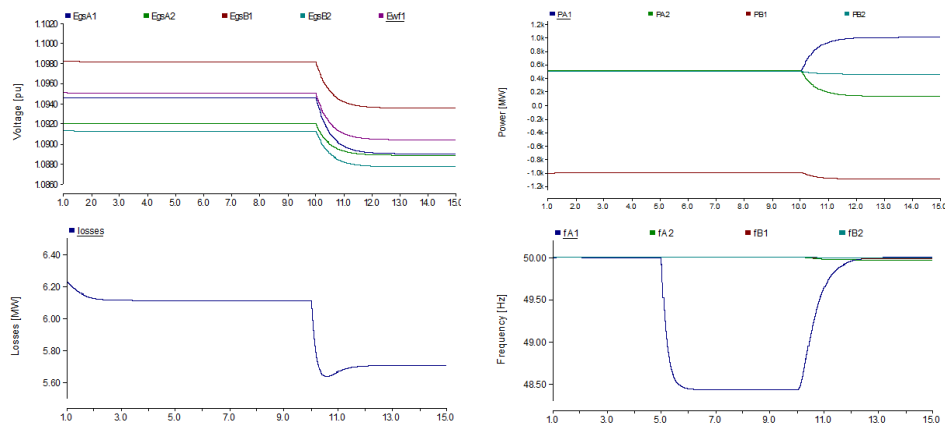
Figure 6.8: Voltages, powers, transmission losses and frequencies responses in ac power system contingency case.

6.10 Discussion

The analytical approach presented in chapter 5 for the higher level in the operation and control of a M-HVDC has been verified and tested with simulation results of a test dc network. Some cases concerning to contingencies and unbalances of such system have been simulated in order to study how the control responses to such disturbances. Simulation results have given a satisfactory performance though it is necessary to focus and analyse some questions.

Voltage boundary. The solution determined by the tertiary control achieves that voltages remain interior the boundary of the feasible region. However, after some disturbances, it is possible that the new operating point determined by the droop controller exceeds the voltage constraints.

By technical or normalization issues, voltages at nodes could not exceed the imposed voltage boundaries. In that case, this can be achieved by doing a N-1 study and limiting the voltage constraints to the maximum values for which the system does not go beyond the imposed voltage limits in the worst of the cases and/or imposing more restrictive boundaries.

Losses minimization. The solution does not manage the transmission losses minimization in all cases. In most of them, it is realized that the problem solution fall into a local minimum due to the intrinsic convergence to a position by the attraction of the best particles in PSO and the premature convergence caused by powers and frequencies penalizations. If transmission losses minimization is prioritized, it is required a scaling of the optimization problem as demonstrated in case 6.5.

Moreover, due to the problem random solution and the premature convergence, it is possible that two executions of the OPF in the same situation provide different solutions. Notwithstanding, it has been checked that the following of identical powers is provided for several executions despite obtaining different voltage levels. Therefore, the problem achieves the optimum power trading but not the minimum of transmission losses.

Transients In the performed simulations, the transient caused by the tertiary control in order to operate in a new equilibrium point has a first order plant behaviour with $\tau = 0.5s$ in order to accelerate simulations and provide clarification in the results. Notwithstanding, the time constant must be designed according to the coordinated performance of the hierarchical control and ac power system dynamics and stability.

To sum up, simulation results of the proposed tertiary control in a M-HVDC network has given a satisfactory performance and has verified the analytical approach previously explained. The controller has demonstrate its capability in the points detailed below.

- It optimizes the operation according to the minimization of losses though there is an important possibility to fall into a local minimum. Hence, the problem can not provide the best solution for the objective function.

- It defines the power exchange between terminals and areas as the power flow which determines the best solution in order to support frequencies.

- It provides N-2 security without reconfiguring the local control scheme.

Chapter 7

Conclusions

The rising importance of M-HVDC systems in the perception of the future grids awakes great interest. It is seen as the most feasible solution for the massive integration of renewables energies, the interconnection among power systems located in remote areas and the interconnection of asynchronous ac grids. The insight is still immature and, thus, it requires an important effort on its research and development. The operation and control of such system is one of the areas which need further research.

In order to gain more in-depth knowledge about the topic, a theoretically approach to the addressed subject is performed. The different control possibilities of such systems, their advantages and drawbacks, and their influence in the operation behaviour have been explained and explored in detail. Furthermore, for the purpose of verifying the theoretically exposed and checking the control behaviour, some practical cases have been performed in the power systems analysis tool PSCAD. To that end, the system modelling and control to be implemented in the simulation tool is presented.

Some conclusions have been confirmed and drawn from the simulated cases. The dc system needs at least one converter controlling the dc voltage for a reliable operation though only one can maintain the voltage at a given reference. The main drawbacks in the centralized control such as its independent scheme in balancing the overall systemand compensating all the disturbances within the network, the need of over-sizing the converter as well as the essential interconnection to a strong power system and the voltage collape and the uncontrollable perform of the system after its disconnection, have been confirmed.

Furthermore, the reasons for which the droop control is generally promoted has been also confirmed. These can be summarized as its autonomous control, the collaborative scheme in balancing the system and the provision of N-1 security. However, the proportional characteristic has an inherent behaviour of considering equally the normal and the disturbed operation. In fact, greater deviations in voltages with reference to the nominal value lead to greater deviation in injected powers.

This can be solved by the secondary controller [70] which allows following refer-

ences determined by the current load flow. Hence, neither the optimization nor any load flow scenario is achieved by itself.

In order to solve the lack of a definition in the power trading between terminals and define an optimization problem and a resolution of such grid, a tertiary controller is presented.

7.1 Main contributions of the research work

The contributions to the research can be categorized in the subjects of operation, control and optimization of M-HVDC systems and are described and discussed below.

i. Load flow analysis of a distributed dc meshed grid.

A Newton-Raphson-based methodology for solving the load flow in a system controlled by the droop strategy is presented. It is solved by expanding equations of currents and not powers [66], as it is commonly done, due to the proportional dependence of currents and voltages according to a droop constant. Results are verified by means of comparing with the steady-state values obtained in the simulations of a power system analysis simulation tool.

ii. Droop design for a scheduled power flow.

An easy and intuitive methodology in dc droop design for achieving a scheduled power flow with reference to the nominal values of a lossless system is presented. In the methodology, the deviation caused by the voltage drop at the injected power in a terminal is partially removed by adapting the droop characteristic. Results show a partial reduction of the deviation at the cost of a greater deviation in one. Therefore, in spite of having an overall reduction it is considered that the droop adaptation has deficiencies.

iii. Optimization of a droop-controlled dc meshed grid.

The losses minimization problem for a droop-controlled M-HVDC network is defined and the challenge in solving the non-convex and non-linear problem with the droop characteristic is explained. Moreover, unlike the literature [75–77] which solve the problem using a distributed slack approach, the problem is defined for bidirectional terminals and, hence, it is capable of achieving any load flow scenario. In order to solve the problem, it is defined an Optimal Power Flow solved by the heuristic method Particle Swarm Optimization with penalty factors in power deviations in order to guarantee the following of the power references.

Therefore, the main contributions to the research of the proposed problem are the optimization of a network with bidirectional and droop-controlled terminals, the optimization problem integration into the control of the operation of such network and the utilization of an OPF solved by PSO in a system of such

characteristics.

However, the resolution presents some limitations due to the random approach of the heuristic method such as the possibility of falling into a local minimum or the premature convergence.

iv. **Tertiary Control of a distributed dc meshed grid.**

A tertiary controller in charge of performing the upper level of the hierarchical control of a M-HVDC system is proposed. The controller performs the operation by means of a set of droop offsets calculated in the optimization problem previously explained. Moreover, in order to impose a hierarchical coherence respect to the lower controllers, it defines the trade of power flows for the purpose of supporting the frequencies of the connected power systems.
The proposed control has been validated and the system operation in contingencies has been studied by means of simulations performed in PSCAD. Moreover, the designed functions for which it conceived have also been demonstrated:

- It defines a coordinated scheme and operation with primary and secondary controllers by means of the optimum droop offsets.

- It defines a power exchange between terminals according to a criterion based on the frequency support. The determined power references are sent to a central controller and then to the secondary.

- It optimizes the operation according to the transmission losses minimization.

- It provides N-2 security, i.e. loss of a terminal and communications, without reconfiguring the local controller.

- It allows any desired load flow scenario.

Nonetheless, it presents the limitations caused by the heuristic resolution of the optimization problem. It has been realized that the problem solution falls into a local minimum due to the premature convergence problem caused by PSO and the penalization of violations of powers and frequencies.

It has been checked that in different executions of the same situation different solutions are provided. Therefore, different voltage levels and, thus, transmission losses, are obtained for differents executions while the same injected powers at terminals are achieved. As explained in the thesis, it can be solved by the scaling of penalization factors according to the criteria though, in the present case, the desired power trading is encouraged.

Moreover, despite the fact that the optimization problem ensures that voltages remain interior the boundary of the feasibe region, it is not guaranteed in dynamic analysis neither in the steady-state after the change in conditions. If voltages at nodes could not exceed the imposed boundaries by technical or normalization issues, the voltage constraints should be sized to the maximum values for which the system does not go beyond the imposed limits in the worst

of the cases and/or imposing more restrictive boundaries.

Furthermore, the time constant of actuation for tertiary controller is not defined in order to ensure a feasible operation and integration between dc and ac systems.

7.2   Suggested Future Works

Before the development of Multi-terminal systems, several challenges to be solved arise. The most important challenges can be categorized into several topic, namely, protection, converter topologies and modelling, cables and transmission design and modelling, system analysis and the problem at hand, the operation and control of such grid. Therefore, despite the large number of work still necessary, only some problems derived from the evidence of their lack during the development of the research performed in the thesis are suggested. These are explained below:

i. Study of the integration and frequency support of ac and dc systems

The frequency support performed in the control is obtained by redistributing the power among terminals by means of power references calculated in the optimization problem. Therefore, the combined performance of the hierarchical control of a dc grid and the power-frequency control of an ac grid is an interesting topic. Moreover, the amount in which the wind farms connected through the dc network could contribute to such frequency support arouse attention.

ii. Study of the time constant of actuation of the tertiary controller

The time constant of actuation of the tertiary controller is not selected in the present thesis. However, it is required to know the operability of the overall system. It must be selected taking into account several issues such as stability, connectedness with the time of actuation the dc nework controllers and the reserves capabilities of the ac power systems.

iii. Study of the performance of having a slack converter in a distributed-controlled system

As mentioned in chapter 4, having a system controlled by a slack converter and supported with droop-controlled converters can be a smart approach. By this, the provision of N-1 security is ensured and the following of power references is partially achieved though the slack converter requires to be over-sized as well. However, in the thesis this approach has not been studied. It is considered that the use of this approach requires the justification of having the slack in the performance of the overall system instead of controlling the system with the explained hierarchical control which also achieves the following of power references. Therefore, justifying the slack in terms of the stability and performance of the overall system is a suggestion to be studied.

iv. Power Flow Controller Devices

Although the power injected to terminals is controlled by the different strategies in converters, the load flow within the system is determined by the line resistances. In order to achieve a flexible and fully controllable dc network, the concept of power flow controllers and different devices is presented [83, 84]. The idea is to implement an element in the dc network which has the same function of FACTS in ac grids. Up to date, there is an insufficient knowledge on its performance and capabilities and control strategies are unsatisfactory compared to the available strategies in the converter control. Therefore, the last points and the addition of it into the optimization problem are suggested as an interesting future research work.

Appendix A

Park

The dq control approach is based upon representing the alternating 3-ph quantities by an equivalent set of two-phase quantities resulting in identical resultant space vector as the original 3ph space-time phasor representation. This control approach widely used in electric machine and drives application areas become the most dominant control approach in applications involving VSCs. Using this approach, the oscillating quantities of 3ph space-time phasor or $\alpha\beta0$ become constant quantities in a synchronous reference frame.

The Park transformation is given by,

$$[x_{qd0}] = [T_{qd0}][x_{abc}] \tag{A.1}$$

and it inverse

$$[x_{abc}] = [T_{qd0}]^{-1}[x_{qd0}] \tag{A.2}$$

where x_{abc} is a vector with the 3ph quantities in the abc frame and x_{qd0} is a vector with the transformed quantities in the $qd0$ frame.

The transformation matrix $T(\theta)$ is defined by

$$T(\theta) = \frac{2}{3} \begin{bmatrix} cos(\theta) & cos(\theta - \frac{2\pi}{3}) & cos(\theta - \frac{2\pi}{3}) \\ sin(\theta) & sin(\theta - \frac{2\pi}{3}) & sin(\theta - \frac{2\pi}{3}) \\ \frac{1}{2} & \frac{1}{2} & \frac{1}{2} \end{bmatrix} \tag{A.3}$$

and its inverse

$$T^{-1}(\theta) = \begin{bmatrix} cos(\theta) & sin(\theta) & 1 \\ cos(\theta - \frac{2\pi}{3}) & sin(\theta - \frac{2\pi}{3}) & 1 \\ cos(\theta + \frac{2\pi}{3}) & sin(\theta + \frac{2\pi}{3}) & 1 \end{bmatrix} \tag{A.4}$$

Figure A.1 illustrates the geometric transformation combining the Clarke transfomation and a rotation.
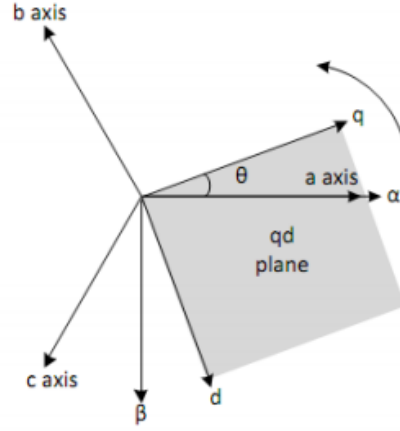
Figure A.1: *qd* frame representation [7].

A.0.1 Application of the Park transformation in the study of the VSC

In this appendix it is also presented the mathematical expand in order to obtain the equations for the study of the voltage source converter and justify the expressions of chapter 3.

Applying the Park transformation to the equation of the inner current controller in 3.12 is obtained,

$$\frac{d}{dt}(P^{-1}PI) = AP^{-1}PI + BP^{-1}PU \qquad (A.5)$$

Where P is the Park transformation matrix and,

$$A = \begin{bmatrix} \frac{R}{L} & 0 & 0 \\ 0 & \frac{R}{L} & 0 \\ 0 & 0 & \frac{R}{L} \end{bmatrix} \qquad (A.6)$$

$$B = \begin{bmatrix} \frac{1}{L} & 0 & 0 \\ 0 & \frac{1}{L} & 0 \\ 0 & 0 & \frac{1}{L} \end{bmatrix} \qquad (A.7)$$

$$I = \begin{bmatrix} i_a \\ i_b \\ i_c \end{bmatrix} \qquad (A.8)$$

$$U = \begin{bmatrix} v_{za} - v_{la} + V_{aN} \\ v_{zb} - v_{lb} + V_{bN} \\ v_{zc} - v_{lc} + V_{cN} \end{bmatrix} \qquad (A.9)$$

Expanding some products and considering the system without homopolar component, some components of equation A.5 are expressed as,

$$PI = I_p \begin{bmatrix} i_q \\ i_d \\ i_0 \end{bmatrix} \qquad (A.10)$$

94

$$PU = U_p \begin{bmatrix} v_{zq} - v_{lq} \\ v_{zd} - v_{ld} \\ v_{z0} - v_{l0} + V_{nN} \end{bmatrix} \tag{A.11}$$

Having all the expressions in terms of Park, it is finally obtained the equation,

$$\frac{d}{dt}(P^{-1}I_p) = AP^{-1}I_p + BP^{-1}U_p \tag{A.12}$$

Expanding the latter equation,

$$\frac{d}{dt}(P^{-1})I_p + \frac{d}{dt}(I_p)P^{-1} = AP^{-1}I_p + BP^{-1}U_p \tag{A.13}$$

$$\frac{d}{dt}(I_p) = P(AP^{-1}I_p + BP^{-1}U_p - \frac{d}{dt}(P^{-1})I_p) \tag{A.14}$$

$$\frac{d}{dt}(I_p) = P(AP^{-1} + -\frac{d}{dt}(P^{-1}))I_p + PBP^{-1}U_p \tag{A.15}$$

The derivative of the inverse of Park transformation matrix is,

$$\frac{d}{dt}P^{-1} = \omega \begin{bmatrix} -sin\theta & cos\theta & 1 \\ -sin(\theta - \frac{2\pi}{3}) & cos(\theta - \frac{2\pi}{3}) & 1 \\ -sin(\theta + \frac{2\pi}{3}) & cos(\theta + \frac{2\pi}{3}) & 1 \end{bmatrix} \tag{A.16}$$

Where it has been taken into account that $\theta = \omega t$. Then, considering some trigonometric identities and that the difference between three trigonometrical functions phase shifted 120º is zero, the product between equation A.16 and the park transformation matrix is,

$$P\frac{d}{dt}P^{-1} = \begin{bmatrix} 0 & -\omega & 0 \\ \omega & 0 & 0 \\ 0 & 0 & 0 \end{bmatrix} \tag{A.17}$$

Finally, equation A.12 is expanded according eq. A.17 as,

$$\frac{d}{dt}\begin{bmatrix} i_q \\ i_d \\ i_0 \end{bmatrix} = -\begin{bmatrix} \frac{R}{L} & -\omega & 0 \\ \omega & \frac{R}{L} & 0 \\ 0 & 0 & \frac{R}{L} \end{bmatrix}\begin{bmatrix} i_q \\ i_d \\ i_0 \end{bmatrix} + \begin{bmatrix} \frac{1}{L} & 0 & 0 \\ 0 & \frac{1}{L} & 0 \\ 0 & 0 & \frac{1}{L} \end{bmatrix}\begin{bmatrix} v_{zq} - v_{lq} \\ v_{zd} - v_{ld} \\ v_{z0} - v_{l0} + v_{nN} \end{bmatrix} \tag{A.18}$$

Appendix B

Modulation techniques

Switches in the inverter must be turned on and off to generate a periodic signal. In the simplest approach, the upper leg switch, top switch, is turned on while the nether is turned off in one cycle. Thus, a square wave waveform results. Including more commutations in a cycle an improved harmonic profile can be achieved.

In inverters a Pulse Width Modulation is required since the converter must generate an output with magnitude and frequency controllable.

The main objective of any modulation technique is to obtain an output variable with a maximum fundamental component and minimum harmonics.

B.1   Sine-PWM

The generation of the desired output waveform voltage can be achieved by comparing the desired reference voltage obtained form the modulation with a high-frequency triangular carrier wave. Depending on the axis on which voltage signal is located, the positive or negative DC voltage is applied at the output.

The triangular waveform, also known as carrier wave, establishes the switching frequency of the converter. The control voltage is used to modulate the switch duty ratio and has a frequency f_1 which is the fundamental frequency of the desired output voltage. The obtained voltage and the switching pulses are shown in figure B.1.
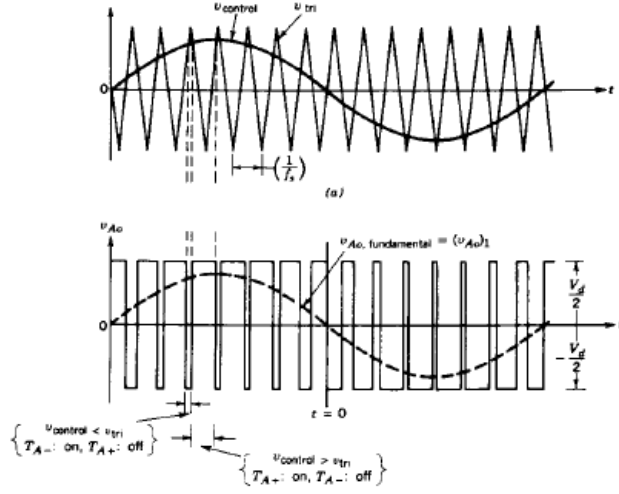
Figure B.1: Output voltage and switching pulses in SPWM [9].

The amplitude modulation ratio is defined as,

$$m = \frac{\hat{V}_{control}}{\hat{V}_{tri}} \tag{B.1}$$

Where $\hat{V}_{control}$ and $\hat{V}_{tri}$ are the peak amplitude of the control and triangular signals respectively.

In the linear region, $m \leq 1$, the fundamental frequency component at the output voltage varies linearly with the amplitude modulation ratio. The peak value of the fundamental frequency component in one of the inverter leg is,

$$\hat{V_{AN}} = m \cdot \frac{E_{DC}}{2} \tag{B.2}$$

Therefore, the line-to-line rms voltage at the fundamental frequency can be written as,

$$V_{LL} = m \cdot \hat{V}_{AN} \frac{\sqrt{3}}{\sqrt{2}} \frac{E_{DC}}{2} \tag{B.3}$$

So the minimum DC voltage level required to avoid converter saturation and to obtain the desired voltage value with m equal to 1 must be,

$$E_{DC_{m}in} = \frac{V_{LL}}{0.612} \tag{B.4}$$

If a higher dc voltage value is desired, the PWM is achieved with a lower amplitude modulation ratio for the new values.

The harmonics in the output voltage generated with SPWM technique appear around the switching frequency and its multiples. Defining a frequency ratio as,

$$m_f = \frac{f_s}{f_1} \tag{B.5}$$

The frequencies at which voltage harmonic occur corresponds to the harmonics,

$$h = j\left(m_f\right) \pm k \tag{B.6}$$

For odd values of j, the harmonic exists only for even values of k, while for even values of j, the harmonics exist for odd values of k. In figure B.2 is shown the harmonic spectra of the output voltage obtained by means of Sinusoidal PWM technique.
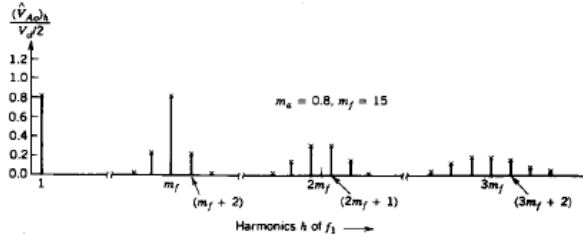

Figure B.2: Harmonic spectra of the output voltage in SPWM [9].

B.2 Space Vector PWM

The Space Vector Modulation technique (SVPWM) is a modulation technique for generating a sine wave which refers to a vector switching scheme of the six power semiconductor switches of a three phase power converter [85]. It was originally developed as a vector approach of the PWM for three phase inverter [86]. SVPWM has become a popular technique for three phase voltage source converters. Some drawbacks of the Sine-PWM are reduced with this modulation. The main advantages of this modulation technique are the lower harmonics and a higher modulation index which means a more efficient use of dc voltage, an excellent output performance, an optimized efficiency and a higher reliability.

B.2.1 Theory

A three phase system can be written in terms of space vectors as:

$$\overrightarrow{v}_s(t) = \overline{v}_{an}(t)e^{j0} + \overline{v}_{bn}(t)e^{j2\pi/3} + \overline{v}_{cn}(t)e^{j4\pi/3} \tag{B.7}$$

Where $\overrightarrow{v}_s(t)$ is a complex variable expressed as a vector which is the average value and contains information of the three phase voltages at any time. The voltage vector varies sinusoidally in time according the frequency and rotates anti-clockwise with a speed $2\pi f$ with a constant amplitude $\widehat{V}_s = \frac{3}{2}\widehat{V}_{ph}$.

$$\overrightarrow{v}_s(t) = \overline{v}_{an}(t)e^{j0} + \overline{v}_{bn}(t)e^{j2\pi/3} + \overline{v}_{cn}(t)e^{j4\pi/3} \tag{B.8}$$

$$\overrightarrow{v}_s(t) = \overline{v}_{aN}(t)e^{j0} + \overline{v}_{bN}(t)e^{j2\pi/3} + \overline{v}_{cN}(t)e^{j4\pi/3} \tag{B.9}$$

A switch state can be 1 or 0, so for three poles, 2^3 combinations are possible. The basic six non-zero vectors are obtained form equation B.9 and the remaining

two vector are the zero vectors because of their zero value for its three phase same switch state. The figure B.3 sketches the eight vectors on complex axis.
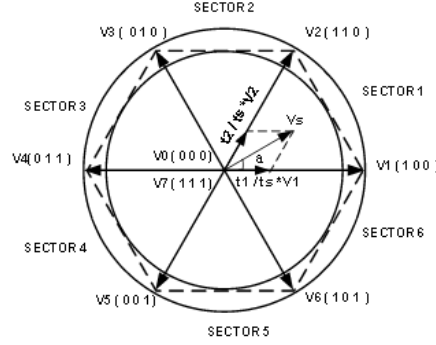

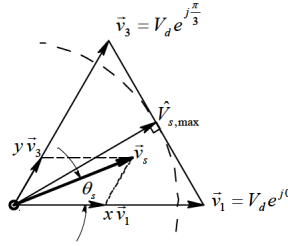Figure B.3: Instantaneous basic vectors [10].

Figure B.4: Synthesis of the voltage space vector [11].

The synthesized voltage vector at a sector has a maximum value limited by the DC voltage bus at an angle of $\pi/6$ rad as is shown in figure B.4.

$$(\widehat{V}_s)_{max} = \frac{\sqrt{3}}{3}E_{dc}(\widehat{V}_s)_{max} = V_d cos\frac{\pi}{6} = \frac{\sqrt{3}}{2}V_d \qquad (B.10)$$

And the corresponding maximum phase voltage peak, $\frac{2}{3}$ times the space vector v_s, is

$$(\widehat{V}_{ph})_{max} = \frac{V_d}{\sqrt{3}}\frac{\sqrt{3}}{2}E_{dc} \qquad (B.11)$$

So the maximum line to line voltage is

$$(\widehat{V}_{LL})_{max} = V_d = \frac{E_{dc}}{2} \qquad (B.12)$$

Which is compared to the Sine-PWM an available output voltage 15 % higher.

B.2.2   Implementation of SVPWM

The SVPWM technique is implemented in PSCAD according [87]. The SVPWM algorithm determines the six switch states of each of the electronic devices for

100

each step time. The switch state at every step time must be three switches in conduction while the other three off. The upper and nether switch of one leg are in a complementary state. The main algorithm steps of SVPWM are:

B.2.2.1 Voltage

Define the voltage space vector as follows:

$$V = \frac{2}{3}(u_a + u_b e^{j2\pi3} + u_c e^{j2\pi3}) = U e^{j\omega t} = V_\alpha + jV_\beta \qquad (B.13)$$

B.2.2.2 Determine the switching cycle iterations

As PSCAD can not do loops is needed that for each calculation or step time the algorithm read the input variables, execute the necessary calculations and send the outputs. Thus, in a switching cycle the algorithm is executed n times where n is the quotient between the simulation time step and a switching cycle.

B.2.2.3 Sector location determination

The sector is determined by the V_α and V_β location in the $\alpha\beta$ axis by the equation B.14 in the case both are positive and the positive direction as anti-clockwise.

$$\gamma = arctan\left(\frac{V_\beta}{V_\alpha}\right) \qquad (B.14)$$

The sector location is defined by the angle γ as,

$$\gamma = \begin{cases} arctan(V_\beta/V_\alpha) & (V_\alpha > 0, V_\beta \geq 0) \\ arctan(V_\beta/V_\alpha) + 2\pi & (V_\alpha > 0, V_\beta < 0) \\ \pi/2 & (V_\alpha = 0, V_\beta \geq 0) \\ 3\pi/2 & (V_\alpha = 0, V_\beta < 0) \\ arctan(V_\beta/V_\alpha) + \pi & (V_\beta < 0) \end{cases} \qquad (B.15)$$

B.2.2.4 Determine the Switching Time duration

The switch conduction time in each adjacent basic vector and in zero vectors is written in the formula B.16.

$$\begin{cases} T_a = mT_s sin(\frac{\pi}{3} - \theta) \\ T_b = mT_s sin(\frac{\pi}{3}) \\ T_c = T_s - (T_a + T_b) \end{cases} \qquad (B.16)$$

Where θ is the angle between voltage space vector V and the beginning basic vector where V locates in the sector. The odd sectors are defined anti-clockwise while the even sectors are defined clockwise. m represents the SVPWM modulation index,

$$m = \frac{\sqrt{3}}{V_{dc}}|V| = \frac{\sqrt{3}}{V_{dc}}\sqrt{V_\alpha^2 + V_\beta^2} \qquad (B.17)$$

B.2.2.5 Generation and distribution of switching

The modulation scheme implemented in the thesis is the symmetrical sequence generation. In order to obtain fixed switching frequency and optimum harmonic distortion the method change the leg switch state to 1 only once in a switching period. This is done by applying the zero vector during the previously calculated working time and then applying the active state vector during the remaining half switching period. The next half is the symmetric mirror of the first half period. As an example, the pulse distribution for the first sector is shown in figure B.5 while figure B.6 sketches the space vector distribution for each period.
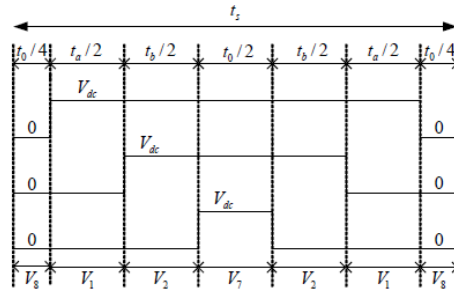

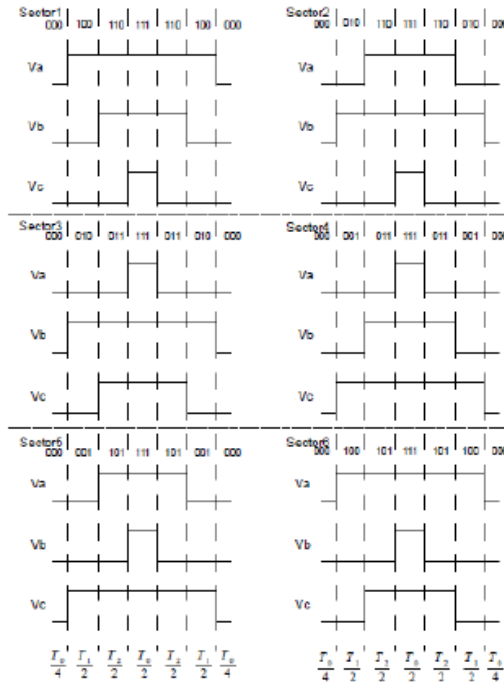Figure B.5: Space Vector distribution in sector I.

Figure B.6: Space Vector distribution.

B.2.3   Determine the time slot

Once the sector has been located and the distribution of switching has been generated, it is only needed the time slot of a switching cycle according the working times previously calculated. In each one of the time slots of a switching cycle as sketched in figure B.6, the current time slot can be determined according table B.1.

TABLE B.1: Time Slots of a switching cycle.

Slot	TIME
t1	$[0, \frac{Tc}{4})$
t2	$[\frac{Tc}{4}, \frac{Tc}{4} + \frac{Ta}{2})$
t3	$[(\frac{Tc}{4} + \frac{Ta}{2}), (\frac{Tc}{4} + \frac{Ta}{2} + \frac{Tb}{2}))$
t4	$[(\frac{Tc}{4} + \frac{Ta}{2} + \frac{Tb}{2}), (\frac{Ts}{4} + \frac{Tc}{4}))$
t5	$[(\frac{Ts}{4} + \frac{Tc}{4}), (\frac{Ts}{4} + \frac{Tc}{4} + \frac{Tb}{2}))$
t6	$[(\frac{Ts}{4} + \frac{Tc}{4} + \frac{Tb}{2}), (\frac{Ts}{4} + \frac{Tc}{4} + \frac{Tb}{2} + \frac{Ta}{2}))$
t7	$[(\frac{Ts}{4} + \frac{Tc}{4} + \frac{Tb}{2} + \frac{Ta}{2}), Ts)$

B.3   Implementation in PSCAD

The switched model of the VSC is implemented into the simulation tool PSCAD as a two level structure composed by six IGBTs with the respective diodes in anti-parallel as shown in figure B.7.
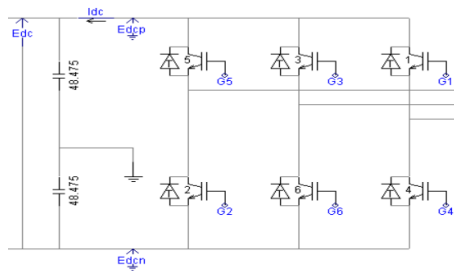

Figure B.7:   Two level switched converter model circuit.

In case of modulation SPWM, the switching is performed by the control structure sketched in figure B.8 and the filtered voltage obtained is shown in figure B.9.
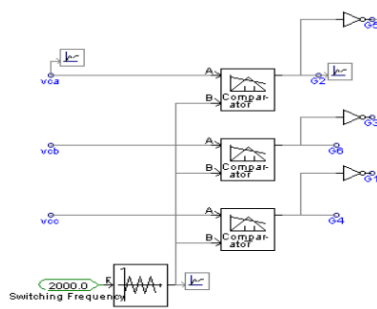
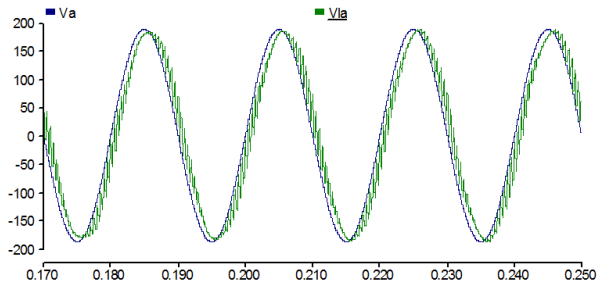Figure B.8:   Switching gate signal generation in SPWM modulation.

Figure B.9:   Filtered ac voltage of phase a at the VSC with SPWM and at the PCC.

In the case of SVPWM, the modulation is implemented in PSCAD by means of a component which contains the algorithm code written in Fortran. Gate signals are obtained from the dq components of voltage and the angle θ as shown in figure B.10.
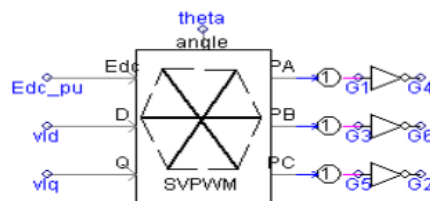

Figure B.10:   SVPWM component implemented in PSCAD.

The filtered line-to-line voltage and phase voltage with the characteristic form due to the over-modulation produced in the basic vectors which can be solved by the addition of a third harmonic are shown in figure B.11.
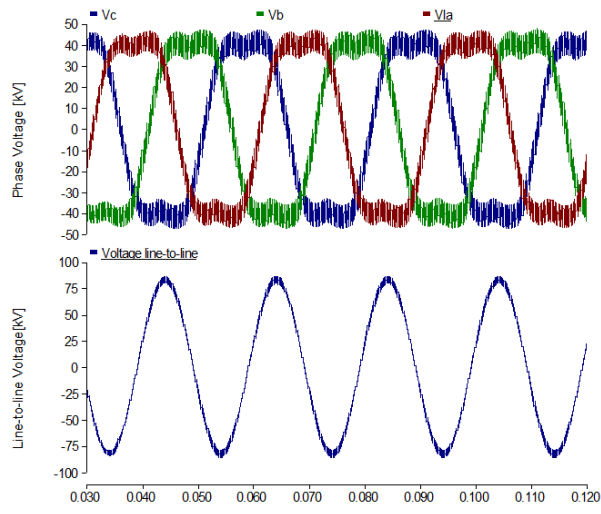
Figure B.11:   Filtered ac line-to-line and phase voltages at the VSC with SVPWM.

Appendix C

Droop Design

The present appendix is focused on the simple droop design on simple cases. By means of the examples, it is observed and studied the behaviour and power sharing of droop-controlled converters. In order to simplify, the dc network is not modelled in these cases. The obtained simulations are also compared with the v-i characteristic of converter in order to verify results.

Point-to-point scheme with droop control A system composed by one WF and one offshore station converter, a back-to-back scheme, has been created in order to show the design and operation of droop control in the simplest case. In first place, taking into account the voltage regulation, a value of 0.985 pu for the dc voltage offset, E_{dc}^*, has been chosen. Accordingly, droop constant can be calculated considering GSVSC rated voltage and power as,

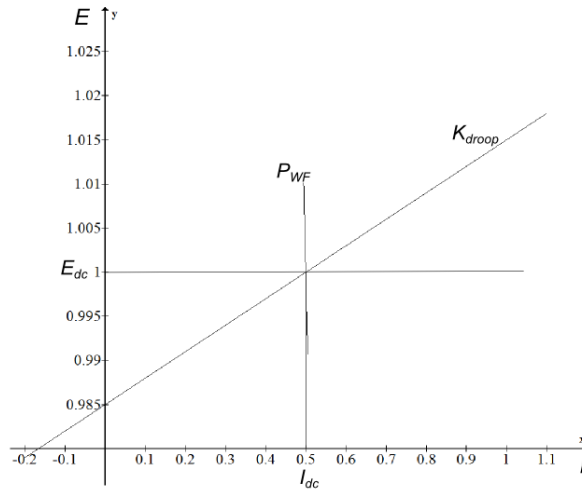$$k_{Droop} = \frac{I_{dcN}}{(E_{dcN} - E_{dc}^*)} \tag{C.1}$$

Figure C.1: V-I characteristic and equilibrium point.

Figure C.1 sketches the voltage-current characteristic of the studied grid while figure C.2 shows the dynamic behaviour of the dc voltage and active power to a generated power step of 500 MW at 0.5 s where the generated power step is injected entirely to the grid side converter while a stationary error in dc voltage is produced.
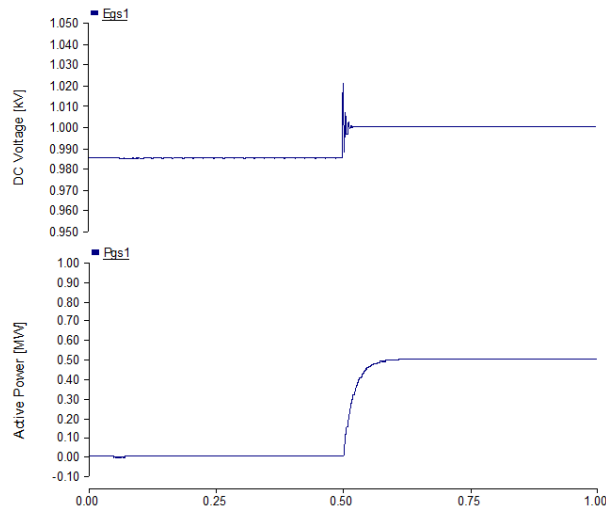

Figure C.2: DC voltage and dc active power in the onshore terminal.

One WF and two GS in parallel   The simulated grid in figure 4.1 is now controlled with droop strategy and its behaviour is shown in figure C.4. The circuit is simulated with a initial generated power equal to zero, a generated power step of 1000 MW at 0.5 s, a power reduction of 500 MW at 1 s and an increase up to 1500 MW generated at 1.5 s. In this case is observed how the two onshore converters share the total generated power for an equal magnitude unlike the case with the converters controlled by the dc voltage controller with PI action at the expenses of generating a stationary error relative to the reference voltage. Figures C.3 and C.4 show the voltage-current characteristic of the M-HVDC and the different equilibrium points at the simulated situations respectively.

TABLE C.1: Droop values and simulation results

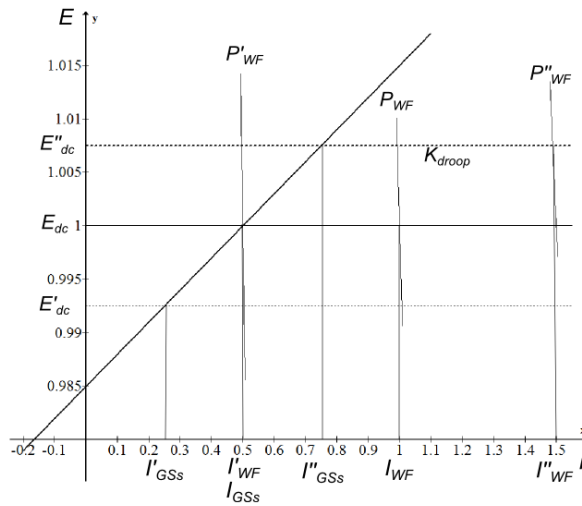| Control parameters				
GSVSC1	$K_{droop} = 33.33$		$E_{dc_0} = 0.985$	
GSVSC1	$K_{droop} = 33.33$		$E_{dc_0} = 0.985$	
DC base voltage	380 kV			
Base power	1000 MW			
Simulation results	t=0s	0.5s	1s	1.5s
P_{WF} [pu]	0	1	0.5	1.5
P_{GSVSC1} [pu]	0	0.5	0.25	0.75
P_{GSVSC2} [pu]	0	0.5	0.25	0.75
E_{dc} [pu]	0.9850	1	0.9926	1.0073

Figure C.3: Voltage-current characteristic of the grid.

The droop control is capable as well of performing a determined power sharing between terminals according to a certain ratio only varying the droop slope.
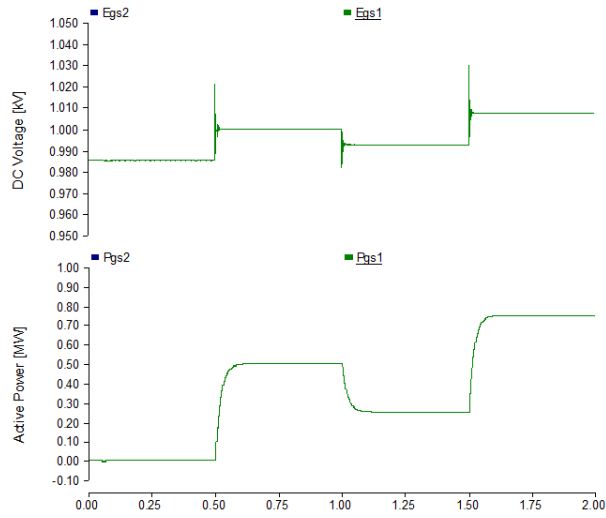
Figure C.4: DC voltage and DC Active Power in the onshore terminals.

As an example, droop control is implemented in a system composed by one WF and two onshore stations in parallel where the generated power is transmitted to two the receiving stations. The total power amount is shared by the two GS terminals which their rated power are P_{GS1} and P_{GS2}. Then, both droop constants can be related by the power sharing ratio as

$$n = \frac{P_{GS1}}{P_{GS2}} = \frac{K_1 \left(E_{DC} - E_{dcset1}\right) E_{DC}}{K_1 \left(E_{DC} - E_{dcset1}\right) E_{DC}} \simeq \frac{K_1}{K_2} \tag{C.2}$$
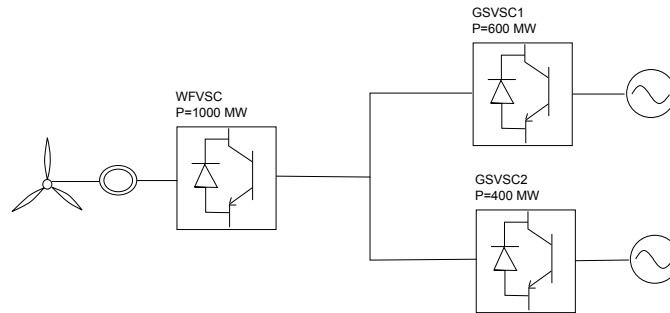
Figure C.5: Circuit of one WF and two GSVSC in parallel with different rated power.

Figure C.5 sketches a circuit with P_{WF}, P_{GS1} and P_{GS2} equal to 1000, 600 and

400 MW respectively. The generated power steps simulated are the same than in the previous case. The V-I characteristics of the two GSVSC and the WF are shown in figure C.6 in which is displayed the different equilibrium points and the obtained simulations are shown in figure C.7. The droop constants of the onshore stations one and two are 40 and 26.67 in pu respectively, which it is the power ratio, and the reference set-point of both is 0.985.

TABLE C.2: Droop values and simulation results

Control parameters			
GSVSC1	$K_{droop} = 40$	$E_{dc_0} = 0.985$	
GSVSC1	$K_{droop} = 26.67$	$E_{dc_0} = 0.985$	
DC base voltage	380 kV		
Base power	1000 MW		
Simulation results	t=0s	0.5s	1s	1.5s
P_{WF} [pu]	0	1	0.5	1.5
P_{GSVSC1} [pu]	0	0.6	0.3	0.9
P_{GSVSC2} [pu]	0	0.4	0.2	0.6
E_{dc} [pu]	0.9850	1	0.9926	1.0073

Figure C.6: Voltage-current characteristic of the grid.

As shown in the figure, initially for a null power injected the power sharing between onshore stations is equal to zero, at the power step of 1000 MW both converters share the rated power of each one and at the following power steps both converters share the total amount of injected power fulfilling the power ratio quotient between them.
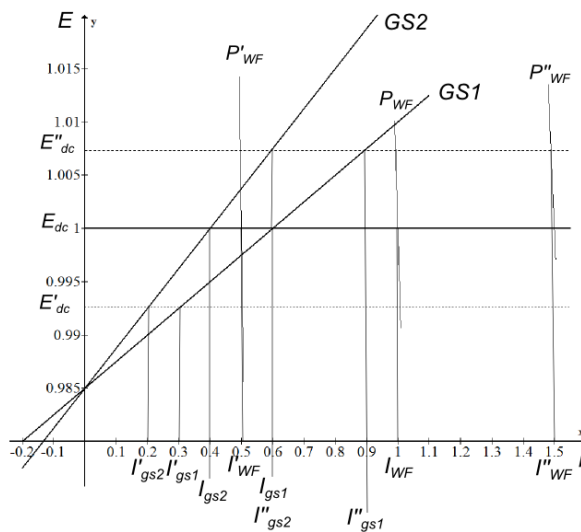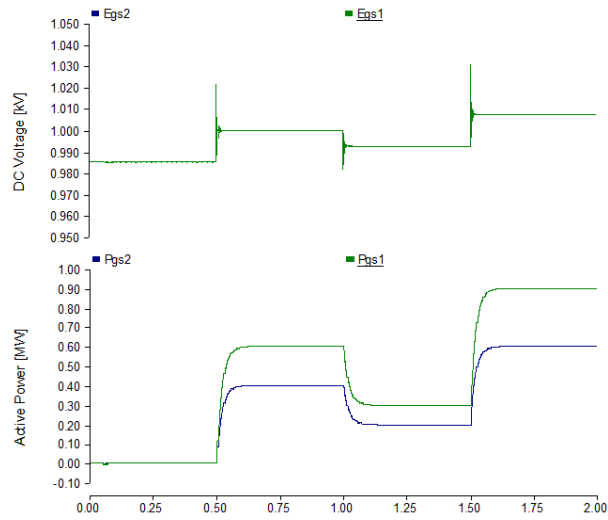
Figure C.7: DC voltage and DC Active Power in the onshore terminals.

Moreover, droop controller is as well capable of achieving power sharing between converters during lack of generation or according to the steady state flow allowing a power flow between the different grids which integrate the system. The dc voltage offset as well as limiting voltage regulation at the converter bus can prioritize the power injection to one terminal regarding the other in the situation of lack of generation and makes possible the power flow between converters in the steady state situation. Thereby, grid side converters can share active power within them being some of them which inject power to the ac grid while the others inject the active power to the dc grid absorbing it from the ac grid.

An example of this is developed in the next paragraphs.

Two WF and two GSVSC scheme A grid composed by two wind farms and two grid side converters is shown in figure C.8 and two cases are simulated on it.

112

Figure C.8: Grid composed by two WFs and two GSCs [12].

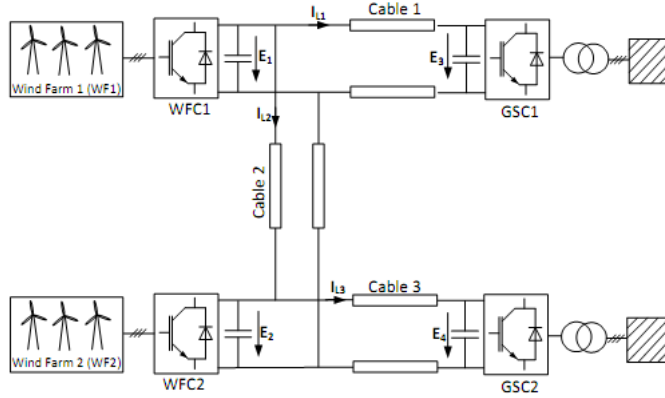In the first case, the two grid side converters absorb their respective rated power at nominal conditions. During the lack of generation, it is prioritized the power injection to GS1 converter which must be provided by GS2. The active power shared between them is determined by the droop constants and the voltage sets of each one of them, the offset also establishes which converter injects power to the dc grid. The equilibrium point in that situation is achieved when both converters currents equalize at a voltage determined by,

$$K_{GS1}\left(E_{dc} - E_{dc0,GS1}\right) = -K_{GS2}\left(E_{dc} - E_{dc0,GS2}\right) \tag{C.3}$$

Focusing on the negative equation must be taking into account its meaning which will be clarified in the following obtained v-i characteristics. It responses to the situation of the characteristic in the second quadrant,i.e. with the negative current, and the converter which work on it will be determined by the higher voltage set of its droop. However it responses as well as the negative slope of the droop constant for which the converter works as a rectifier in the first quadrant and the two parts of the previous equation would be equal. The election of this sign will be determined by the sign convention of the system.

In the studied case the system has been simulated with the control design and the values shown in C.3 and considering non-resistive lines with the same power ratings of onshore converter than the previous case. The v-i characteristic of the system is shown in figure C.9 where is chosen a sign convention that the power injected to the converter is positive, i.e converters work as an inverter. The dynamical behaviour of injected power to converters and grid voltage is observed in figure C.10 in which the system is initially at nominal conditions and then it is applied null generation at 0.5s.

TABLE C.3: Droop values and simulation results

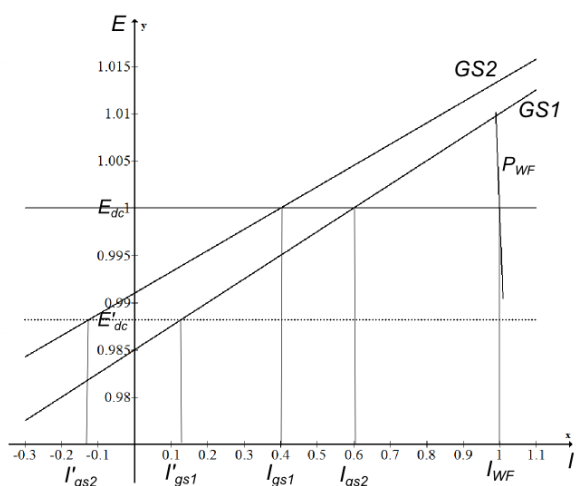| Control parameters			Power rating [MW]
GSVSC1	$K_{droop} = 40$	$E_{dc_0} = 0.985$	600
GSVSC2	$K_{droop} = 44.44$	$E_{dc_0} = 0.991$	400
DC base voltage	380 kV		
Base power	1000 MW		
Simulation results	t=0s	0.5s	
$P_{WF1} + P_{WF2}$ [pu]	1000	0	
P_{GSVSC1} [pu]	0.6000	0.1248	
P_{GSVSC2} [pu]	0.4000	-0.1248	
E_{dc} [pu]	1	0.9882	

Figure C.9: Voltage-current characteristic of the system.

As observed, at nominal conditions the two onshore stations achieve their rated power while during loss of generation the GS2 supplies all the power injected to GS1 as expected in the v-i characteristic and obtaining the same results by both methods.
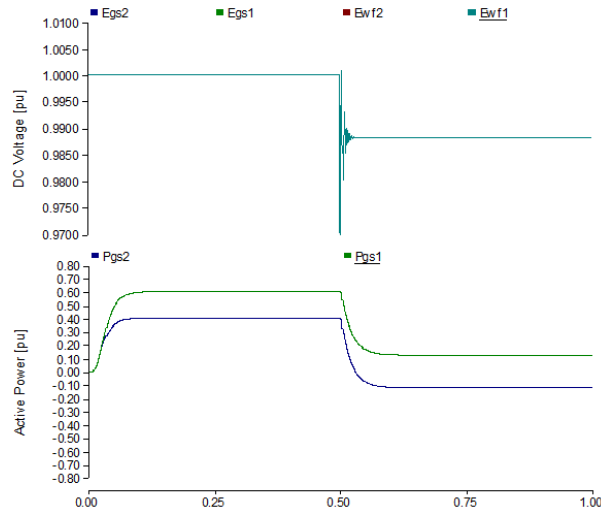
Figure C.10: DC voltage and DC Active Power in the onshore terminals.

In the following case it is considered that in steady state GS2 and wind farms inject to GS1 its rated power, in this case 0.7 pu. Thereby, droop constants are designed to satisfy $P_{WF} + P_{GS2} = P_{GS1}$ in nominal conditions. So GS1 droop constant is designed considering its rated power at rated voltage and the voltage regulation limitation. On the other hand, GS2 could be designed following the same conditions but, in this case, it is done taking another point in the v-i characteristic. When GS1 reaches an injected power equal to 0.9 pu, GS2 must start to work as an inverter, so from this value both converters start to share the generated power. With two points in the v-i characteristic, the droop constant is easily calculated.

Droop constants, the system base and rated values and simulation results are shown in table C.3. On its behalf, figure C.11 shows the v-i characteristic with the equilibrium points and figure C.12 shows the behaviour of active power and dc voltage of grid side converters. Is important to mention that in the v-i characteristic GS1 has been considered as an inverter and GS2 as a rectifier while in the graphics both converters have been considered as inverters to make clear the flow direction in the system. For this reason, some results have the same value with the opposite sign. The system is simulated initially at nominal conditions, to a power step of generation up to 1100 MW at 0.5 s and a decrease up to null generation at 1 s.

115

TABLE C.4: Droop values and simulation results

Control parameters			Power rating [MW]
GSVSC1	$K_{droop} = 46.67$	$E_{dc_0} = 0.985$	700
GSVSC2	$K_{droop} = -70.09$	$E_{dc_0} = 1.004$	-300
DC base voltage	380 kV		
Base power	1000 MW		
Simulation results	t=0s	0.5s	1s
$P_{WF1} + P_{WF2}$ [pu]	0.40	1.10	0
P_{GSVSC1} [pu]	0.70	0.98	0.54
P_{GSVSC2} [pu]	-0.30	0.12	-0.54
E_{dc} [pu]	1	1.0059	0.9966

Figure C.11:   Voltage-current characteristic of the system.
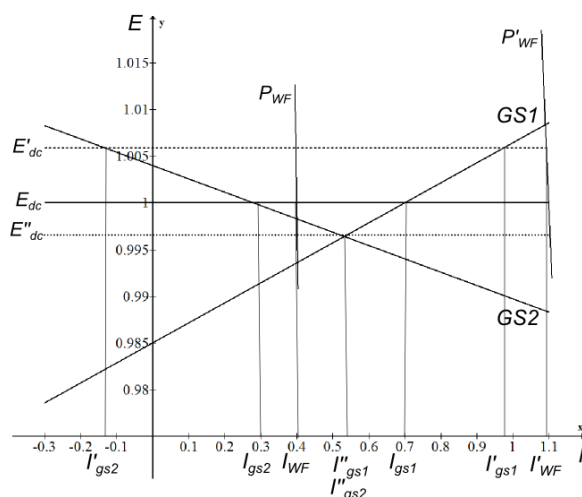
As observed the results obtained in the simulation reach the same equilibrium points than the found analytically in the characteristic.
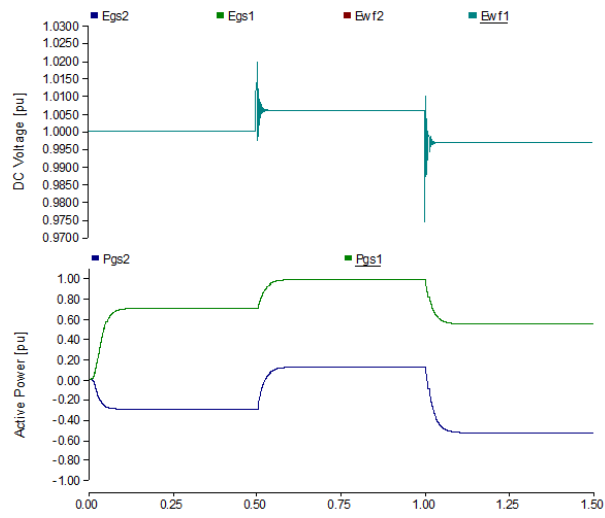
116

Figure C.12: DC voltage and dc Active Power in the onshore terminals.

The examples have been performed with the only focus of explaining different methodology for the droop design and studying its operation and capabilities.

Bibliography

[1] O. Heyman, L. Weimers, and M.-L. Bohl, "Hvdc - a key solution in future transmission systems," tech. rep., ABB Technical reports., ,. xvii, 5

[2] D. Van Hertem and M. Ghandhari, "Multi-terminal vsc hvdc for the european supergrid: Obstacles," *Renewable & Sustainable Energy Reviews*, vol. vol. 14, no. 9, pp. pp. 3156–3163, 2010. xvii, 6, 14, 15

[3] C. Du, *VSC-HVDC for Industrial Power Systems*. PhD thesis, Energy and Environment Dept., Chalmers University of Technology, Goteborg, Sweden, 2007. xvii, 7, 8, 22, 27

[4] S. G. Johansson, G. Asplund, E. Jansson, and R. Rudervall, "Power system stability benefits with vsc dc-transmission systems," tech. rep., Cigré B4-204, 2004. xvii, 8

[5] J. Glasdam, J. Hjerrild, L. H. Kocewiak, and C. L. Bak, "Review on multilevel voltage source converter based hvdc technologies for grid connection of large offshore wind farms," *Power System Technology (POWERCON), 2012 IEEE International Conference on*, vol. ,, pp. pp 1–6, 2012. xvii, 10, 11

[6] B. Qahraman, *Series / Parallel Hybrid VSC-LCC for HVdc Transmission Systems*. PhD thesis, Department of Electrical and Computer Engineering, University of Manitoba, 2010. xvii, 12

[7] A. Egea-Alvarez, A. Junyent-Ferré, and O. Gomis-Bellmunt, *Modeling and Control of Sustainable Power Systems*, ch. Active and reactive power control of grid connected distributed generation systems, pp. pp. 47–81. ser. Green Energy and Technology, L. Wang, 2012. xvii, xviii, 20, 25, 26, 29, 94

[8] L. Zhang, *Modeling and Control of VSC-HVDC Links Connected to Weak AC Systems*. PhD thesis, KTH Electrical Engineering, 2010. xvii, 21

[9] R. W. Mohan N., Undeland T.M., *Power Electronics- Converters, Applications and Design*. John Wiley & Sons, 2003. xviii, 98, 99

[10] S. Bowes and Y. Lai, "The relationship between space vector modulation and regular-sampled pwm," *IEE Trans.Power Electron*, vol. vol. 14, pp. pp. 670–679, 1997. xviii, 100

[11] N. Mohan, P. Jose, T. Brekken, and W. Sulkowski, "Explaining synthesis of three-phase sinusoidal voltages using sv-pwm in the first power electronics course.," *Power Electronics Education, 2005. IEEE Workshop*, vol. June 16-17, 2005, pp. pp. 40–44, 2005. xviii, 100

[12] A. Egea-Alvarez, F. Bianchi, A. Junyent-Ferre, G. Gross, and O. Gomis-Bellmunt, "Voltage control of multiterminal vsc-hvdc transmission systems for offshore wind power plants: Design and implementation in a scaled platform," *Industrial Electronics, IEEE Transactions on*, vol. Vol. 60 no. 6, pp. pp. 2381 – 2391, 2013. xix, 37, 113

[13] E. Commission, "Investing in the development of low carbon technologies - set plan." Available: http://ec.europa.eu. 1

[14] EWEA, "The european offshore wind industry key trends and statistics 2009." Available: http://www.ewea.org. 1

[15] G. S., "Supergrid to the rescue," *Power Engineer*, vol. 20, pp. 30–33, 2006. 3

[16] R. V. Robles, A. Sumper, A. Suwannarat, B. Bak-Jensen, R. Ramirez, O. Gomis, and A. Sudria, "On wind power integration into electrical power system: Spain vs. denmark," in *Electrical Power Quality and Utilization, EPQU*, 2007. 4

[17] *Demand power web of REE. Visited the May 14th. https://demanda.ree.es/demanda.html.* 4

[18] P. Francos, S. Verdugo, H. Alvarez, S. Guyomarch, and J. Loncle, "Inelfe - europe's first integrated onshore hvdc interconnection," *Power and Energy Society General Meeting, 2012 IEEE*, vol. ., pp. pp. 1 – 8, 2012. 4

[19] T. Economist, "When the wind blows," in *http://www.economist.com/node/9539765*, July 2006. 4

[20] ETSO., "European wind integration study towards a successful integration of wind power into european electricity grids, project report (january 2007)," in *http://www.wind-integration.eu/downloads/library/EWIS-phase-I-finalreport.pdf*, . 4

[21] P. Kundur, *Power System Stability and Control*. McGraw-Hill Professional, 1994. 6

[22] B. Andersen, "Hvdc transmission-opportunities and challenges," *AC and DC Power Transmission, 2006. ACDC 2006. The 8th IEE International Conference on*, vol. ., pp. 24–29, 2006. 6

[23] A. Nabae, I. Takahashi, and H. Akagi, "A new neutral-point clamped pwm inverter," , vol. 17, pp. 518-523, 1981.," *IEEE Trans. Ind. Application*, vol. vol. 17, pp. pp. 518–523, 1981. 9

[24] J. Rodriguez, J. Lai, and F. Peng, "Multilevel inverters: A survey of topologies, controls, and applications," *IEEE Transactions on Industrial Electronics*, vol. vol. 49, pp. pp. 724–738, 2002. 9

[25] B. R. Andersen, L. Xu, and K. T. G.Wong, "Topologies for vsc transmission," *Proc. 7th Int. Conf. AC-DC Power Transm., London, U.K.*, vol. ,, pp. pp. 298–304, Nov. 2001. 9

[26] A. Lesnicar and R. Marquardt, "An innovative modular multilevel converter topology suitable for a wide power range," *IEEE PowerTech Conference, Bologna, Italy*, vol. ., p. ., 2003. 9

[27] P. Boonchiam and N. Mithulananthan, "Diode-clamped multilevel voltage source converter for medium voltage dynamic voltage restorer," *ESD2006 conj, Phuket*, vol. ., p. ., 2006. 9

[28] L. Franquelo, J. Rodríguez, J. Leon, S. Kouro, R. Portillo, and M. Prats, "The age of multilevel converters arrives," *IEEE Ind. Electron. Mag.*, vol. vol. 2, no. 2, pp. pp. 28–39, Jun. 2008. 9, 10

[29] S. Allebrod, R. Hamerski, and R. Marquardt, "New transformerless, scalable modular multilevel converters for hvdc-transmission," *Proc. IEEE Power Electron. Spec. Conf*, vol. ,, pp. pp. 174–179., Jun. 2008. 10

[30] M. Natale, F. Lane, and T. Calverley, "The sardinianitalian mainland hvdc interconnection," *IEE Conf.*, vol. No. 22, p. p. 42, 1966. 13

[31] "Abb. power transmission and distribution.the hvdc transmission québec - new england. available from: http://www.abb.com/cawp/gad02181/c1256d71001e0037c12568340029b5c4.aspx," Visited on April 18th, 2013. 13

[32] T. Nakajima and S. Irokawa., "A control system for hvdc transmission by voltage sourced converters.," *Power Engineering Society Summer Meeting.*, vol. IEEE, pp. ,, 1999. 13

[33] T. Nakajima and S. Irokawa, "A control system for hvdc transmission by voltage sourced converters," *in 1999 IEEE Power Engineering Society Summer Meeting.*, vol. vol. 2, pp. pp. 1113–1119, 1999. 13, 35

[34] L. Xu, B. Williams, and L. Yao, "Multi-terminal dc transmission systems for connecting large offshore wind farms," *Power and Energy Society General Meeting- Conversion and Delivery of Electrical Energy in the 21st Century*, vol. ,, pp. pp. 1–7, 2008. 13, 35

[35] L. Xu, L. Yao, and M. Bazargan, "Dc grid management of a multi-terminal hvdc transmission system for large offshore wind farms," *International Conference on Sustainable Power Generation and Supply, 2009. SUPERGEN 09*, vol. ,, pp. pp. 1–7, 2009. 13, 35

[36] J. Liang, O. Gomis-Bellmunt, J. Ekanayake, and N. Jenkins, "Control of multi-terminal vsc-hvdc transmission for offshore wind power," in *EPE2009, 13th European conference on Power Electronics and Applications*, 2009. 13, 35

[37] O. Gomis-Bellmunt, J. Liang, J. Ekanayake, and N. Jenkins, "Voltage current characteristics of multiterminal hvdc-vsc for offshore wind farms," *Electric Power Systems Research*, vol. vol. 81, pp. pp. 440 –450, 2011. 13, 35, 37

[38] R. Hendriks, G. Paap, and W. Kling, "Control of a multi-terminal vsc transmission scheme for connecting offshore wind farms," *Proc. European Wind Energy Conference & Exhibition*, vol. Milan, Italy, pp. May 7–10, 2007. 13, 35

[39] A. Egea-Alvarez, A. Junyent-Ferre, O. Gomis-Bellmunt, J. Liang, J. Ekanayake, and N. Jenkins, "Operation and control of vsc-hvdc multiterminal grids for offshore wind," *Power Electronics and Applications (EPE 2011), Proceedings of the 2011-14th European Conference on*, vol. ., pp. pp: 1–9, 2011. 13, 31

[40] B. Silva, C. Moreira, L. Seca, Y. Phulpin, and J. Peas Lopes, "Provision of inertial and primary frequency control services using offshore multiterminal hvdc networks," *Sustainable Energy, IEEE Transactions on*, vol. vol. 3 Issue:4, pp. pp: 800–808, 2012. 13

[41] T. Haileselassie, R. Torres-Olguin, T. Vrana, K. Uhlen, and T. Undeland, "Main grid frequency support strategy for vsc-hvdc connected wind farms with variable speed wind turbines," *Dept. of Electr. Power Eng., Norwegian Univ. of Sci. & Technol., Trondheim, Norway*, vol. ., pp. pp: 1–9, 2011. 13

[42] A. Sarlette, J. Dai, Y. Phulpin, and D. Ernst, "Cooperative frequency control with a multi-terminal high-voltage dc network," *Elsevier, Automatica*, vol. vol. 48, pp. pp. 3128–3142, 2012. 13

[43] O. Gomis-Bellmunt, J. Liang, J. Ekanayake, R. King, and N. Jenkins, "Topologies of multiterminal hvdc-vsc transmission for large offshore wind farms.," *Electric Power Systems Research*, vol. 81, pp. 271–281, 2011. 13

[44] J. Arrillaga and P. Bodger, "Integration of h.v.d.c. links with fast-decoupled load-flow solutions," *Electrical Engineers,Proceedings of the Institution of* ., vol. vol. 124, pp. pp. 463–468, 1977. 13, 41

[45] M. El-Marsafawy and R. Mathur, "A new, fast technique for load-flow solution of integrated multi-terminal ac/dc systems," *IEEE Trans.Power App. Syst., vol. PAS-99, no. 1, pp. 246-255,*, vol. vol.1, pp. pp. 246–255, Jan Feb. 1980. 13, 41

[46] T. M. Haileselassie and K. Uhlen, "Power flow analysis of multi-terminal hvdc networks," *in PowerTech, 2011 IEEE Trondheim*, vol. ,, pp. pp. 1–6, 2011. 13, 41

[47] J. Reeve, G. Fahny, and B. Stott, "Versatile load flow method for multiterminal hvdc systems," *Power Apparatus and Systems, IEEE Transactions on, ,*, vol. vol. 96, pp. pp. 925–933, 1977. 13, 41

[48] M. E. El-Hawary and S. T. Ibrahim, "A new approach to ac-dc load flow analysis," *Electric Power Systems Research*, vol. vol. 33, pp. pp. 193–200, 1995. 13, 41

[49] J. Beerten, S. Cole, and R. Belmans, "Implementation aspects of a sequential ac/dc power flow computation algorithm for multi-terminal vsc hvdc systems," *in AC and DC Power Transmission, 2010. ACDC. 9th IET International Conference on*, vol. ., pp. pp. 1–6, 2010. 13, 41

[50] M. Baradar, M. Hesamzadeh, and M. Ghandhari, "Modelling of multi-terminal hvdc systems in optimal power flow formulation," *Electrical Power and Energy Conference (EPEC), 2012 IEEE*, vol. ., pp. pp. 170–175, 2012. 13

[51] G. Kalcon, G. P. Adam, O. Anaya-Lara, S. Lo, and K. Uhlen, "Small-signal stability analysis of multi-terminal vsc-based dc transmission systems," *IEEE Transactions on Power Systems*, vol. vol. 27 issue.44, pp. pp. 1818 – 1830, 2012. 13

[52] E. Prieto-Araujo, F. Bianchi, A. Junyent Ferre, and O. Gomis-Bellmunt, "Methodology for droop control dynamic analysis of multiterminal vsc-hvdc grids for offshore wind farms," *Power Delivery, IEEE Transactions on*, vol. vol. 26 no 4, pp. pp. 2476– 2485, 2011. 13, 37

[53] T. M. Haileselassie, *Control, Dynamics and Operation of Multi-terminal VSC-HVDC Transmission Systems*. PhD thesis, Norwegian University of Science and Technology, Department of Electric Power Engineering, December, 2012. 13, 41

[54] D. Van Hertem, M. Ghandhari, J. Curis, O. Despouys, and A. Marzin, "Protection requirements for a multi-terminal meshed dc grid," in *Cigre symposium The elec-tric power system of the figure, Bologna*, 2011. 14

[55] C. Franck, "Hvdc circuit breakers: A review identifying future research needs," *Power Delivery, IEEE Transactions on*, vol. vol. 26 , Issue: 2, pp. pp. 998 – 1007, 2011. 14

[56] M. Callavik, A. Blomberg, J. Häfner, and B. Jacobson, "The hybrid hvdc breaker: An innovation breakthrough enabling reliable hvdc grids," *ABB Grid Systems*, vol. ., p. ., 2012. 14

[57] "Abb solves 100-year-old electrical puzzle - new technology to enable future dc grid. http://www.abb.com/cawp/seitp202/65df338284e41b3dc1257aae0045b7de.aspx," Visited on April 19th. 14

[58] K. D. Kerf, K. Srivastava, M. Reza, D. Bekaert, S. Cole, D. V. Hertem, and R. Belmans, "Wavelet-based protection strategy for dc faults in multi-terminal vsc hvdc systems," *Generation,Transmission & Distribution, IET*, vol. vol. 5, no. 4,, pp. pp. 496–503, 2011. 14

[59] J. Murthy, P.K.and Amarnath, Kamakshiah.S., and B. Singh, "Wavelet transfor approach for detection and location of faults in hvdc system," *IEEE Region 10 Colloquium and 3rd International Conference on Industrial and Information systems*, vol. ., p. ., 8-10 Dec.2008. 14

[60] M. Shukr, D. Thomas, and P. Zanchetta, "Vsc-hvdc transmission line faults location using active line impedance estimation," *Energy Conference and Exhibition (ENERGYCON), 2012 IEEE International*, vol. Florence, 9-12 Sept. 2012, pp. pp. 244–248, 2012. 14

[61] "Ewea: Eu energy policy to 2050.," 2010. 16

[62] "Build a european supergrid for jobs and energy-interview to ana aguado. http://www.ewea.org/blog/2012/12/build-a-european-supergrid-for-jobs-and-energy/ visited on april 20th.," 2012. 16

[63] R. Park, "Two reaction theory of synchronous machines," *AIEE Transactions*, vol. vol. 48, pp. pp. 716–730, 1929. 20

[64] H. Akagi and A. Nabae, "The p-q theory in three-phase systems under nonsinusoidal conditions," *European Trans. on Electric Power, ETEP*, vol. vol. 3 no. 1, pp. pp. 27–31, 1993. 20

[65] K. D. Brabandere, B. Bolsens, J. van den Keybus, A. Woyte, J. Driesen, and R. Belmans, "A voltage and frequency droop control method for parallel inverters," *IEEE Transactions on Power Electronics*, vol. vol. 22, no. 4, pp. pp. 1107–1115, 2007. 27

[66] J. Beerten, D. V. Hertem, and R. Belmans, "Vsc mtdc systems with a distributed dc voltage control - a power flow approach," *in PowerTech, 2011 IEEE Trondheim*, vol. ., pp. pp. 1–6, 2011. 34, 36, 41, 43, 88

[67] T. Haileselassie and K. Uhlen, "Primary frequency control of remote grids connected by multi-terminal hvdc," *Proc. IEEE PES GM 10*, vol. Minneapolis, USA, pp. Jul. 25–29, 2010. 36

[68] F. Bianchi and O. Gomis-Bellmunt, "Droop control design for multi-terminal vsc-hvdc grids based on lmi optimization," *Decision and Control and European Control Conference (CDC-ECC), 2011 50th IEEE Conference on*, vol. ., pp. pp. 4823– 4828, 2011. 37

[69] T. Haileselassie and K. Uhlen, "Precise control of power flow in multiterminal vsc-hvdcs using dc voltage droop control," *Power and Energy Society General Meeting, 2012 IEEE*, vol. ., pp. pp. 1–9, 2012. 39

[70] A. Egea-Alvarez, J. Beerten, D. V. Hertem, and O. Gomis-Bellmunt, "Primary and secondary power control of multiterminal hvdc grids.," *AC/DC IET Conference 2012 Procedings*, 2012. 41, 70, 87

[71] C. Barker and R. Whitehouse, "Autonomous converter control in a multi-terminal hvdc system," *AC and DC Power Transmission, 2010. ACDC. 9th IET International Conference on*, vol. ., pp. pp. 1–5, 2010. 41

[72] C. Barker and R. Whitehouse, "Further developments in autonomous converter control in a multi-terminal hvdc system," *AC/DC IET Conference 2012 Procedings*, 2012. 41

[73] J. Beerten, S. Cole, and R. Belmans, "A sequential ac/dc power flow algorithm for networks containing multiterminal vsc hvdc systems," *in Power and Energy Society General Meeting, 2010 IEEE*, vol. ., pp. pp. 1–7, 2010. 41

[74] F. Gonzalez-Longatt, J. Roldan, and C. A. Charalambous, "Power flow solution on multi-terminal hvdc systems: Supergrid case," *International Conference on Renewable Energies and Power Quality (ICREPQ12)*, vol. Santiago de Compostela, Spain, pp. March, 28–30, 2012. 41

[75] M. Aragüès-Peñalba, A. Egea-Àlvarez, O. Gomis-Bellmunt, and A. Sumper, "Optimum voltage control for loss minimization in hvdc multi-terminal transmission systems for large offshore wind farms," *Electric Power System Research,Elsevier*, vol. vol. 89, pp. pp. 54–63, 2012. 60, 88

[76] R. Pinto, P. Bauer, S. Rodrigues, and E. Wiggelinkhuizen, "A novel distributed direct-voltage control strategy for grid integration of offshore wind energy systems through mtdc network," *Industrial Electronics, IEEE Transactions on*, vol. Vol. 60 no. 6, pp. pp. 2429 – 2441, 2013. 60, 88

[77] R. T. Pinto, S. F. Rodrigues, E. Wiggelinkhuizen, R. Scherrer, P. Bauer, and J. Pierik, "Operation and power flow control of multi-terminal dc networks for grid integration of offshore wind farms using genetic algorithms," *Energies ISSN 1996-1073*, vol. vol. 6, pp. pp. 1–26, 2013. 60, 88

[78] J. Carpentier and J. Siroux, "L'optimisation de la production de l'electricite de france," *Bulletin de la Societe Francaise de l'Electricite*, vol. B4, pp. pp. 121–129, 1963. 61

[79] H. Domme and W. Tinney, "Optimal power flow solutions," *IEEE Trans.*, vol. PAS 87, pp. pp. 1866–1876, 1968. 61

[80] J. Kennedy and R. Eberhart, "Particle swarm optimization," *in Proc. Conf. IEEE Int Neural Networks*, vol. vol. 4, pp. pp. 1942–1948, 1995. 61

[81] M. A. Abido, "Optimal power flow using particle swarm optimization," *International Journal of Electrical Power Energy Systems*, vol. vol. 24, no. 7, pp. pp. 563–571, 2002. 63

[82] J. Morren, S. de Haan, W. Kling, and J. Ferreira, "Wind turbines emulating inertia and supporting primary frequency control," *Power Systems, IEEE Transactions on*, vol. vol. 21 no. 1, pp. pp. 433–434, 2006. 75

[83] E. Veilleux and B.-T. Ooi, "Multiterminal hvdc with thyristor power-flow controller," *Power Delivery, IEEE Transactions on*, vol. vol. 27 no. 3, pp. pp. 1205–1212, 2012. 91

[84] Q. Mu, J. Liang, Y. Li, and X. Zhou, "Power flow control devices in dc grids," *Power and Energy Society General Meeting, 2012 IEEE*, vol. 22-26 July 2012, pp. pp. 1–7, 2012. 91

[85] O. Ogasawara, H. Akagi, and A. Nabel, "A novel pwm scheme of voltage source inverters based on space vector theory," *Proc. EPE European Conf. Power Electronics and Applications*, vol. ,, pp. pp. 1197–1202, 1989. 99

[86] H. W. v. d. Brocker, H. C. Skudenly, and G. Stanke, "Analysis and realization of a pulse width modulator based on the voltage space vectors," *Conf. Rec. IEEE-IAS Annu. Meeting, Denver*, vol. ,, pp. pp. 244–251, 1986. 99

[87] J. Liu, L. Yao, T. Wu, and Y. An, "Implementation of two-level svpwm algorithm in pscad/emtdc," *Power and Energy Engineering Conference (APPEEC), 2010 Asia-Pacific*, vol. ,, pp. pp. 1–5, 2010. 100